

Utilization of *K*-Region Oxidation for the Synthesis of Functional Materials

by

© Joshua C. Walsh

A thesis submitted to the

School of Graduate Studies

in partial fulfillment of the requirements for the degree of

Master of Science

Department of Chemistry

Memorial University of Newfoundland

July 2016

St. John's, Newfoundland and Labrador

Abstract

Pyrene with its long fluorescence lifetime, large Stokes shift and proclivity towards excimer formation has become the gold standard in the sensing of microenvironments using fluorescence spectroscopy.^[1] Derivatives of pyrene find applications in a broad range of fields.^{[2][3]} However, the design of more complex systems is hampered by the lack of selectivity one encounters when working with pyrene. Alkylation, halogenation and nitration produce practically inseparable isomers. Methods that desymmetrize pyrene are currently of high value. Known methods have recently been improved and applied to a number of systems within the Bodwell group. The optimization of a *K*-region oxidation reaction and utilization of desymmetrized pyrene in the synthesis of redox-active molecules and progress towards a 2,7-pyrenylene-ethynylene macrocycle is investigated in this thesis work.

References

- [1] R. Rieger, K. Müllen, *J. Phys. Org. Chem.*, **2010**, 23, 315-325.
- [2] J. Andréasson, U. Pischel, *Chem. Soc. Rev.*, **2015**, 44, 1053-1069.
- [3] P. Conlon, C. J. Yang, Y. Wu, Y. Chen, K. Martinez, Y. Kim, N. Stevens, A. A. Marti, S. Jockusch, N. J. Turro, W. Tan, *J. Am. Chem. Soc.*, **2008**, 130, 336-342.

Acknowledgements

Firstly, thank you to my supervisor Dr. Graham J. Bodwell for his constant support over the last two years, without his valuable advice and patient guidance the work presented here would have not been possible.

Thanks go out as well to the entire Bodwell group past and present with special mention to Kiran Sagar Unikela who's mentoring early in the program was invaluable to me.

I would like to thank my supervisory committee, Dr. Raymond Poirier and Dr. Sunil Pansare for helpful suggestions during committee meetings and for proof reading this thesis. I am grateful to Dr. Céline Schneider and Ms. Linda Winsor for instrument training and help with NMR and mass spectrometry respectively.

Finally I thank Nicole, Leo, Sofia and my parents Carl and Joy Walsh for love and support throughout my undergraduate and graduate degrees.

Table of Contents

Abstract	I
Acknowledgements	II
List of Tables	IV
List of Figures	IV
List of Schemes	VII
List of Symbols, Nomenclature or Abbreviations	IX
Chapter 1: Introduction	1
Chapter 2: <i>K</i> -region oxidation of selected PAHs	31
Chapter 3: Progress towards a 2,7-pyrenylene-ethynylene macrocycle	58
Chapter 4: Synthesis of functional materials base on TTFV-PAH hybrid	78
Appendix	101

List of Tables

Table 1.1	Heptafused PAHs studied by Balaban and Klein.	6
Table 2.1	NMI as an additive in the oxidation of pyrene (2.1) to afford pyrene-4,5-dione (2.2).	37
Table 2.2	Ligands screened for the oxidation of pyrene (2.1).	39
Table 2.3	Scale-up of the <i>K</i> -region oxidation of pyrene (2.1) to afford pyrene-4,5-diketone (2.2).	43
Table 2.4	Oxidation of pyrene derivatives as well as some selected PAHs.	44

List of Figures

Figure 1.1	Clar analyses of the Kekulé resonance structures of phenanthrene (1.1) and anthracene (1.2).	2
Figure 1.2	Examples of PAHs containing the four types of rings defined by Clar.	3
Figure 1.3	Heptafused PAHs studied by Balaban and Klein.	5

Figure 1.4	HOMA and NICS values of phenanthrene (1.1).	7
Figure 1.5	Various edge features of polycyclic aromatic hydrocarbons.	8
Figure 1.6	Annulation of a bay region producing <i>K</i> -regions.	9
Figure 1.7	The formal definition of a shape-persistent macrocycle as described by Höger.	10
Figure 1.8	Three possible side group orientations in SPMs.	11
Figure 1.9	Influence of substitution pattern in SPMs on their supramolecular chemistry.	12
Figure 1.10	Superstructure 1.17c formed in the solid state reported by Gattuso <i>et al.</i>	13
Figure 1.11	AEM 1.18 , a SPM with extraannular substitution.	13
Figure 1.12	Inclusion complex formed between SPM 1.19 and two tetrapentylammonium cations.	14

Figure 1.13	Examples of AEMs displaying exclusive ortho (1.20), meta (1.21) and para (1.22) substitution.	15
Figure 1.14	An onion complex of C ₆₀ @dibenzo[6]CPPA \rhd tribenzo[9]CPPA (1.33).	21
Figure 1.15	Important molecules in the chemical history of TTF.	23
Figure 1.16	Parent TTFV (1.45) and a derivative showing conformational switching.	24
Figure 1.17	Polymer capable of the reversible dispersion of SWCNTs reported by Zhao <i>et al.</i>	25
Figure 1.18	Zhao's TTFV-pyrene hybrid molecular tweezer with C ₆₀ .	27
Figure 1.19	Pyrene-TTFV-copolymer (1.52).	28
Figure 2.1	Direct oxidation of pyrene using RuCl ₃ /NaIO ₄ .	35
Figure 2.2	Extractions of reaction mixtures obtained from <i>K</i> -region oxidations of pyrene (2.1).	39

Figure 2.3	Proposed mechanism of the ruthenium catalyzed oxidation of pyrene (2.1) to diketone (2.2).	41
Figure 2.4	Proposed mechanism of the oxidative ring opening of corannulene (2.25).	47
Figure 2.5	Proposed mechanism of the oxidative ring opening of corannulene (2.25) under optimized conditions.	48
Figure 3.1	Synthetic targets of this work.	58
Figure 4.1	Parent compounds, TTF (4.1) and TTFV (4.2).	78
Figure 4.2	Redox switchability of tetrathiafulvalenes.	80
Figure 4.3	pH-induced conformational switching of TTFV.	80
Figure 4.4	Cyclic voltammogram of (4.11) (V vs. Ag/AgCl)	85
Figure 4.5	Proposed resonance hybrid accounting for low reactivity of 4.11 .	86
Figure 4.6	UV-vis absorption spectrum of 4.13 titrated with sodium	86

periodate.

Figure 4.7	Bulk Raman spectra of 4.13 aluminium and product of mechanochemical reaction.	87
Figure 4.8	Expected product from the oxidation of 4.13 with iodine and reductive workup.	88
Figure 4.9	Proposed radical ring closure regenerating corannulene system 4.16 .	90
Figure 4.10	Charge separated resonance form resulting in two sextets.	91
Figure 4.11	Proposed synthetic route to homocorannulene (4.18).	94
Figure 4.12	Proposed delocalization resulting in both anti- and aromatic character.	94

List of Schemes

Scheme 1.1	Reactions of tribenzoperylenes 1.6 and 1.8 with maleic anhydride.	4
------------	---	---

Scheme 1.2	Diels-Alder reaction of perylene (1.14) with benzyne (1.14a).	9
Scheme 1.3	The synthesis of <i>ortho</i> -AEM (1.20) by Campbell <i>et al.</i>	16
Scheme 1.4	Bodwell's synthesis of AEMs 1.24 and 1.25 .	17
Scheme 1.5	Sondheimer's 1974 synthesis of dibenzocyclooctadiyne (1.27).	18
Scheme 1.6	[5]-[9]CPPAs (1.28-1.32) reported by Kawase <i>et al.</i> between 1996 and 2006.	19
Scheme 1.7	Attempted synthesis of [4]CPPA by Kawase <i>et al.</i>	20
Scheme 1.8	Oxidative dimerization of dithiafulvenes producing tetrathiafulvalenes.	25
Scheme 1.9	Classical synthesis of monosubstituted dithiafulvenes 1.50 .	26
Scheme 1.10	Bryce's olefination reaction.	26
Scheme 2.1	Direct and indirect <i>K</i> -region oxidation of pyrene to pyrene-4,5-dione (2.2).	31

Scheme 2.2	Dewar localization energies of positions in pyrene (2.1) and phenanthrene (1.1).	32
Scheme 3.1	Retrosynthetic analysis of 2,7-pyrenylene-ethynylene macrocycle 3.1 .	61
Scheme 3.2	Retrosynthetic analysis of cyclophanetetraene 3.3 .	62
Scheme 3.3	Continued retrosynthetic analysis of tetrathiacyclophane 3.2 .	63
Scheme 3.4	Retrosynthetic analysis of dithiol 3.5 .	63
Scheme 3.5	Retrosynthetic analysis of dialdehyde 3.7 .	64
Scheme 3.6	Synthesis of building block 3.13 .	65
Scheme 3.7	Synthesis of building block 3.15 .	65
Scheme 3.8	Synthesis of building block 3.17 .	67
Scheme 3.9	Attempted synthesis of various electrophiles 3.18-3.21 .	68

Scheme 3.10	Synthesis of disulfide-containing macrocycle 3.22 .	70
Scheme 3.11	Desulfurization revealing the target tetrathiacyclophane 3.2 .	71
Scheme 4.1	General strategies for the synthesis of TTFVs from aldehydes.	79
Scheme 4.2	The synthesis of dialdehyde 4.10 .	81
Scheme 4.3	The synthesis of diDTFVpyrene 4.11 .	82
Scheme 4.4	Knoevenogel condensations of pyrene dialdehyde 4.10 .	83
Scheme 4.5	Oxidation of 4.11 and the expected product of polymerization.	84
Scheme 4.6	Reduction of black material yielding starting material (4.13).	89
Scheme 4.7	Proposed olefination of benzofluoranthenedialdehyde (4.26).	89
Scheme 4.8	Unexpected seven-membered ring formation during olefination.	91
Scheme 4.9	Proposed mechanism of the reaction yielding homocorannulene derivative (4.17).	93

List of Symbols, Nomenclature or Abbreviations

SI units and symbols for elements do not appear in this list of abbreviations.

ASE	aromatic stabilization energy
Bipy	2,2'-bipyridine
δ	chemical shift (NMR)
d	doublet
DBU	1,8-diazobicyclo[5.4.0]undec-7-ene
dien	diethylenetriamine
eq	equivalent(s)
h	hour(s)
HOMO	highest occupied molecular orbital
LC-MS	liquid chromatography mass spectrometry
LUMO	lowest unoccupied molecular orbital
m	multiplet
MTO	methyltrioxorhenium

min	minute(s)
NFP	<i>N</i> -formylpiperidine
NMI	<i>N</i> -methylimidazole
NMR	nuclear magnetic resonance spectroscopy
R_f	retention factor
s	singlet
t	triplet
THF	tetrahydrofuran
TLC	thin layer chromatography
TTF	tetrathiafulvalene
TTFV	tetrathiafulvalene vinylogue
VID	valence isomerization / dehydrogenation

Introduction

1.1 Clar's rule

Erich Hückel published his widely known Hückel's rule in 1931; in short, the rule allowed chemists to accurately determine if a molecule would display additional stability known as aromaticity. Hückel reported four criteria that, if satisfied, indicated that a given molecule was aromatic. Put simply, the criteria are as follows: if a molecule is monocyclic, planar, fully conjugated and contains a number of π -electrons that satisfies the equation $4n + 2$ where $n = \mathbb{Z}_{\geq 0}$ then the compound is deemed to be aromatic.^[1] Hückel's rule cannot technically be applied to polycyclic systems, and many attempts were made to develop new models that could be extended to the superfamily of polycyclic aromatic hydrocarbons (PAHs). The most successful of these was reported in 1972, by another Erich, Erich Clar, in a published work for which he is best known: *The Aromatic Sextet*. Clar popularized the term 'aromatic sextet', which was actually coined by Armit and Robinson nearly 50 years earlier. As they put it: "These are, of course, the chief characteristics of benzenoid systems, and here the explanation is obviously that six electrons are able to form a group which resist disruption and may be called the aromatic sextet".^[2] Clar's extension of this concept, which was based on the observed characteristics of known PAHs, allowed chemists to easily describe the aromaticity of polycyclic benzenoid systems in qualitative terms. Clar's rule states that the Kekulé resonance structure of a PAH that contains the greatest number of aromatic sextets,^[3]

defined as distinct benzene-like rings separated by neighboring rings by single bonds (Figure 1.1), is the resonance structure that best represents the chemical and physical properties of the PAH in question. Clar's rule can be applied to two simple PAHs to illustrate its power. First, for phenanthrene (Figure 1.2), two Kekulé resonance structures can be drawn, which differ in the number of aromatic sextets. According to Clar's rule, **(1.1a)** contains the greater number of disjoint aromatic sextets (two, versus one for **1.1b**), so it should provide the best picture of phenanthrene's actual properties.

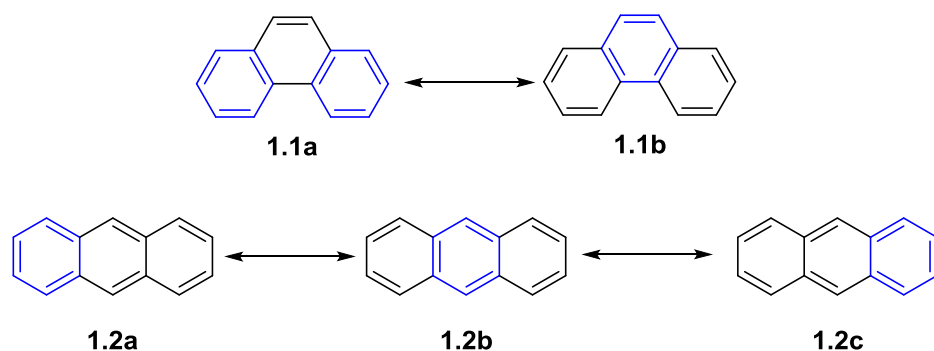


Figure 1.1 Clar analyses of the Kekulé resonance structures of phenanthrene (**1.1**) and anthracene (**1.2**).

On the other hand, anthracene only has a single aromatic sextet in all three of the possible resonance structures and thus is predicted to be less kinetically stable in comparison to its constitutional isomer phenanthrene. Furthermore Clar's rule tells us that in phenanthrene we can expect the outer rings to be more aromatic in character and less reactive than the central ring. In contrast, with respect to Clar's rule, all Kekulé resonance structures of anthracene (and for that matter of all higher homologues known as the acenes) are

degenerate. This insight has been confirmed by numerous aromaticity criteria and by experiment (*vide infra*).

In *The Aromatic Sextet*, Clar further defines four types of rings in PAHs (Figure 1.3).^[3] The first is the aromatic sextet discussed previously. The second is the migrating sextet, which may migrate to adjacent rings providing structures that are equivalent in the Clar analysis. Examples of migrating sextets can be seen in the [*n*]acenes, *e.g.* anthracene (1.2).

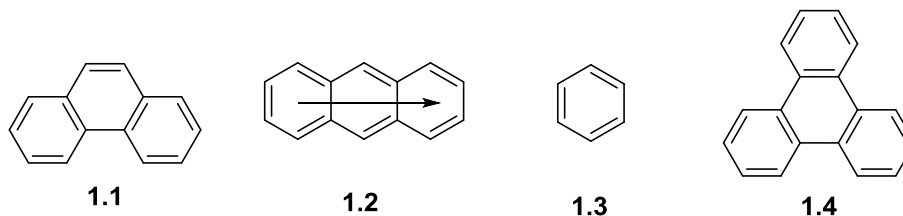
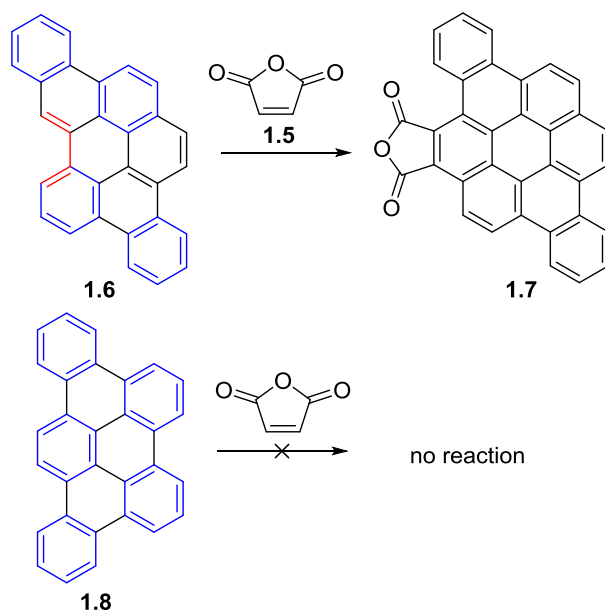


Figure 1.2 Examples of PAHs containing the four types of rings defined by Clar.

The third type of ring is the empty ring, alternating bonds of which are fused to aromatic sextets. The central ring of triphenylene (1.4) is the simplest example. The fourth and final type of ring contains one localized double bond, *e.g.* the central ring of phenanthrene (1.1). Clar further defined PAHs that contain only aromatic sextets and empty rings such as triphenylene as “fully benzenoid PAHs”. Such structures, which all contain $6n$ π -electrons, typically display greater stability than other PAH constitutional isomers. A powerful example of the insight of Clar in this respect is triphenylene, which is the smallest fully benzenoid PAH after the parent compound, benzene. Triphenylene

has the largest resonance energy, highest first ionization potential and the largest HOMO-LUMO gap among the C₁₈H₁₂ isomers.^[4]

Clar himself developed numerous experiments to support his theory and demonstrate its predictive power. For example, tribenzoperylene **1.6** (4 sextets) and **1.7** (5 sextets) were synthesized (an example of Clar's numerous contributions to the synthesis of PAHs) because the Clar analysis pointed toward different reactivity as dienes in the Diels-Alder reaction. Whereas Diels-Alder reaction of **1.6** (diene unit indicated in red) would result in the destruction of one aromatic sextet, analogous reaction in **1.7** would destroy two aromatic sextets. Indeed, it was found that the two isomers had markedly different reactivity toward maleic anhydride. Tribenzoperylene (**1.6**) reacted quantitatively to afford **1.7** (via a Diels-Alder/dehydrogenation sequence) while **1.8** was completely unreactive under the same conditions (Scheme 1.1).^[5]



Scheme 1.1 Reactions of tribenzoperylene (**1.6**) and (**1.8**) with maleic anhydride.

Balaban and Klein provided a truly amazing affirmation of Clar's rule,^[6] by comparing the properties of five carefully chosen PAHs **1.9-1.13** (Figure 1.3). Each of these PAHs contains seven fused rings, but they differ in their connectivity such that each member of the series contains an additional aromatic sextet (Table 1.1). It was found that

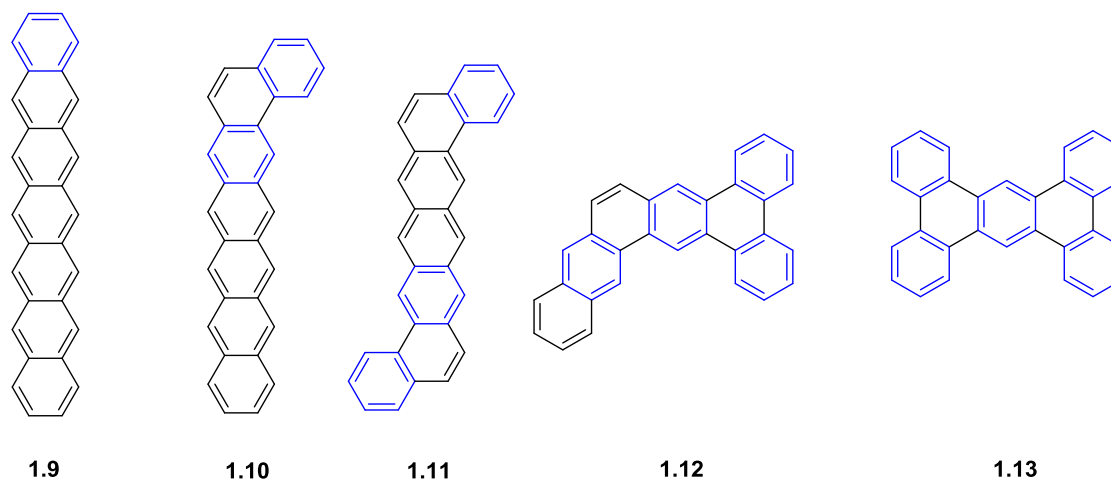


Figure 1.3 Heptafused PAHs studied by Balaban and Klein.

increasing the number of aromatic sextets resulted in a dramatic hypsochromic shift (*ca.* 100 nm per sextet) in the UV-vis spectrum, which indicates a strong increase in the HOMO-LUMO gap.

Table 1.1 Photophysical properties of Balaban and Klein's hydrocarbons

Entry	λ_{\max} (nm)	Color	Number of Sextets
(1.9)	840	Deep-green	1
(1.10)	651	Blue-green	2
(1.11)	523	Red	3

(1.12)	425	Yellow	4
(1.13)	328	Colorless	5

Computational and theoretical chemistry has also lent support to Clar's rule. Of the many indices that have been used to quantify local aromaticity, the two most popular at the time of writing are HOMA and NICS.^[7] HOMA (the harmonic oscillator model of aromaticity) is a geometry-based index, which is defined as:

$$HOMA = 1 - \frac{\alpha}{n} \sum_{i=1}^n (R_{opt} - R_i)^2$$

where α is an empirical constant of carbon-carbon bonds, n is the number of bonds the molecule in question contains, R_{opt} is 1.388 Å (the supposed optimum bond length for aromatic delocalization) and R_i is the observed bond length. HOMA calculations necessarily yield a number between 0 and 1, whereby a value of zero represents a nonaromatic system with maximal bond length alternation and a value of 1 represents a perfect aromatic system with no bond length alternation and bond lengths equal to an optimal 1.388 Å as defined by the equation.

NICS (the nucleus-independent chemical shift) is a magnetism-based index for aromaticity. It is a computational method that calculates the absolute magnetic shielding arising from diamagnetic ring current at any desired point (usually the center) of a ring. The computed values are represented with reversed sign to draw a parallel between the more familiar NMR shift convention; thus a more negative number indicates higher

aromaticity. A value of zero indicates a nonaromatic system and a large positive value indicates antiaromaticity. The excellent agreement of these two aromaticity indices with predictions made using Clar's rule is striking. For example, the HOMA and NICS values for phenanthrene shown in Figure 1.4 show the central ring of phenanthrene is indeed less aromatic than the distal rings with pronounced bond length alternation, nearly double that of the rings containing sextets. The NICS values show more pronounced ring current in the distal rings as well, with the central ring possessing only two thirds as much ring current.

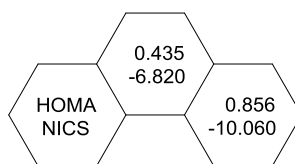


Figure 1.4 HOMA and NICS values of phenanthrene.^[7]

1.1.1 *K*-regions

The periphery of PAHs can contain a number of edge features that can introduce interesting physical properties and affect their reactivity. Due to the rising popularity of carbon nanotube chemistry, two edge topologies (zigzag and armchair) are well-known, but there are several other important edge features that are common in PAH chemistry (Figure 1.5). The topology of the edge can have effects on the properties of molecules. For example, single-walled carbon nanotubes with zigzag edges are metallic while

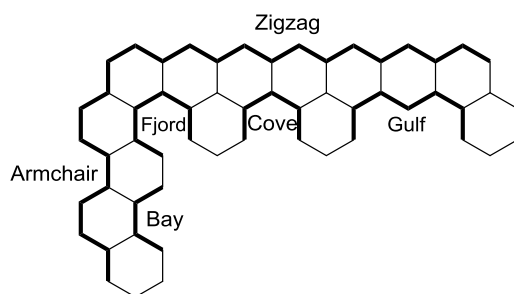
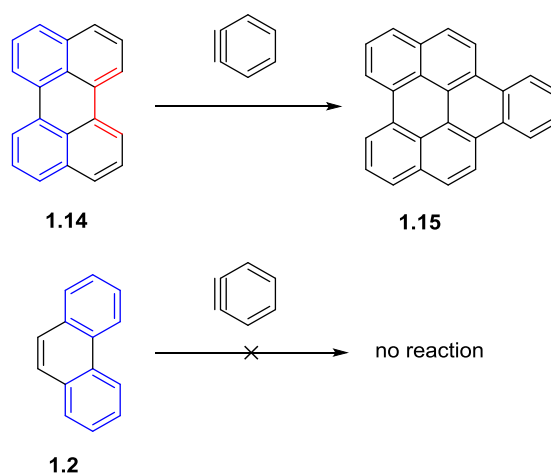


Figure 1.5 Various edge features of polycyclic aromatic hydrocarbons.

armchair nanotubes are semiconducting.^[8] Other notable edge features are the fjord and cove regions, which introduce nonplanarity into a PAH system. In fact, the smallest possible PAHs containing fjord and cove regions are [5]helicene and [4]helicene, respectively. As discussed earlier the bay region (Figure 1.5), (a repeating feature of the armchair edge) is very interesting because it can, in some cases, display significant diene-like behaviour and thus undergo Diels-Alder reactions with appropriate dienophiles. The reactivity in Diels-Alder reactions can be easily predicted by Clar analysis elucidating



Scheme 1.2 Diels-Alder reaction of perylene with benzyne

why perylene will undergo cyclization but phenanthrene will not (Scheme 1.2). Annulation of a fully benzenoid PAH bay region produces a Clar ring with a localized double bond.

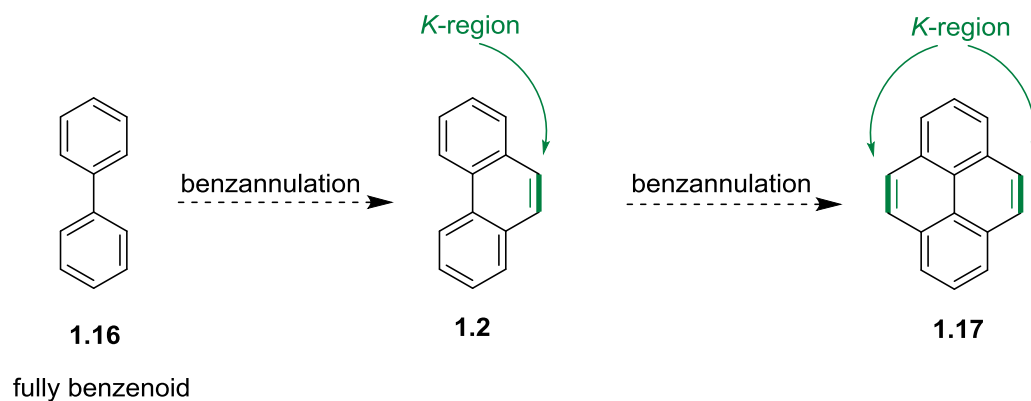


Figure 1.6 Annulation of bay region producing *K*-regions.

The new ring displays reduced aromaticity (*vide supra*) and contains a double bond with significant olefinic character. If this hybrid alkene is located at an edge, the region is known as a *K*-region (Figure 1.6). The *K*-region holds a special place in PAH chemistry. It has been widely studied due to its involvement in the carcinogenicity of PAHs and displays unique reactivity that has been utilized across the chemical sciences. These topics are discussed in detail in Chapter 2.

1.2 Shape-Persistent Macrocycles

Shape-persistent macrocycles (SPMs) are a broad class of large organic molecules that are rigid and non-collapsible in contrast to other macrocycles such as the highly flexible crown ethers and macrolides. A more formal definition was given by Höger:

“shape-persistent macrocycles have an interior (lumen) d that is, on average equal to the contour length l of their molecular backbone divided by π (Figure 1.7).^[9]

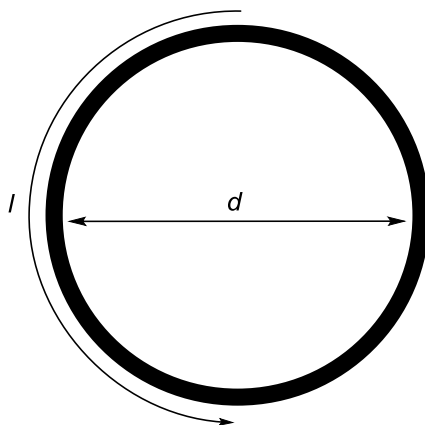


Figure 1.7 The formal definition of a shape-persistent macrocycle as described by Höger (when $d \approx l/\pi$).

SPMs are highly interesting targets, as the rigid backbone allows the chemist to know precisely where functional groups integrated into the macrocycles will be located. Many known SPMs display lumen sizes on the order of single nanometers, giving rise to rich host-guest chemistry that has been widely exploited.^[10] Unlike their flexible counterparts, the rigidity of SPMs allows three different orientations of side groups. Two orientations have the side groups in the plane of the ring (contour length). First, there are extraannular substituents, which lie in the plane of the ring but outside the lumen (Figure 1.8A). Then there are intraannular substituents, which again lie in the plane of the ring, but are oriented inside the lumen (Figure 1.8B). Finally, side groups can be oriented orthogonal to the plane of the ring (Figure 1.8C). Each orientation gives rise to unique properties.

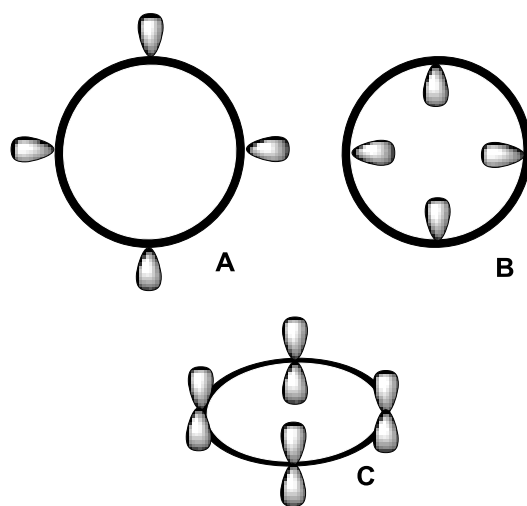


Figure 1.8 Three possible side group orientations in SPMs, A=extraannular, B=intraannular, C=orthogonal.

Orthogonally and extraannularly substituted SPMs are best known for forming superstructures in the solid state. Orthogonally substituted SPMs with appropriate functionality are known to form tubular superstructures (Figure 1.9A), while extraannular substitution leads to a propensity to form 2-dimensional networks on surfaces (Figure 1.9B). On the other hand, intraannular substitution does not project functionality for self-aggregation. Nevertheless, internal functional groups have been utilized in host-guest chemistry where complementary groups on the surfaces of hosts can bind strongly (Figure 1.9C).^[11] Examples of all three types of SPMs have been synthesized and utilized in host-guest chemistry. In 1997, Gattuso *et al.* reported the remarkable supramolecular chemistry of a cyclodextrin (**1.17a**).^[13] Strictly speaking, the cyclodextrins are not SPMs because the shape of the cavity is quite fluxional in solution.

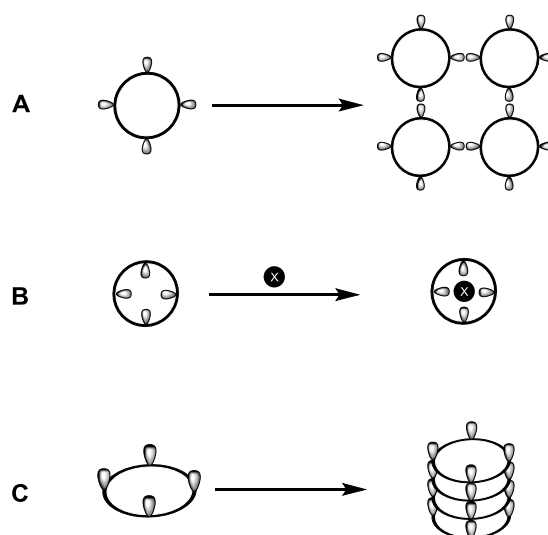


Figure 1.9 Influence of substitution pattern in SPMs on their supramolecular chemistry.

However, several important researchers in the field consider them to be in this class nonetheless.^{[9],[11]} In the solid state, cyclodextrins adopt a rigid conformation with the hydroxyl groups lying orthogonal to the ring structure. As such, the cyclodextrin molecules are predisposed to form tubular superstructures (nanotubes) with a diameter of 1.3 nm (Figure 1.10).

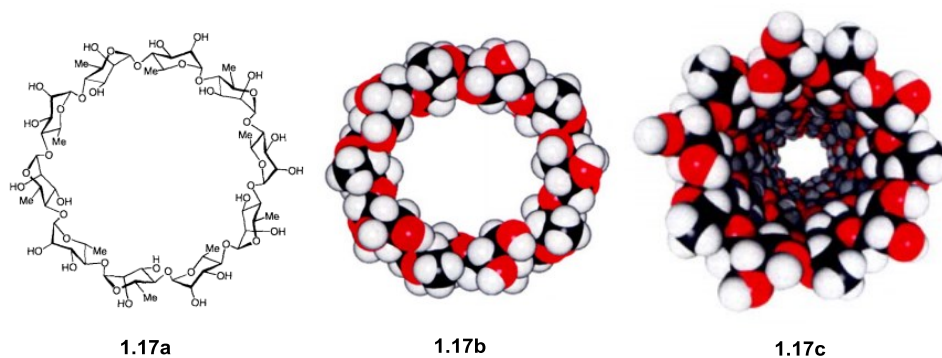


Figure 1.10 Superstructure (1.17c) formed in the solid state reported by Gattuso *et al.*^[13] (Used with permission)

Arlyene-ethynylene macrocycles (AEMs) frequently fall into the category of extraannularly-substituted SPMs. For example, as reported by Höger, macrocycle **1.18** features four extraannular 1,2,3-tridodecoxyphenyl groups,^[13] a common functional group in liquid crystal chemistry. The macrocycle (**1.18**) did not form a liquid crystalline phase, but this did not surprise the authors as it had been known for some time that large internal voids usually preclude liquid crystal formation.^[14]

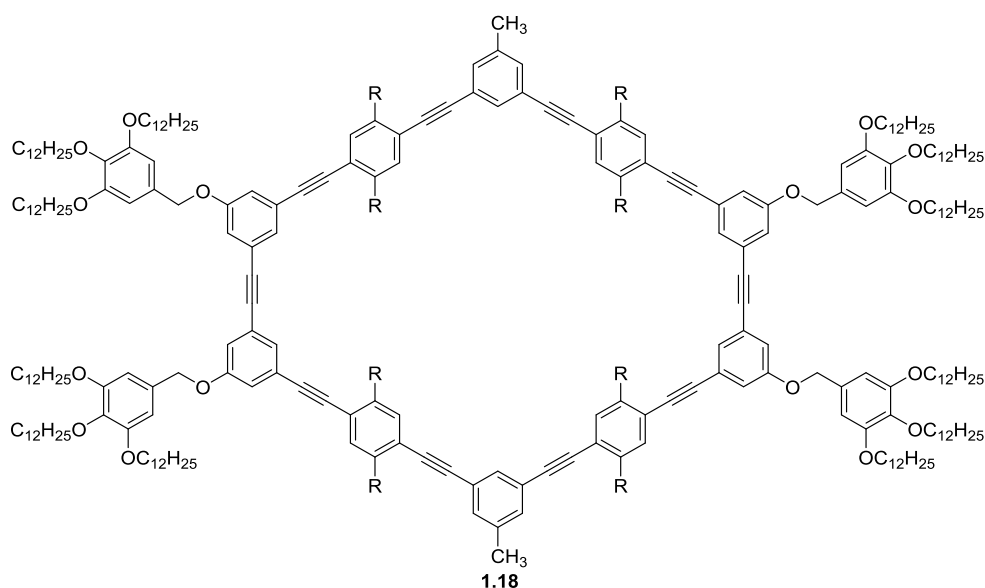


Figure 1.11 AEM **1.18**, a SPM with extraannular substitution.

The compound did, however, form a highly-ordered 2-dimensional network when a monolayer was applied to highly-ordered pyrolytic graphite (HOPG).^[14] Two years later, an example of an SPM with intraannular substitution **1.19** was reported by the same group.^[15] The presence of two internal substituents bearing negatively charged sulfonate

groups and the large internal diameter make **1.19** an excellent host for cations. Indeed, macrocycle **1.19** formed an air and water stable inclusion complex with two tetrapentylammonium cations (Figure 1.12).

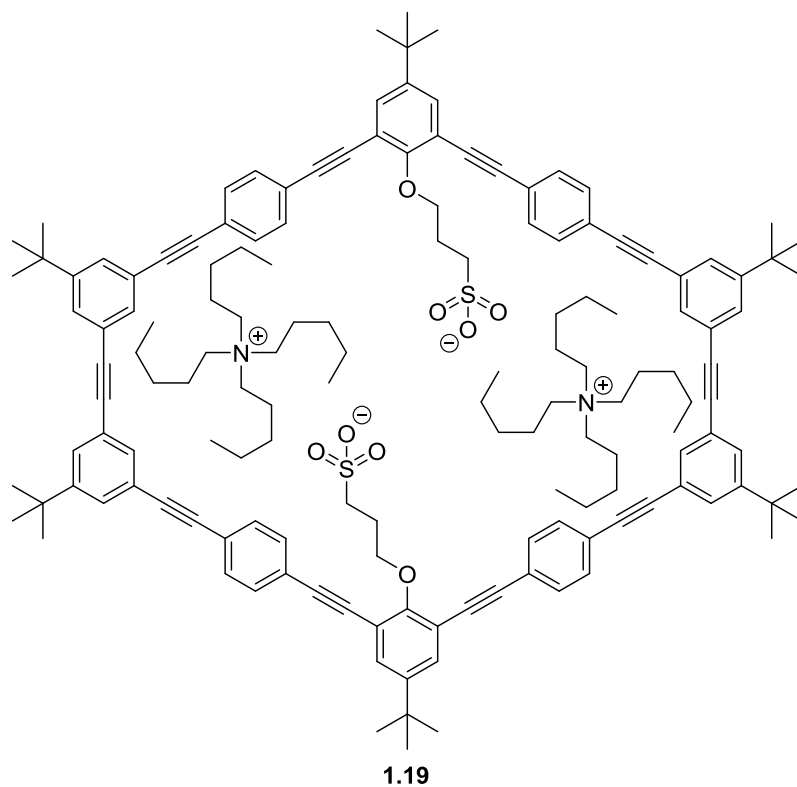


Figure 1.12 Inclusion complex formed between SPM (**1.19**) and two tetrapentylammonium cations.

The SPMs are a large family, differing as much in structure as in function.^[5] With the opportunity to select different substitution motifs, modification of the rigid backbone and the endless array of functional groups available to today's chemists, the possibilities for future development are essentially limitless.

1.2.1 *Para*-arylene-ethynylene Macrocycles

Of the numerous SPMs that have been reported in the literature, the most well-represented subgroup are the AEMs. Their prevalence is due mainly to their relative ease of synthesis.^[10] This, in turn, is due to the availability of reliable synthetic methodology for forming C-C triple bonds (double dehydrohalogenation of geminal dihalides, alkyne metathesis), the homocoupling/cross-coupling of terminal alkynes (Eglinton reaction, Glaser coupling, Hay coupling, Cadiot-Chodkiewicz coupling) and the ease with which terminal alkynes can be linked to appropriately substituted arenes (Sonogashira coupling). The shape of AEMs is determined primarily by the substitution pattern of the constituent arenes.

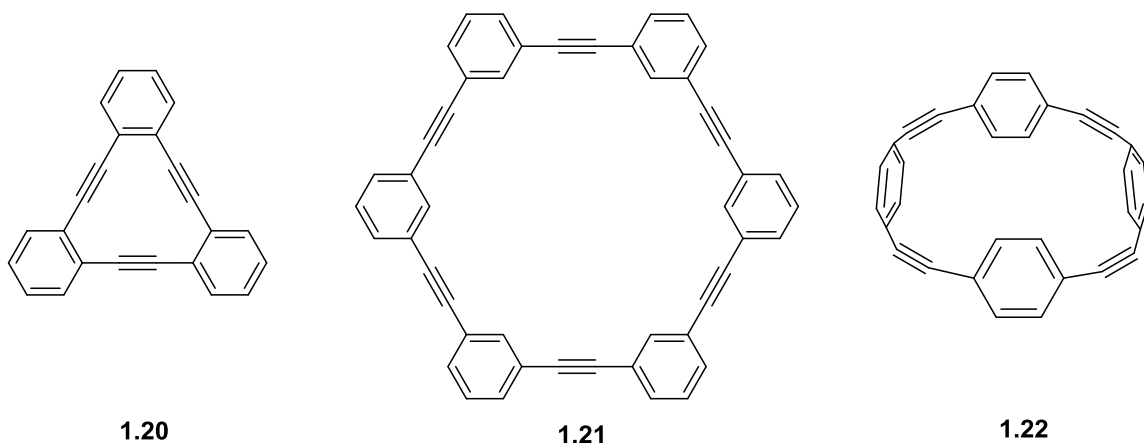
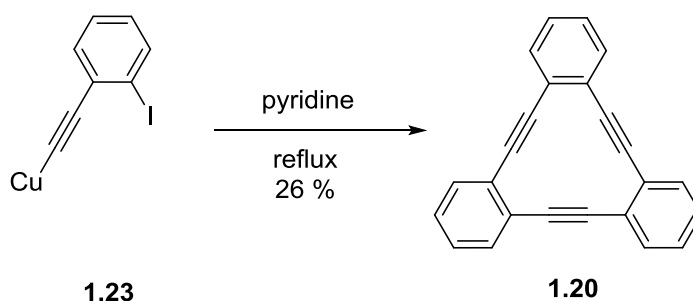


Figure 1.13 Examples of AEMs displaying exclusive *ortho* (1.20), *meta* (1.21) and *para* (1.22) substitution.

When disubstituted benzene is employed as a vertex, three substitution patterns are available: *ortho*, *meta* and *para*. These building blocks impart 120°, 60° and 0° turns to AEMs in which they are incorporated. When the sum of the turns comes to 360°, then the

resulting AEM is essentially strain free. Thus, AEM **1.20** has three *ortho*-substituted benzene rings and **1.21** has six *meta*-substituted benzene rings (Figure 1.13). The absence of strain means that the key challenge in the synthesis of such compounds is macrocyclization and not overcoming strain. For example, **1.20** was first prepared by Campbell *et al.* in 1966 through a trimerization of ((2-iodophenyl)ethynyl)copper(I) (**1.23**) in anhydrous pyridine (Scheme 1.3).^[16]

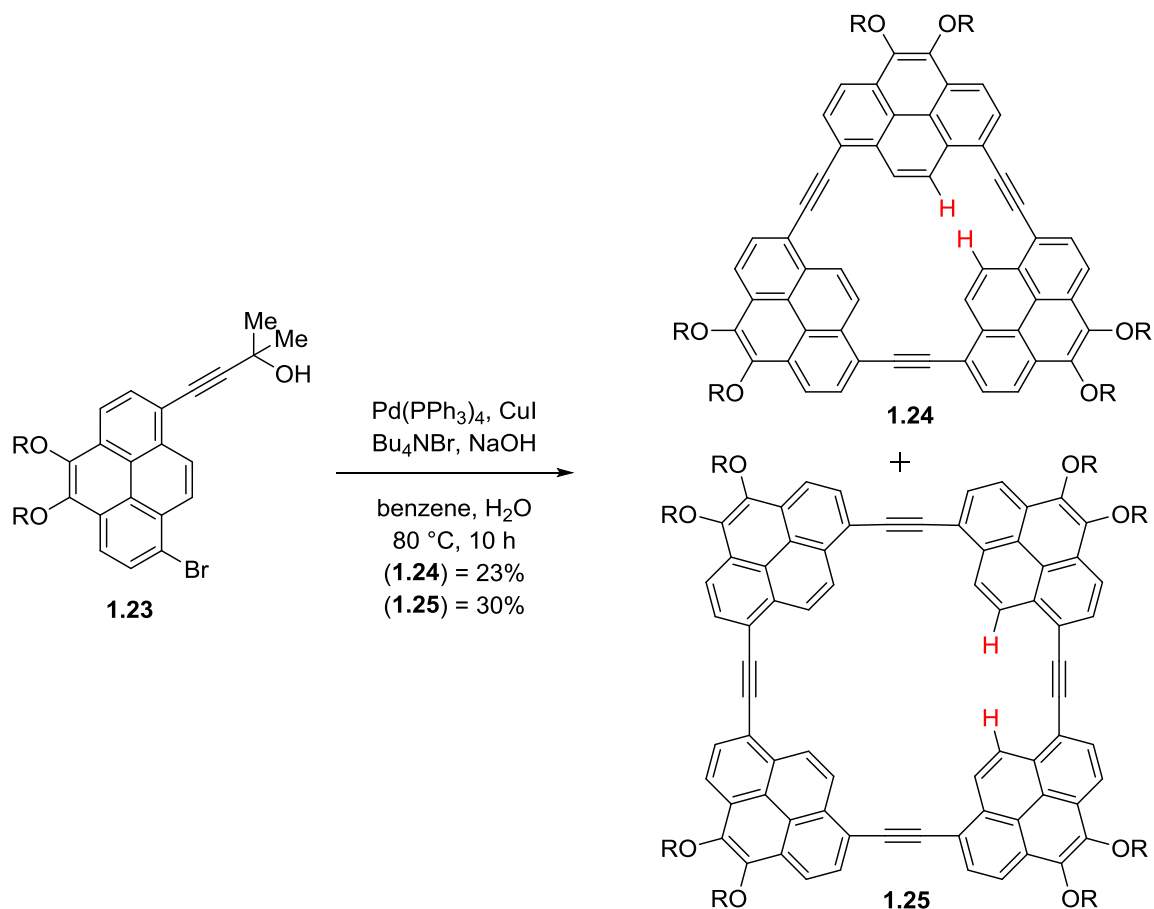


Scheme 1.3 The synthesis of *ortho*-AEM (**1.20**) by Campbell *et al.*^[16]

The vast majority of unstrained AEMs are synthesized in a similar fashion, but typically using the Sonogashira reaction or alkyne metathesis. In contrast, these methods fail to produce AEMs containing only *para*-connected AEMs. Such systems are highly strained because both the benzene rings and ethynylene units must distort from their ideal geometries for a macrocycle to form (*vide infra*).

Of the AEMs reported in the literature to date, relatively few contain aryl groups larger than benzene. Indeed, as the arene becomes larger, the number of examples drops off precipitously. In 2011, the Bodwell group reported the synthesis and characterization of two pyrenylene-ethynylene macrocycles **1.24** and **1.25** (Scheme 1.4), which were the

first examples of pyrene-containing shape-persistent macrocycles.^[17] Like *ortho*-substituted benzene, the 1,8- substitution pattern on pyrene introduces a 120° turn in the macrocycle, thus like AEM **1.19** the cyclic trimer **1.24** is planar and unstrained.



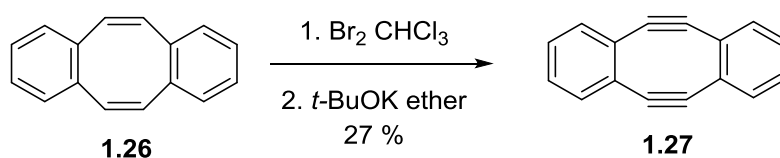
Scheme 1.4 Bodwell's synthesis of AEMs **1.24** and **1.25**.

On the other hand, cyclic tetramer **1.25** adopts a saddle-shaped conformation akin to that of tetrabenzocyclooctatetraene.

As introduced earlier, AEMs with only *para*-substituted benzene rings differ drastically from those with *ortho* and *meta*-substituted rings due to their 0° turn angles.

Not only do they differ in their structures, but also in their properties and the way in which they are synthesized. In most AEMs with *ortho* and *meta*-substituted arenes, the arenes lie in the plane of the macrocycle and this places the substituents in the same plane (Types A, B, Figure 1.8). On the other hand, in AEMs with *para*-substituted benzenes, the benzene rings are puckered into boat conformations and their planes are orthogonal to the plane of the AEM. This necessarily puts any substituents on the aryl rings orthogonal to the plane (Type C, Figure 1.8).

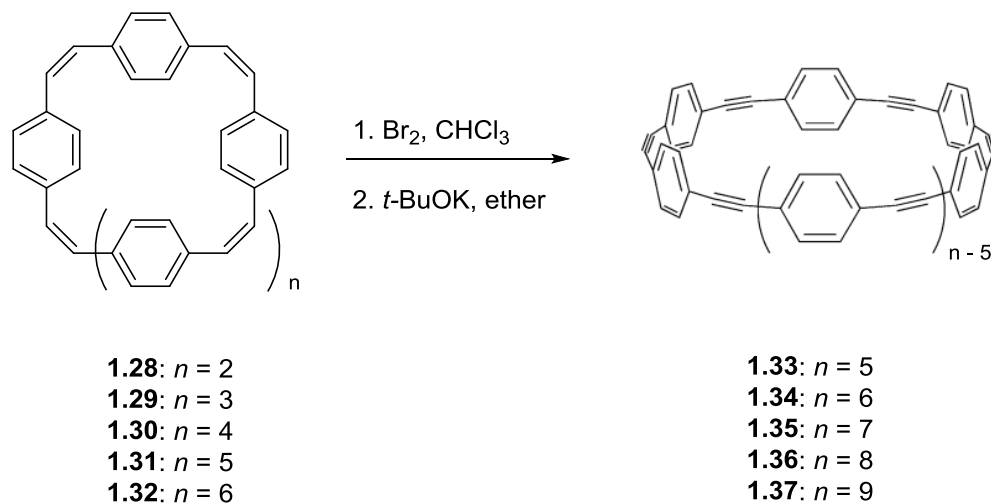
The majority of the known chemistry published on AEMs with *para*-substituted benzenes has been reported by Takeshi Kawase of Osaka University. Kawase took advantage of a strategy first utilized by Sondheimer *et al.* in 1974, which involves the synthesis of a cyclic system consisting of arylene and ethenylene (alkene) units and the conversion of the alkenes into strained alkynes. For examples, **1.26** was converted into highly strained *ortho*-phenyleneacetylene **1.27** by bromination of the alkenes followed by twofold double dehydrobromination.^[18]



Scheme 1.5 Sondheimer's 1974 synthesis of dibenzocyclooctadiyne.

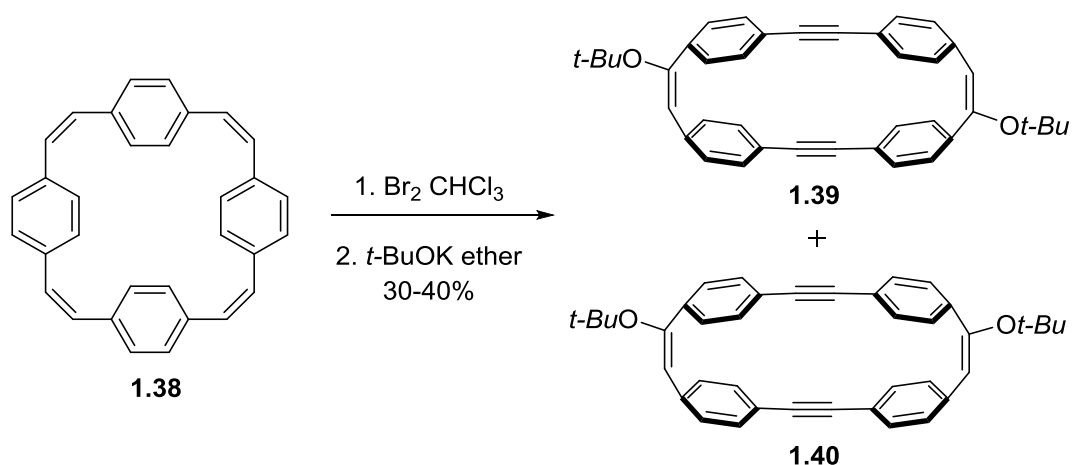
Kawase reasoned that since this reaction was capable of producing such a strained structure, then it should have a good chance of working on the comparatively less strained cycloparaphenyleneacetylenes (CPPAs), the size of which should allow the strain energy

to be dispersed over many bonds. Between 1996 and 2006 he reported the synthesis of $[n]$ CPPAs (where $n = 5-9$) (Scheme 1.6).



Scheme 1.6 [5]-[9]CPPAs reported by Kawase *et al.* between 1996 and 2006.

It is instructive to note that the key alkyne-forming methodology failed when called upon to generate [4]CPPA from tetraene **1.38**, but rather led to the formation of a mixture of isomeric *tert*-butyl alcohol adducts **1.39** and **1.40** (Scheme 1.7).^[19] Since [5]CPPA was easily generated under these conditions, it is evident that either the methodology or the stability of the CPPA under the conditions of its formation reaches a hard limit somewhere between [5] and [4]CPPAs.



Scheme 1.7 Attempted synthesis of [4]CPPA by Kawase *et al.*

The strain energies of the CPPA series have been calculated at the B3LYP/6-31G* level of theory by Krishna.^[20] Analysis of this data shows the gap between the strain energies of the CPPA homologues is not linear. While the difference in strain energy calculated for [10]CPPA and [9]CPPA is only 18 kJ/mol (59 and 75 kJ/mol respectively) the gap between [5] and [4]CPPA is 63 kJ/mol (197 and 264 kJ/mol respectively).^[20]

Table 1.2 Comparison of CPPA strain energies by Krishna *et al.*

Compound	Strain energy	Strain energy/ <i>n</i>	Calculated alkyne
[<i>n</i>]CPPA	(kJ/mol)	kJ/mol/ <i>n</i>	Bend angle
[4]CPPA	266	66.5	157.99
[5]CPPA	203	40.6	162.79
[6]CPPA	164	27.3	165.28
[7]CPPA	133	19.0	167.65

[8]CPPA	109	13.6	169.16
[9]CPPA	90.5	10.1	170.64
[10]CPPA	73.3	7.33	171.43

The reaction that inspired the synthetic route utilized so fruitfully by Kawase must itself be near the limit of what is possible under those conditions since the alkyne bend angle in **1.27** (162°) is only 4° larger than those calculated for [4]CPPA (158°).^[21]

Following the synthesis of the CPPAs, some interesting host-guest chemistry was discovered. [6]CPPA (**1.34**) was found to form exceptionally strong inclusion complexes with C_{60} and C_{70} fullerenes ($C_{60}@[6]CPPA$ $K_a = (1.6 \pm 0.3) \times 10^4$ M^{-1} in benzene at $30^\circ C$).^[22] Further work discovered that strong ring-in-ring complexes were also easily formed, the inclusion complexes [5]CPPA \supset [8]CPPA and [6]CPPA \supset [9]CPPA as well as onion type complexes (Figure 1.14) were reported by Kawase in 2007.^[23]

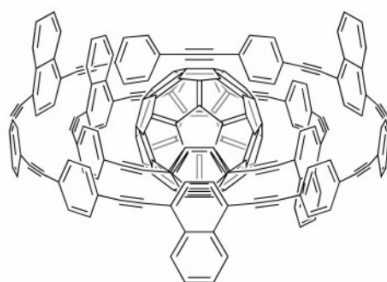


Figure 1.14 An onion complex of $C_{60}@dibenzo[6]CPPA \supset tribenzo[9]CPPA$.

As previously stated, larger PAHs have received very limited attention in the field of AEMs and this is even more true for the strained CPPAs. Preliminary work involving the

incorporation of naphthalene units in the CPPA skeleton led to some very exciting results, which indicated that relatively small increases in the π -surface area can have dramatic effects on the strength of association complexes. In going from inclusion complex [9]CPPA \supset [6]CPPA to tribenzo[9]CPPA \supset dibenzo[6]CPPA, there is a 33% increase in π -surface area, but this is accompanied by a 1000% increase in association constant.^[23] This result suggests that the incorporation of even larger PAHs into CPPAs should provide very strong fullerene receptors. Work aimed at the synthesis of a CPPA in which the *para*-substituted benzenes are replaced by 2,7-pyrenylene units, which also have 0° turn angles, is presented in Chapter 3.

1.3 TTF, TTFV and PAH Hybrids

The first molecule reported bearing the tetrathiafulvalene (TTF) core, a dibenzo derivative **1.41**, was reported in 1926 by Hurtley and Smiles.^[24] Unadorned TTF (**1.42**) was first reported by Wudl in 1970^[25] and has since been the subject of over 13,000 publications in the chemical literature.^[26] In the three years following Wudl's synthesis, the field developed rapidly. Wudl reported the first organic conductor, the chloride salt of TTF-radical-cation (**1.43**) in 1972^[27] and arguably the most

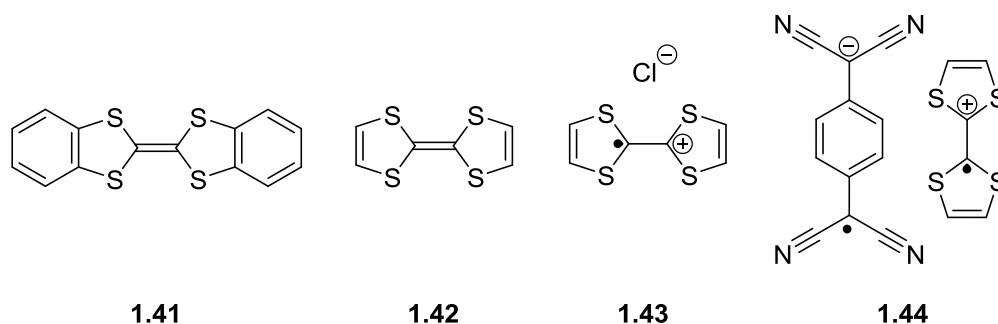


Figure 1.15 Important molecules in the chemical history of TTF.

important publication in TTF chemistry came a year later in 1973, when Ferraris *et al.* reported that the donor-acceptor complex TTF-TCNQ (**1.44**) was in fact a highly conductive organic metal with a near-zero band-gap.^[28] The remarkable properties of **1.44** were attributed to two unique characteristics of TTF: (1) it has high symmetry (D_{2h}), which mitigates random potentials caused by disorder, (2) the presence of four sulfur atoms renders the TTF group highly polarizable, which minimizes Coulombic repulsion between neighboring TCNQ radical anions.^[28] The excellent donor properties of TTF come from the aromaticity of the dithiolane rings that develops upon loss of two electrons. Indeed, both the radical-cation and dication are formally Hückel aromatic.

A more recent development in the field of TTFs is the insertion of π -conjugated spacers between the dithiolane rings. Such extended TTFs (ex-TTFs) have garnered significant attention over the past several years. An important subset of the ex-TTFs are the tetrathiafulvalene vinologues (TTFVs). The parent compound, TTFV (**1.45**), which adopts a planar shape has received little attention. In contrast to this, many of its

derivatives, especially diaryl TTFVs have been the subjects of considerable recent interest.

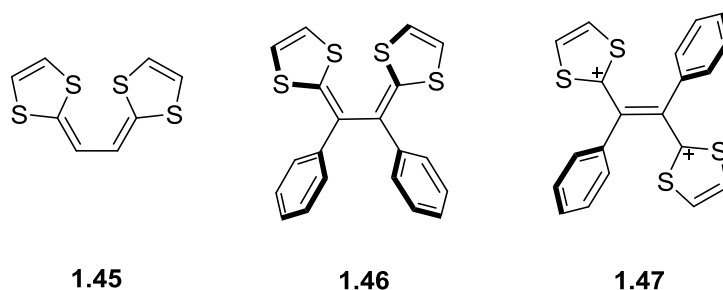


Figure 1.16 Parent TTFV and a derivative showing conformational switching.

Diaryl TTFVs such as the diphenyl derivative **1.46** adopt a *pseudo-cis* conformation driven by attractive sulfur-sulfur interactions and steric repulsion of the benzene rings (Figure 1.16). Like TTF, the TTFVs undergo reversible oxidation driven by the aromaticity of the cationic dithiolinium rings. In the case of the TTFVs, the oxidation to the dication **1.47** is accompanied by a change in conformation to *trans*, which is driven by Coulombic repulsion between the dithiolinium rings. This switchable behavior coupled with a drastic change in conformation has been taken advantage of in very interesting ways. In 2012 the Zhao group reported a TTFV-containing polymer (**1.48**) that exploits the ability of the *pseudo-cis* conformation of the TTFVs to put ‘kinks’ in the polymer, rendering it helical. The polymer, which is adorned with numerous solubilizing groups, is capable of dispersing single-walled carbon nanotubes (SWCNTs) in solution. Upon addition of an oxidant, the TTFV units are switched to the *trans* conformation (**1.49**) (Figure 1.17), which releases the tubes and causes instantaneous precipitation of the SWCNTs.^[29]

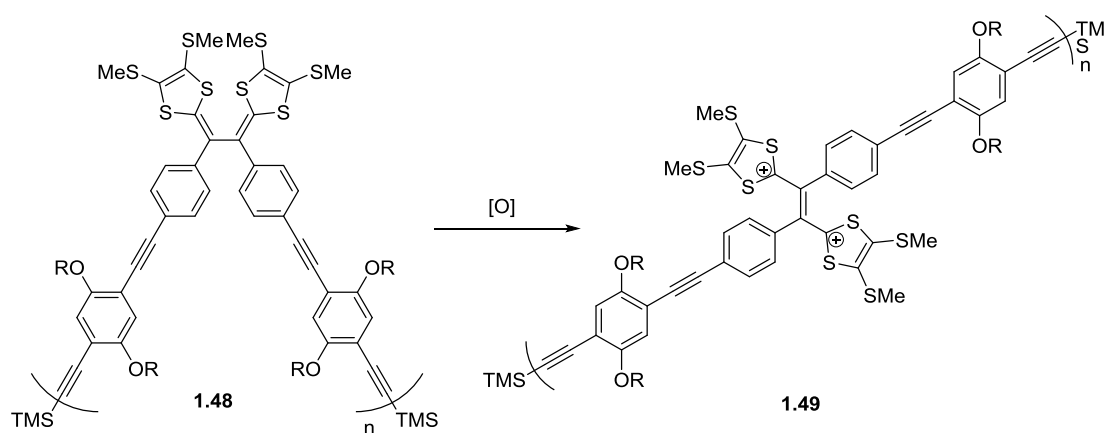
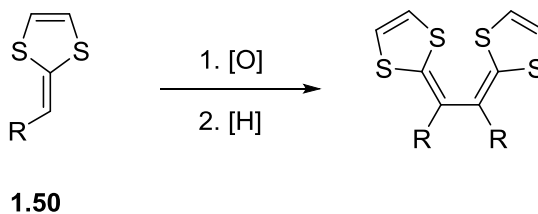
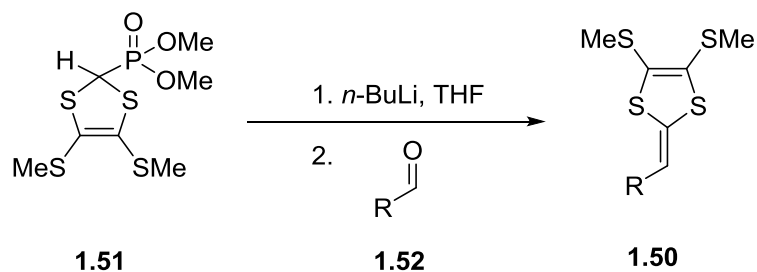


Figure 1.17 Polymer capable of the reversible dispersion of SWCNTs reported by Zhao *et al.*

TTFVs can be synthesized easily from monosubstituted dithiafulvenes through oxidative or electrochemical dimerization (Scheme 1.8). Until recently, the required dithiafulvenes (**1.50**) were synthesized through a Horner-Wadsworth-Emmons reaction involving an aldehyde (**1.52**) and a dithiafulvene phosphonate (**1.51**) (Scheme 1.9) that required laborious multistep synthesis.^[30]

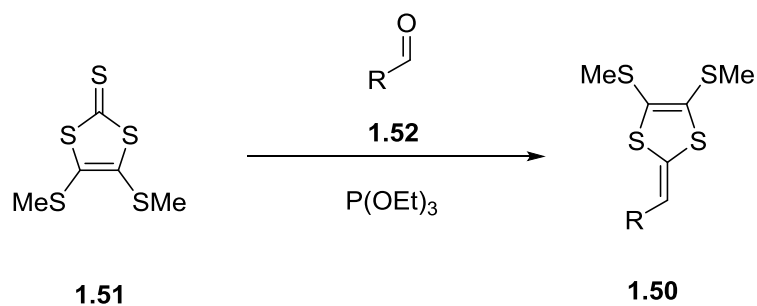


Scheme 1.8 Oxidative dimerization of dithiafulvenes producing tetrathiafulvalenes.



Scheme 1.9 Classical synthesis of monosubstituted dithiafulvenes.

In 2007, Bryce *et al.* reported a phosphite-mediated olefination that is compatible with dithiolethiones (**1.51**) (Scheme 1.10).^[31] They are themselves easily prepared using a two-step-one-pot procedure beginning with carbon disulfide, circumventing the need for multistep synthesis.



Scheme 1.10 Bryce's olefination reaction.

Given the broad scope of applications, the availability of reliable synthetic procedures and tremendous diversity in the structure of aldehydes that can be used in the synthesis of TTFVs, TTFVs have been exploited widely in the chemical sciences. In many of these cases TTFVs have been attached to other structural motifs in order to

couple its electroactive behavior with whatever interesting behavior its partner brings. For example, TTFV-PAH hybrids are interesting and valuable targets. PAHs such as pyrene have long been known to have high affinity for SWCNTs and fullerenes (*vide infra*).

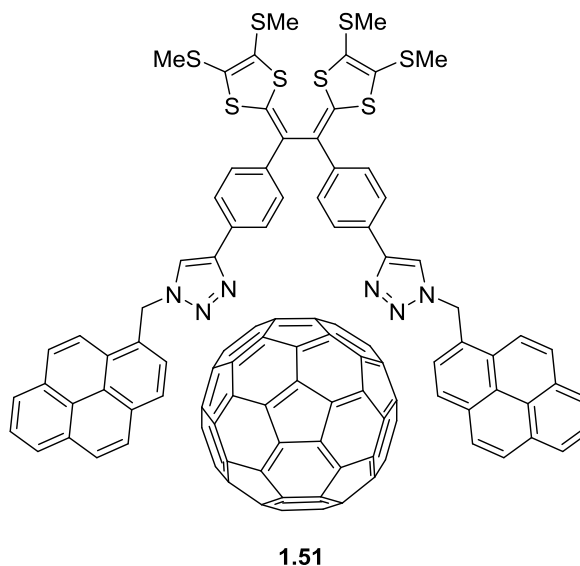


Figure 1.18 Zhao's TTFV-pyrene hybrid molecular tweezer with C_{60} .

Coupling this behavior with the conformational switchability of TTFVs has been demonstrated to have great utility in supramolecular chemistry. The TTFV-pyrene hybrid (**1.51**) was shown by Zhao *et al.* to bind C_{60} and C_{70} fullerenes strongly (Figure 1.18).^[32] Even more recently, a collaboration between the Bodwell and Zhao groups resulted in the synthesis of a TTFV-pyrene-based copolymer (**1.52**) (Figure 1.19), which exhibited interesting aggregation properties in the solid state.^[33] In Chapter 4, the synthesis and properties of some other PAH-TTFV hybrids are described.

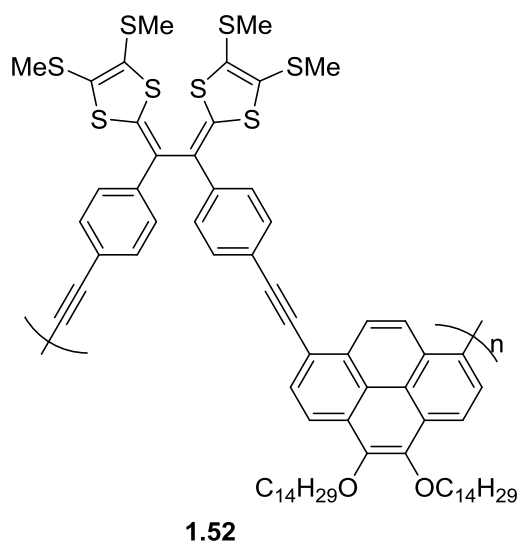


Figure 1.19 Pyrene-TTFV-copolymer (**1.52**).

1.4 References

- [1] E. Hückel, *Z. Phys. Chem.*, **1931**, 70, 204–286.
- [2] J. W. Armit, R. Robinson, *J. Chem. Soc.*, **1925**, 127, 1604–1618.
- [3] E. Clar, *The Aromatic Sextet*; Wiley: New York, **1972**.
- [4] D. Moran, F. Stahl, H. E. Bettinger, H. F. Schaefer, P. v. R. Schleyer, *J. Am. Chem. Soc.*, **2003**, 125, 6746-6752.
- [5] E. Clar, M. Zander, *J. Chem. Soc.*, **1958**, 1861-1865.
- [6] A. T. Balaban, D. J. Klein, *J. Phys. Chem. C.*, **2009**, 113, 19123-19133.
- [7] G. Portella, J. Poater, M. Sola, *J. Phys. Org. Chem.*, **2005**, 18, 785-791.
- [8] V. Barone, O. Hod, G. E. Scuseria, *Nano Lett.*, **2006**, 6, 2748-2754.
- [9] S. Höger, *Chem. Eur. J.*, **2004**, 10, 1320-1329.

- [10] M. K. Smith, O. S. Miljanic, *Org. Biomol. Chem.*, **2015**, 13, 7841-7845.
- [11] F. Diederich, P. J. Stang, R. R. Tykwinski, *Acetylene Chemistry: Chemistry, Biology and Material Science*; Wiley: New York, **2005**.
- [12] G. Gattuso, S. Menzer, S. A. Nepogodiev, J. F. Stoddart, D. J. Williams, *Angew. Chem. Int. Ed.*, **2003**, 36, 1451-1454. (got permission)
- [13] S. Höger, K. Bonrad, A. Mourran, U. Beginn, M. Möller, *J. Am. Chem. Soc.*, **2001**, 123, 5651-5659.
- [14] S. Höger, V. Enkelmann, K. Bonrad, C. Tschierske, *Angew. Chem. Int. Ed.*, **2000**, 39, 2267-2270.
- [15] M. Fischer, S. Höger, *Eur. J. Org. Chem.*, **2003**, 441-446.
- [16] I. D. Campbell, G. Eglinton, W. Henderson, R. A. Raphael, *Chem. Commun.*, **1966**, 87-89.
- [17] G. Venkataramana, P. Dongare, L. N. Dawe, D. W. Thompson, Y. Zhao, G. J. Bodwell, *Org. Lett.*, **2011**, 13, 2240-2243.
- [18] H. N. C. Wong, P. J. Garratt, F. J. Sondheimer, *J. Am. Chem. Soc.*, **1974**, 96, 5604.
- [19] T. Kawase, H. R. Darabi, M. Oda, *Angew. Chem. Int. Ed.*, **1996**, 35, 2664-2666.
- [20] M. A. Ali, M. S. Krishnan, *Mol. Phys.*, **2009**, 107, 2149-2158.
- [21] T. Kawase, H. Kurata, *Chem. Rev.*, **2006**, 106, 5250-5273.
- [22] T. Kawase, H. R. Darabi, K. Tanaka, M. Oda, *Angew. Chem. Int. Ed.*, **2003**, 42, 1624-1628.
- [23] T. Kawase, Y. Nishiyama, T. Nakamura, T. Ebi, K. Matsumoto, H. Kurata, M. Oda, *Angew. Chem. Int. Ed.*, **2007**, 46, 1086-1088.
- [24] W. R. H. Hurtley, S. Smiles, *J. Chem. Soc.*, **1926**, 129, 2263-2270.

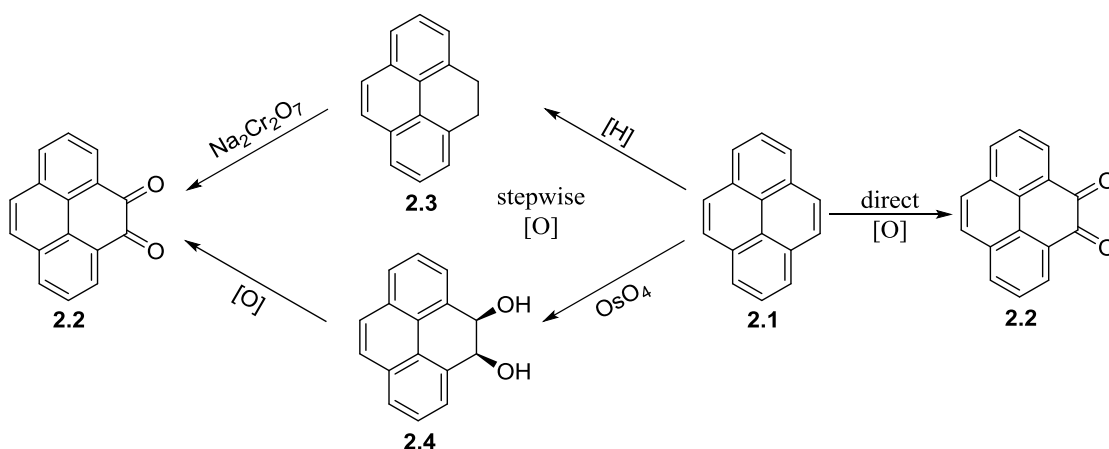
- [25] F. Wudl, G. M. Smith, E. J. Hufnagel, *J. Chem. Soc., Chem. Commun.*, **1970**, 1453–1454.
- [26] M. Bendikov, F. Wudl, D. F. Perepichka, *Chem. Rev.*, **2004**, 104, 4891-4946.
- [27] F. Wudl, D. Wobschall, E. J. Hufnagel, *J. Am. Chem. Soc.*, **1972**, 94, 670-672.
- [28] J. Ferraris, D. O. Cowan, V. V. Walatka, J. H. Perlstein, *J. Am. Chem. Soc.*, **1973**, 95, 948-955.
- [29] S. Liang, G. Chen, J. Peddle, Y. Zhao, *Chem. Commun.*, **2012**, 48, 3100-3102.
- [30] Y. Zhao, G. Chen, K. Mulla, I. Mahmud, S. Liang, P. Dongare, D. W. Thompson, L. N. Dawe, S. Bouzan, *Pure Appl. Chem.*, **2012**, 84, 1005-1025.
- [31] C. A. Christensen, A. S. Batsanov, M. R. Bryce, *J. Org. Chem.*, **2007**, 72, 1301-1308.
- [32] K. Mulla, H. Shaik, D. W. Thompson, Y. Zhao, *Org. Lett.*, **2013**, 15, 4532-4535.
- [33] E. A. Younes, K. M. Williams, J. C. Walsh, C. M. Schneider, G. J. Bodwell, Y. Zhao, *RSC Adv.*, **2015**, 5, 23952-23956.

Chapter Two

K-region Oxidation of Selected PAHs

2.1 Introduction

The selective oxidation of PAH *K*-regions is a powerful method for functionalizing PAHs and modifying their reactivity. The products of *K*-region oxidation are interesting both from organic synthetic and biological points of view, in that they are useful precursors to larger conjugated systems and precursors to *K*-region oxides, which are responsible for the known carcinogenicity of PAHs.^{[1],[2]}



Scheme 2.1 Direct and indirect *K*-region oxidation of pyrene to pyrene-4,5-dione.

Classically, PAH-based *ortho*-quinones have been synthesized in three different ways. The oldest approach is direct oxidation with chromic acid, which is highly substrate dependent in how well it works. The distribution of the various quinones produced by this

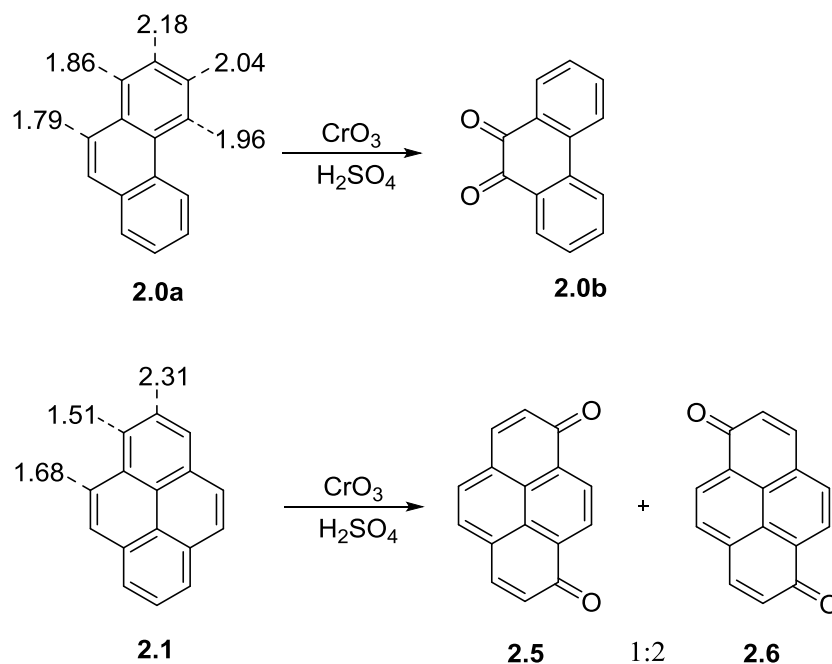
method is influenced by subtle electronic effects. The positions in which oxidation should occur by a given reagent has been calculable since the early 1950s. M. J. S. Dewar reported in Part 6 of his famous series of papers titled, “A Molecular Orbital Theory of Organic Chemistry” a powerful semi-quantitative estimation of the relative rates of substitution at different positions in aromatic hydrocarbons.^[3] The approach involved separating the activation energy (ΔE) of a particular reaction into two terms: (1) a constant (C) representing the characteristics of the leaving group and the reagent in question and (2) the change in electron binding energy, ΔE_{π} representing the difference in binding energy between initial and transition states. ΔE_{π} is independent of the type of substitution occurring since the intermediates (Wheland intermediate, Meisenheimer complex and aryl radical) only differ by the number of electrons in the non-bonding molecular orbital of the transition state.

$$\Delta E = C + \Delta E_{\pi}$$

Equation 2.1 The activation energy of aromatic substitution.

The energy difference ΔE_{π} is known as the localization energy since the value represents the amount of energy needed to isolate a π -electron from the remaining conjugated system. It follows that positions with lower localization energy will undergo substitution more readily. Dewar calculated the localization energies at every position for several PAHs and the results agree perfectly with experimental results. Interestingly, K -regions are rarely the position(s) of lowest localization energy and this illustrates a fundamental problem in the synthesis of K -region *ortho*-quinones by direct oxidation. In fact, the only

PAH calculated to have a preference for *K*-region reactivity is phenanthrene (**2.0a**). In agreement with Dewar's predictions, the direct oxidation of phenanthrene with $\text{CrO}_3/\text{H}_2\text{SO}_4$ yields the *K*-region quinone (**2.0b**) (Scheme 2.2).^[4] In contrast, pyrene (**2.1**) yields a mixture of 1,6-pyrenedione (**2.5**) and 1,8-pyrenedione (**2.6**) with only a trace of the derivative resulting from *K*-region oxidation.^[5]



Scheme 2.2 Dewar localization energies of positions in pyrene and phenanthrene (thermodynamic β units).

The oxidation reactions shown in Scheme 2.1 involve the oxidation of two carbon atoms and, in line with Dewar's predictions, reaction takes place on the two atoms with the minimum combined localization energy. This behaviour is intrinsic to oxidants that proceed through acyclic intermediates, *e.g.* $\text{CrO}_3/\text{H}_2\text{SO}_4$. If oxidation occurs through a cyclic transition state, (*e.g.* using OsO_4) the two carbon atoms that undergo oxidation

must be adjacent. In such cases, the two *adjacent* carbon atoms with the lowest sum of localization energies is almost exclusively the *K*-region. For example, in pyrene (**2.1**), the sum of the localization energies of two adjacent *K*-region carbon atoms is 3.36, as compared to 3.82 for the carbon atoms at C-1 and C-2

PAHs that suffer from poor selectivity under direct oxidation conditions (*i.e.* many of them) can be transformed more efficiently into the corresponding *K*-region quinones by indirect methods. More specifically, Harvey and co-workers reported two indirect methods for the *K*-region oxidation in the 1970s, which far surpassed the older direct oxidation methods in practicality and yield in most cases. This method took advantage of the low combined localization energies typical of *K*-regions. For example, it was found that pyrene's *K*-region could be oxidized to the corresponding *cis*-diol **2.4** using osmium tetroxide. Further oxidation using DDQ or SO₃/pyridine in DMSO afforded quinone (**2.2**) (Figure 2.1). This methodology was also applied to the synthesis of *K*-region quinones of benz[*a*]anthracene and benzo[*a*]pyrene.^[6] Alternatively, catalytic hydrogenation of the *K*-region of pyrene afforded dihydro derivative **2.3**, which was then oxidized directly to the quinone (**2.2**) using sodium dichromate (Scheme 2.1). The latter method has two main advantages over the former: it avoids the use of the very expensive and highly toxic OsO₄ and, using Harvey's own words, the procedure is "adaptable to preparation on any scale".^[7]

In 2005, Hu, Zhang and Harris published a direct oxidation method for pyrene utilizing catalytic amounts of ruthenium chloride in conjunction with sodium metaperiodate as a stoichiometric oxidant to generate and regenerate the presumed active

species, RuO_4 .^[8] The main advantage of this method over previous literature reports is that it achieved *K*-region oxidation in a single step. On the other hand, a major drawback of the reaction is that the workup is singularly difficult.

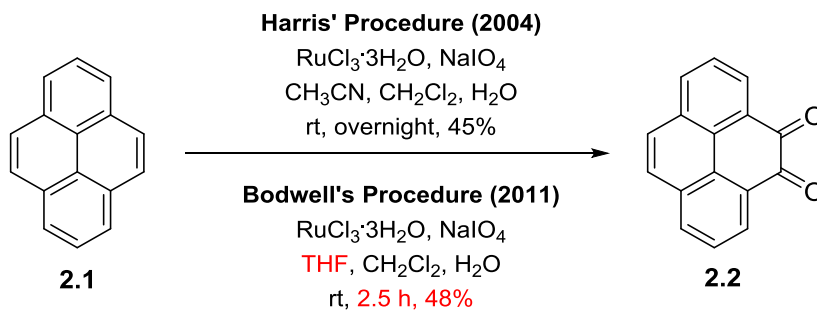


Figure 2.1 Direct oxidation of pyrene using $\text{RuCl}_3/\text{NaIO}_4$.

.Black, tarry byproducts form during the reaction, which preclude efficient filtration or separation. This point is not made in Harris and Zhang's paper, but becomes immediately evident to anyone performing the reaction. Colloquial terms such as "gunky" (gunk: An unpleasantly sticky or messy substance) are commonly employed by such people. Column chromatography requires unusually large volumes of dichloromethane (>1 L per gram of pyrene) and the yield is only modest (45%). Practically, these issues limit the scale of the reaction to *ca.* 2 g of pyrene.

In 2011, the Bodwell group reported an improvement to this procedure. Changing one of the co-solvents from acetonitrile to THF allowed the reaction to be completed in 2.5 h without significantly changing the yield.^[9] This small success meant that a gram of dione **2.2** could be synthesized and isolated by one researcher in a single working day. However, the workup was still as problematic as before.

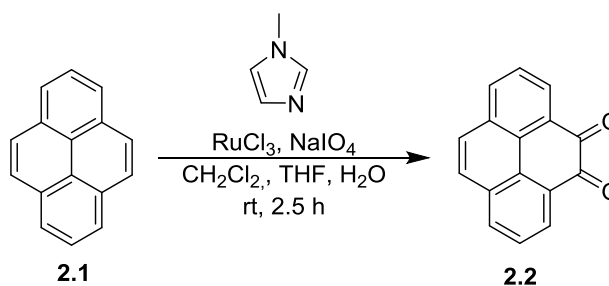
Over the past several years, pyrene-4,5-dione (**2.2**) has been a compound of considerable interest, not only in the Bodwell group, but also to other researchers in the field worldwide. Although it was first reported nearly 80 years ago, 60% of SciFinder hits are within the last 10 years. At the time the work described in this thesis was initiated, several projects in the Bodwell group relied upon pyrene-4,5-dione as a starting material, including those described in Chapters 3 and 4. Progress was limited by the inability to produce multigram quantities of pyrene-4,5-dione (**2.2**). Consequently, work aimed at the development of new or modified procedures that addressed the major issues (workup, yield and scale) was initiated. It is worth noting that pyrene-4,5-dione (**2.2**) is commercially available from a number of suppliers, but it is prohibitively expensive (\$800-2500/g).

2.1 Results and Discussion

The addition of nitrogen-containing heterocycles to transition metal-catalyzed oxidations has been shown to have a significant effect on the rate and outcome of certain reactions. In 1997, Sharpless reported that pyridine and various pyridine derivatives had beneficial effects when added to the methylrhodium trioxide-mediated epoxidation of stilbenes.^[10] The ligand was found to play three roles: (1) to speed up catalytic turnover, (2) to prevent the hydrolysis of the epoxides that were produced and, (3) above a threshold concentration, to increase the catalyst lifetime in solution. These results contrasted the effect observed when using nonaromatic tertiary amines, which were found to strongly inhibit catalyst activity. This contrasting behavior was explained using HSAB theory, *i.e.* that a soft transition-metal has a more favorable interaction with the relatively

softer aromatic amine rather than with the hard aliphatic triamine. A plethora of nitrogen-based heteroaromatic ligands are available, but *N*-methylimidazole (NMI) was chosen for initial work on the basis of a suggestion by Dr. J. P. Lumb (McGill University) at the Calix 2013 conference in St. John's.

Table 2.1 NMI as an additive in the oxidation of pyrene (**2.1**) to afford pyrene-4,5-dione (**2.2**)



Entry	<i>N</i> -methylimidazole (mol%)	Yield (2.2)
1	1	44
2	5	52
3	10	45
4	15	39
5	20	30
6	25	12
7	50	17
8	100	21

To probe the effect of NMI as an additive, eight oxidation reactions were performed on 2 g of pyrene using Bodwell's 2011 procedure while varying the loading of NMI (Table 2.1). It is important to note that these reactions are somewhat mercurial. Two reactions run side by side under the same conditions can yield crude reaction mixtures that appear very different. As such, assessing the 'cleanliness' of a reaction can be tricky. The

addition of 1 mol%, 5 mol% and 10 mol% NMI (with respect to pyrene had a drastic effect on the “cleanliness” of the reactions (Table 2.1, Entries 1-3). A substantial reduction in “gunk” formation was observed and this meant that the work-up could be performed quickly and easily, *i.e.* like most normal organic reactions. The best yield (52%) was obtained when 5 mol% NMI was used (Table 2.1, Entry 2). As the loading of NMI was further increased to 25 mol% in increments of 5 mol%, the yield of **2.2** had decreased to just 12%, although the workups were still as manageable as before. Interestingly, the downward trend in yield was steepest when the loading of NMI reached and then surpassed two equivalents with respect to RuCl₃ (Table 2.1, Entries 5-6). Upon progressing from 25 mol% to 100 mol% loading of NMI, a slight increase in yield was observed (up to 21%), but nothing close to the previously obtained levels was achieved. The dramatic effect of adding just 5 mol% NMI on the workup of the reaction can be seen in the pictures shown in Figure 2.2. Extractions during the workup of reactions using Harris’ 2004 procedure and Bodwell’s 2011 procedure are awash with large amounts of a tarry substance that obscure the phase boundary and complicate both separation and subsequent filtration (Figure 2.2, A, B). In contrast, the extraction associated with the reaction utilizing 5 mol% NMI as an additive has a clear phase boundary and the organic

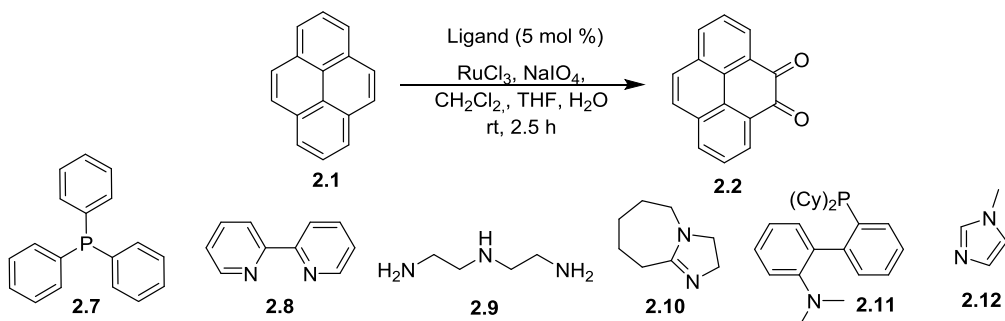


Figure 2.2 Extractions of reaction mixtures obtained from *K*-region oxidations of pyrene (**2.1**) using three different procedures: A = Harris *et al.* 2004, B = Bodwell *et al.* 2011, C = This work (using 5 mol% NMI).

layer is so free of tar that the deep orange colour of the quinone **2.2** can be seen easily (Figure 2.2, C).

With the extremely encouraging result using NMI, other ligands were tested (Table 2.2). The ligands (**2.7-2.12**) varied greatly in structure and included a phosphorus based ligand (PPh₃) (**2.7**), a bidentate aromatic amine (2,2'-bipyridine) (**2.8**), a tridentate aliphatic amine (diethylenetriamine) (**2.9**), an amidine base (DBU) (**2.10**) and a P-N hybrid ligand (Davephos) (**2.11**).

Table 2.2 Ligands screened for the oxidation of pyrene (**2.1**).



Ligand	Yield (%)
PPh ₃ (2.7)	36
bipy (2.8)	43
dien (2.9)	43
DBU (2.10)	45
Davephos (2.11)	45
NMI (2.12)	52

The use of triphenylphosphine as an additive resulted in a significant decrease in the yield and had no apparent effect on the amount of tar formed in the reaction (Table 2.2, Entry 1). It is possible that the phosphine was oxidized under the reaction conditions

to triphenylphosphine oxide, but this was not confirmed. The amine ligands bipy (**2.8**), dien (**2.9**) and DBU (**2.10**) were found to have little effect on the yield and only a moderate cleaning effect on the crude reaction mixture. Davephos (**2.11**), a popular Buchwald-Hartwig ligand, had no effect on the yield, but resulted in a much cleaner workup, even cleaner than when NMI was employed. However NMI is 2 orders of magnitude cheaper than Davephos and resulted in a modest increase in yield along with an adequate cleaning effect.

It is still unclear what role the NMI or any of the tested ligands play in the reaction mechanism. In fact, the mechanism has not been studied rigorously to date. The only mechanism to have been proposed was the one by Tabatabaeian *et al.* (Figure 2.5),^[11] which does not appear to be unreasonable, since it has many precedents in similar reactions with high oxidation state metals (albeit equally speculative).

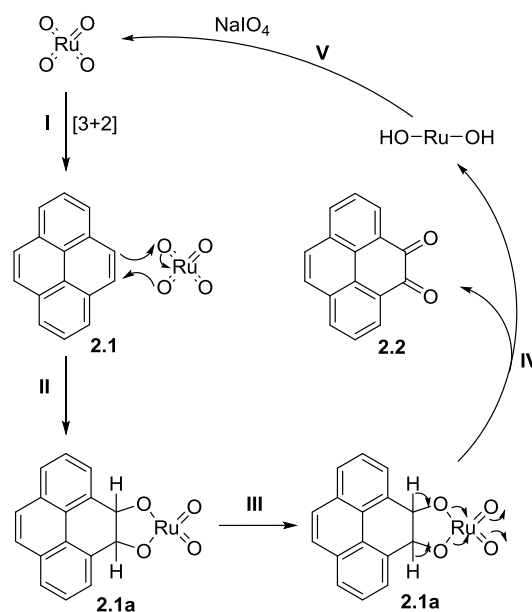


Figure 2.3 Tabatabaeian *et al.*'s proposed mechanism of the ruthenium catalyzed oxidation of pyrene to diketone (**2.2**).

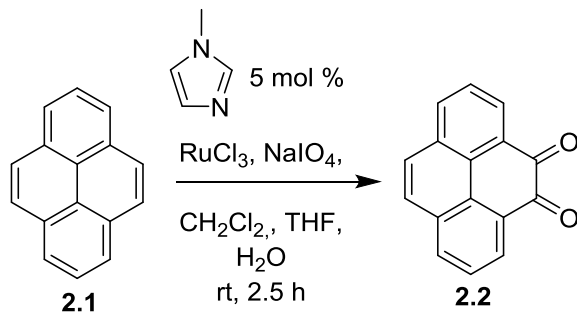
It is proposed^[11] that RuO₄, like OsO₄, first undergoes a [3+2] cycloaddition at the 4 and 5-positions of pyrene (Figure 2.3 I, II) to afford a ruthenate ester **2.1a**. Unlike the corresponding osmate ester, it is proposed that the ruthenate ester **2.1a** does not undergo hydrolysis, but rather, that a double 1,2-elimination to furnish the dione **2.2** and a reduced ruthenium species (Figure 2.3 III, IV). The NaIO₄ is then proposed to serve as the oxidant to regenerate RuO₄.

With regard to the role of NMI, it could be acting as a ligand for Ru at any point and/or serve as a base for the double elimination step. Beyond that, it is unclear exactly why a ligand or base would (at 5 mol%) have such a pronounced effect on the amount of tar that is produced in the reaction. For that matter, it is unknown what the nature of the tarry substance is, which makes it hard to assess the factors leading to its formation. Drawing a parallel with OsO₄ oxidations, the mechanisms are generally poorly understood, but appear to be very complicated. Furthermore, the role that added amines play often depends on subtle electronic differences.^[12] Thus, getting to the bottom of why 5 mol% NMI has such a strong cleaning effect and why it outperforms other ligands is a formidable challenge, which is beyond the scope of the work described in this thesis.

To summarize, the first additive investigated (NMI) had proved to be the best. Its use resulted in the highest yield (modestly higher than the original reaction and the reactions with some other additives) and the work-up was far easier than that of the original reaction. Although the addition of Davephos resulted in an even cleaner work-up and a comparable yield, the cost of NMI is less than 1% of that of Davephos. It was therefore decided to investigate scale-up with NMI as an additive. As previously

mentioned, the original reaction was limited to a 2 g scale. Increasing the scale to 5, 10 and 25 g, proved to be straightforward (Table 2.3). The work-up was as easy on the larger scales as it was on the 2 g scale. The yield was also stable over the change in scale. Strikingly, it appeared as though the reaction with 5 mol% NMI on the 25 g scale proceeded with the formation of less tar than a reaction on the 2 g scale without NMI using the older procedure (Table 2.3).

Table 2.3 Scale-up of the *K*-region oxidation of pyrene to afford pyrene-4,5-diketone (**2**).



Scale (g)	Yield (%)
2	52
5	52
10	51
25	52
100*	41

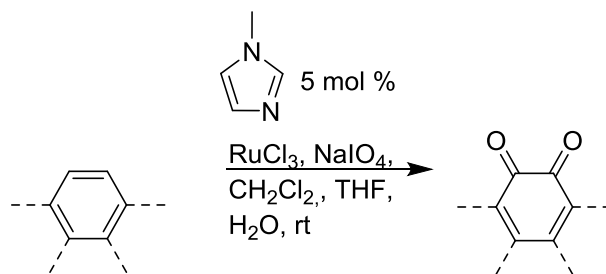
* reaction performed by K. M. Williams

A previous member of the Bodwell group attempted a 100 g scale reaction. Although the reaction proceeded smoothly, readily available standard laboratory glassware was not large enough to perform to the workup. Consequently, specialized glassware was required. Ultimately, Soxhlet extraction was used to extract the product from the tarry residue. It is likely that the somewhat lower yield (41%) yield at this scale

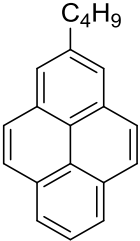
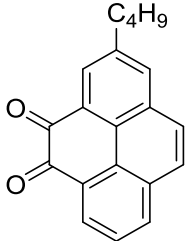
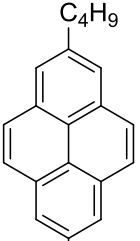
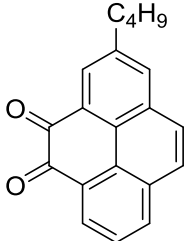
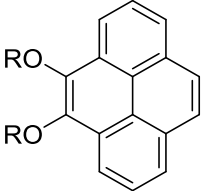
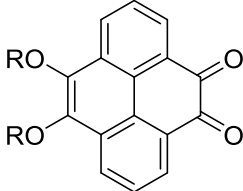
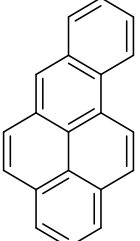
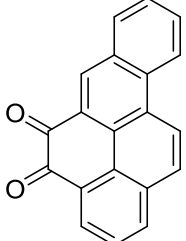
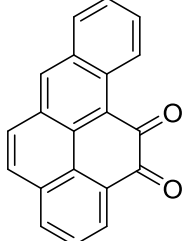
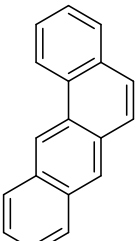
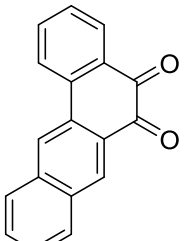
is due to transfer losses and incomplete extraction. The 25 g scale remains the scale of choice because it can be performed comfortably using regular laboratory glassware and it delivers *ca.* 15 g of product. Using the original procedure, at least 15 reactions would have had to have been performed to produce the same amount of dione **2.2**.

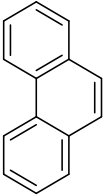
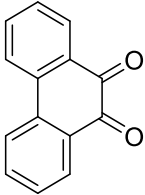
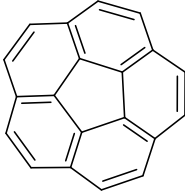
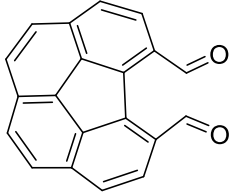
With a reliable large-scale synthesis of pyrene-4,5-dione (**2.2**) in hand, it was of interest to see if the optimized reaction could be utilized in oxidising pyrene derivatives and other *K*-region-containing PAHs to the corresponding diones (Table 2.4). Pyrene derivatives, 2-*tert*-butylpyrene (**2.13**) and 2,7-di-*tert*-butylpyrene (**2.15**) smoothly underwent oxidation easily under these conditions on a 1-2 g scale and scale-up to 25 g was achieved easily. The yields of *tert*-butylated pyrenediones **2.14** (48%) and **2.16** (44%) were a little lower than that obtained with **2.2** (52%) at the same scale.

Table 2.4 Oxidation of some pyrene derivatives and some selected PAHs.



Starting Material	Product	Yield (%)	Time (h)	Scale (g)
 2.1	 2.2	52	2.5	25

 <p>2.13</p>	 <p>2.14</p>	48	2	25
 <p>2.15</p>	 <p>2.16</p>	44	1.5	25
 <p>2.17</p>	 <p>2.18</p>	55	0.75	5
 <p>2.19</p>	 <p>2.20a</p>	50	2	0.1
	 <p>2.20b</p>			
 <p>2.21</p>	 <p>2.22</p>	56	2	0.1

		48	2.5	2
2.23	2.24			
		19 51 brsm	2.5	0.5
2.25	2.26			

4,5-Dihexoxypyrene (**2.17**) was oxidized smoothly under the new conditions on a 2 g scale to afford 4,5-dihexoxy-9,10-pyrenedione (**2.18**). This blood-red dione is a push-pull chromophore, which makes it a compound of interest to the Bodwell group. Unfortunately, a white impurity was always present, which precluded the precise determination of the yield and proper characterization. The impurity could only be partly removed by sublimation. Despite considerable effort, the structure of the impurity could not be determined. Not surprisingly, the apparent rates of consumption of the starting materials (TLC analysis) for compounds **2.1**, **2.13**, **2.15** and **2.17** increased with the presence of electron-donating groups to the pyrene system.

Benzo[*a*]pyrene (**2.19**) underwent oxidization as expected, but the two inequivalent *K*-regions were oxidized unselectively, which resulted in the formation of an inseparable mixture of **2.20a** and **2.20b**. Oxidation of benz[*a*]anthracene (**2.21**) afforded quinone **2.22** in 56% yield after a 2 hour reaction, Not only was the yield the highest of any of the PAH substrates that were investigated, but no evidence for 1,4-oxidation of the

central ring of the anthracene subsystem was obtained. Phenanthrene, unsurprisingly, furnished phenanthrene-9,10-dione (**2.24**) in 48% yield. By comparison, however it is important to note the yield is slightly better and the procedure vastly more practical than the published procedure.^[12] Lastly, corannulene was oxidized in hopes of generating corannulene-1,2-dione, which would offer numerous opportunities for building onto the corannulene system. Unexpectedly, benzo[*ghi*]fluoranthene-5,6-dicarboxaldehyde (**2.23**) was formed instead (Figure 2.4). Nevertheless, this was an exciting result because dialdehyde (**2.26**) is also a potentially useful compound for the synthesis of functionalized corannulenes (*vide infra*). The anomalous behaviour of corannulene (**2.25**) most likely has its origin in the resulting strain relief upon oxidation. If one follows the reaction mechanism proposed by Tabatabaeian (Figure 2.5), cyclic ruthenate ester **2.25a** could conceivably collapse to afford dialdehyde **2.26** and RuO₂.

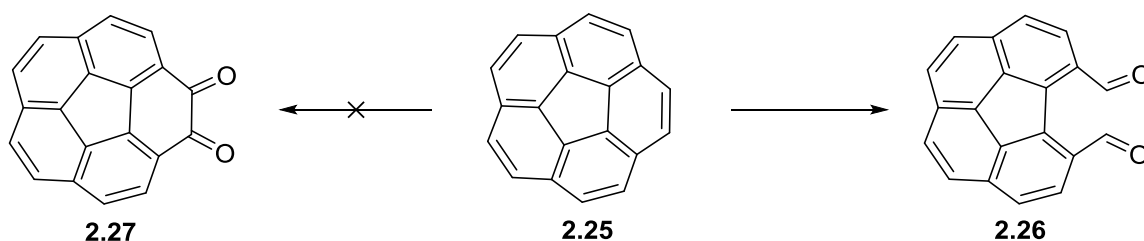


Figure 2.4 The expected **2.27** and the obtained **2.26** products of the oxidation of corannulenes *K*-region.

Again, strain relief would be the driving force for this system. The strain energy of corannulene (**2.25**) has been calculated to be 62.4 kcal/mol and the conversion of ruthenate ester **2.25a** to dialdehyde **2.26** would be expected to relieve a large part of this strain energy.

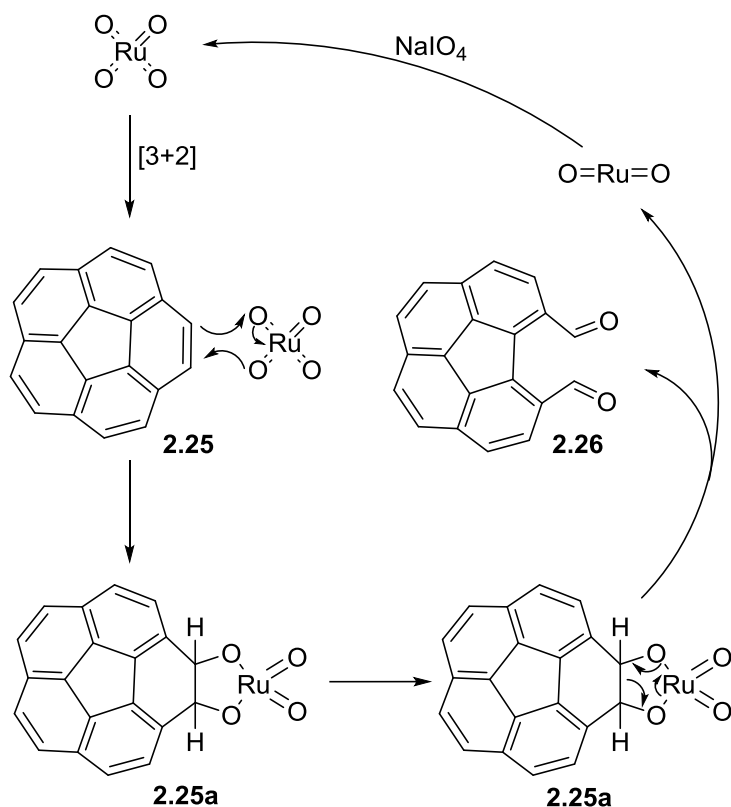


Figure 2.5 Proposed mechanism of the oxidative ring opening of corannulene (**2.25**) under optimized conditions.

The oxidation of corannulene (**2.25**) was also noteworthy because it was the only PAH among those tested that was not completely consumed during the reaction (TLC analysis). The yield of 51% is based on recovered starting material. The absolute yield was 17%.

2.2 Conclusion

The *K*-region oxidation of pyrene to form pyrene-4,5-dione (**2.2**) was improved through the addition of 5 mol% NMI. This resulted in a much cleaner workup, which allowed the reaction to be scaled up by over an order of magnitude with respect to the

amount of pyrene (**2.1**) that can be oxidized in a single reaction. Whereas the original reaction procedure had a practical limit of about 2 g of pyrene (**2.1**), the reaction can now be performed relatively easily on a 25 g scale using regular laboratory glassware. The yield (52%) is slightly better than before. The reaction was then performed on a selected set of *K*-region-containing PAHs and the reaction showed good generality with a tight spread in the yields obtained (44-56%). An unexpected result was obtained for the oxidation of corannulene (**2.25**), which led to the formation of a potentially useful dialdehyde (**2.26**), which would otherwise have required multistep synthesis.

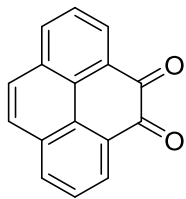
2.3 Experimental section

All reagents utilized in the work described in this chapters work were used as received from commercial chemical suppliers (Aldrich, Alfa Aesar, TCI, Matrix Scientific and Precious Metals Online). All reactions were performed without an inert atmosphere unless otherwise indicated. THF was dried over activated 4 Å molecular sieves for 24 h prior to use. Hexanes were distilled before use in column chromatography. Methyl *tert*-butyl ether was subjected to three freeze-pump-thaw cycles before use. Flash chromatography was performed using ZEOChem 60 eco 40-63 µ. Compounds on TLC plates were visualized with UV light (254 and 365 nm) and chemical staining methods (phosphomolybdic acid, 2,4-dinitrophenylhydrazine and iodine).

Instrumentation:

Melting points were measured on an OPTImelt automated melting point system and are uncorrected, recrystallization solvents are presented in brackets ^1H NMR (300 MHz) and ^{13}C NMR (75 MHz) were recorded on a Bruker AVANCE III instrument (CDCl_3 , unless otherwise indicated). Chemical shifts are reported relative to internal standards: Me_4Si (δ 0.00 ppm) and CDCl_3 (δ 77.23 ppm). ^1H NMR data are presented as follows: chemical shift, multiplicity (s=singlet, d=doublet, t=triplet, q=quartet, m=multiplet, brs=broad singlet, dd=doublet of doublets), coupling constant (J in Hz), integration (number of ^1H). IR spectra were obtained using a Bruker TENSOR 27 FTIR. Low-resolution mass spectra (MS) were taken on LC/MSD (Trap) Agilent 1100 series SL. High resolution mass spectra (HRMS) of some compounds were obtained using a Waters Micromass GCT premier instrument. MS data are presented as follows: m/z (relative intensity), assignment (when appropriate), calculated mass for corresponding molecular formula. UV-vis and fluorescence spectra were recorded using Agilent HP8453A UV-Visible absorbance spectrophotometer and PTI QuantaMaster 6000 spectrofluorometer.

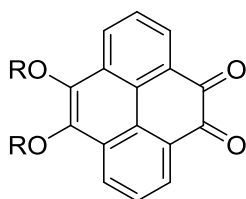
Pyrene-4,5-dione (2.2)



To a solution of pyrene (10.0 g, 49.4 mmol) in CH_2Cl_2 (400 mL) and THF (400 mL) was added $\text{RuCl}_3 \cdot 3\text{H}_2\text{O}$ (1.29 g, 4.94 mmol), 1-methylimidazole (0.203 g, 2.47 mmol), H_2O (500 mL) and NaIO_4 (47.6 g, 222 mmol). The black solution was stirred at room temperature for 2.5 h. Organic

solvents were removed under reduced pressure. CH₂Cl₂ (400 mL) and H₂O (500 mL) were added and the layers separated. The aqueous phase was extracted with CH₂Cl₂ (3 × 100 mL). The CH₂Cl₂ extracts were combined and washed with H₂O (3 × 500 mL). The organic phase was dried over Na₂SO₄ and the solvent removed under reduced pressure to afford a dark orange solid. Column chromatography (CH₂Cl₂) gave pyrene-4,5-dione as bright orange crystals (5.97 g, 52%) R_f (40% EtOAc/hexanes) = 0.50: mp: > 300 °C decomp.; ¹H NMR (CDCl₃, 300 MHz) δ 8.46 (dd, *J* = 6.2, 1.3 Hz, 2H), 8.15 (dd, *J* = 6.7, 1.3 Hz, 2H), 7.83 (s, 2H), 7.74 (t, *J* = 7.5 Hz, 2H) ppm; ¹³C NMR (CDCl₃, 75 MHz) δ 180.4, 135.7, 132.0, 130.2, 130.1, 128.4, 128.0, 127.3 ppm. HRMS [APCI(+)] calcd for C₁₆H₈O₂ 232.0524, found: 232.0523.

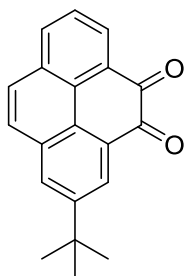
Pyrene-4,5-dihexoxy-9,10-dione (2.18)



To a solution of 4,5-dihexoxypyrene (5.01 g, 12.4 mmol) in CH₂Cl₂ (50 mL) and THF (50 mL) were added RuCl₃·3H₂O (331 mg, 1.24 mmol). To the resulting dark brown solution *N*-methylimidazole (51 mg, 0.62 mmol) and 65 mL H₂O were added. Over a 20-min period NaIO₄ (12.0 g, 55.9 mmol) was added in small portions. The slurry was stirred at room temperature for 0.75 h. The reaction contents were then suction filtered and the filtrate was stripped of solvent under reduced pressure. CH₂Cl₂ (100 mL) and H₂O (200 mL) were added to dissolve the residue and the layers were separated. The aqueous phase was extracted with CH₂Cl₂ (2 × 100 mL) and the combined organic layers were washed with water (2 × 200 mL) to

afford a deep red solution which was dried over anhydrous Na₂SO₄ and the solvent was removed by rotary evaporator. The residue was adsorbed onto silica gel and subjected to flash chromatography (5 × 15 cm) using 50% CH₂Cl₂/hexanes as eluent to yield crude pyrene-4,5-dihydroxy-9,10-dione (**2.18**) as a blood red solid *R_f*(20% EtOAc/Hexanes) = 0.4.

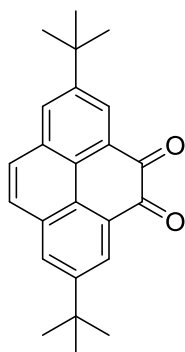
2-*tert*-Butylpyrene-4,5-dione (**2.14**)



To a solution of 2-*tert*-butylpyrene (25.0 g, 97.0 mmol) in CH₂Cl₂ (400 mL) and THF (400 mL) were added RuCl₃·3H₂O (2.59 g, 9.70 mmol). To the resulting dark brown solution *N*-methylimidazole (0.398 mg, 4.85 mmol) and H₂O (500 mL) were added. Over a 20-min period NaIO₄ (93.5 g, 437 mmol) was added in small portions. The slurry was stirred at room temperature for 2 h. The reaction contents were then suction filtered and the filtrate was stripped of solvent under reduced pressure. CH₂Cl₂ (500 mL) and H₂O (1500 mL) were added to dissolve the residue and the layers were separated. The aqueous phase was extracted with CH₂Cl₂ (2 × 200 mL) and the combined organic layers were washed with water (2 × 500 mL) to afford a dark orange solution which was dried over anhydrous Na₂SO₄ and the solvent was removed by rotary evaporator. The residue was adsorbed onto silica gel and subjected to flash chromatography (10 × 25 cm) using CH₂Cl₂ as eluent to yield 2-*tert*-butylpyrene-4,5-dione (**2.14**) as an orange solid (13.4, 48%): *R_f* (20% EtOAc/hexanes) = 0.4. ¹H NMR (CDCl₃, 300 MHz) 2.07 (d, *J* = 2.07 Hz, 1H), 8.44

(dd, $J = 1.27, 6.18$ Hz, 1H), 8.14 (dd, $J = 1.28, 4.96$ Hz, 1H), 8.14 (d, $J = 2.06$ Hz, 1H), 7.81 (s, 2H), 7.70 (t, $J = 7.85$ Hz, 1H), 1.49 (s, 9H) ppm; ^{13}C NMR (CDCl_3 , 75 MHz) 180.8, 151.6, 135.7, 132.2, 131.8, 130.0, 129.9, 128.5, 128.4, 127.6, 127.3, 127.0, 126.4, 35.26, 31.19 ppm. MS [APCI(+)] m/z (%): 311 ($[\text{M}+\text{Na}]^+$, 100); HRMS [APCI(+)] calcd for $\text{C}_{20}\text{H}_{16}\text{O}_2$ 288.1153, found: 288.1150.

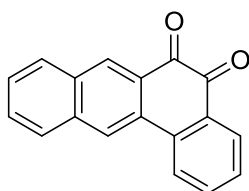
2,7-Bis(*tert*-butyl)pyrene-4,5-dione (**2.16**)



To a solution of 2,7-bis(*tert*-butyl)pyrene (25.0 g, 81.2 mol) in CH_2Cl_2 (350 mL) and THF (350 mL) were added $\text{RuCl}_3 \cdot 3\text{H}_2\text{O}$ (2.17 g, 8.11 mol). To the resulting dark brown solution *N*-methylimidazole (0.333 g, 4.06 mol) and H_2O (420 mL) were added. Over a 20-min period NaIO_4 (78.3 g, 365 mol) was added in small portions. The slurry was stirred at room temperature for 1.5 h. The reaction contents were then suction filtered and the filtrate was stripped of solvent under reduced pressure. CH_2Cl_2 (500 mL) and H_2O (1500 mL) were added to dissolve the residue and the layers were separated. The aqueous phase was extracted with CH_2Cl_2 (2×200 mL) and the combined organic layers were washed with water (2×500 mL) to afford a dark orange solution which was dried over anhydrous Na_2SO_4 and the solvent was removed by rotary evaporator. The residue was adsorbed onto silica gel and subjected to flash chromatography (10×25 cm) using CH_2Cl_2 as eluent to yield 2,7-di-*tert*-butylpyrene-4,5-dione (**2.16**) as an orange solid (12.1, 44%): R_f (20% EtOAc/hexanes) = 0.55. ^1H NMR (CDCl_3 , 300 MHz) 8.55 (d, $J = 2.05$ Hz, 2H), 8.12 (d, J

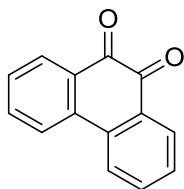
= 2.05 Hz, 2H), 7.80 (s, 2H), 1.49 (s, 18H) ppm; ^{13}C NMR (CDCl_3 , 75 MHz) 181.1, 151.09, 131.94, 131.78, 129.75, 128.37, 127.28, 126.48, 35.22, 31.21 ppm. MS [APCI(+)] m/z (%): 367 ($[\text{M}+\text{Na}]^+$, 100); HRMS [APCI(+)] calcd for $\text{C}_{24}\text{H}_{24}\text{O}_2$ 344.1777, found: 344.1776.

Benz[*a*]anthracene-5,6-dione (**2.22**)



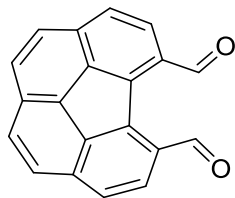
To a solution of benz[*a*]anthracene (0.103 g, 0.438 mmol) in CH_2Cl_2 (5 mL) and THF (5 mL) were added $\text{RuCl}_3 \cdot 3\text{H}_2\text{O}$ (12.0 mg, 0.043 mmol). To the resulting dark brown solution *N*-methylimidazole (0.181 mg, 0.022 mmol) and H_2O (7 mL) were added. Over a 20-min period NaIO_4 (421 mg, 1.97 mmol) was added in small portions. The slurry was stirred at room temperature for 2 h. The reaction contents were then suction filtered and the filtrate was stripped of solvent under reduced pressure. CH_2Cl_2 (25 mL) and H_2O (100 mL) were added to dissolve the residue and the layers were separated. The aqueous phase was extracted with CH_2Cl_2 (2×25 mL) and the combined organic layers were washed with water (2×100 mL) to afford a dark orange solution which was dried over anhydrous Na_2SO_4 and the solvent was removed by rotary evaporator. The residue was adsorbed to silica gel and subjected to flash chromatography (3×15 cm) using CH_2Cl_2 as eluent to yield benz[*a*]anthracene-5,6-dione (**2.22**) as orange needles. (63.5 mg): R_f (20% EtOAc/hexanes) = 0.35.

Phenanthrene-9,10-dione (2.24)



To a solution of phenanthrene (2.03 g, 11.2 mmol) in CH₂Cl₂ (90 mL) and THF (90 mL) were added RuCl₃·3H₂O (300 mg, 1.12 mmol). To the resulting dark brown solution *N*-methylimidazole (46.1 mg, 0.561 mmol) and 110 mL H₂O were added. Over a 20-min period NaIO₄ (10.8 g, 50.5 mmol) was added in small portions. The slurry was stirred at room temperature for 2 h. The reaction contents were then suction filtered and the filtrate was stripped of solvent under reduced pressure. CH₂Cl₂ (50 mL) and H₂O (100 mL) were added to dissolve the residue and the layers were separated. The aqueous phase was extracted with CH₂Cl₂ (2 × 50 mL) and the combined organic layers were washed with water (2 × 100 mL) to afford a dark orange solution which was dried over anhydrous Na₂SO₄ and the solvent was removed by rotary evaporator. The residue was adsorbed to silica gel and subjected to flash chromatography (3 × 15 cm) (dichloromethane) to yield phenanthrene-9,10-dione (**2.24**) as a yellow solid. (1.12 g, 48%): *R*_f(10% EtOAc/hexanes) = 0.45.

Benzo[ghi]fluoranthene-5,6-dicarboxaldehyde (2.26)



To a solution of corannulene (0.499 g, 2.00 mmol) in CH₂Cl₂ (10 mL) and THF (10 mL) were added RuCl₃·3H₂O (53.4 mg, 0.200 mmol). To the resulting dark brown solution *N*-methylimidazole (8.20 mg, 0.100 mmol) and H₂O (12.5 mL) were added. Over a 20-min period NaIO₄

(1.92 g, 8.99 mol) was added in small portions. The slurry was stirred at room temperature for 2.5 h. The reaction contents were then suction filtered and the filtrate was stripped of solvent under reduced pressure. CH₂Cl₂ (100 mL) and H₂O (100 mL) were added to dissolve the residue and the layers were separated. The aqueous phase was extracted with CH₂Cl₂ (2 × 100 mL) and the combined organic layers were washed with water (2 × 100 mL) to afford a dark orange solution which was dried over anhydrous Na₂SO₄ and the solvent was removed by rotary evaporator. The residue was adsorbed to silica gel and subjected to flash chromatography (3 × 15 cm) using 50% CH₂Cl₂/hexanes as eluent to yield benzo[ghi]fluoranthene-5,6-dicarboxaldehyde (**2.26**) as a yellow solid. (106 mg, 19%): *R_f*(75% CH₂Cl₂/hexanes) = 0.40, ¹H NMR (CDCl₃, 300 MHz) 10.7 (s, 2H), 8.14 (d, *J* = 8.4 Hz, 2H), 8.07 (d, *J* = 8.4 Hz, 2H), 8.00 (d, *J* = 8.7 Hz, 2H), 7.96 (d, *J* = 8.7 Hz, 2H) ppm. MS [APCI(+)] *m/z* (%): 283 ([M+H]⁺, 100); HRMS [APCI(+)] calcd for C₂₀H₁₀O₂ 282.0681, found: 282.0678.

2.4 References

- [1] M. Kastler, J. Schmidt, W. Pisula, D. Sebastiani, K. Müllen, *J. Am. Chem. Soc.*, **2006**, 128 (29), 9526-9534.
- [2] R. G. Harvey, *Polycyclic Aromatic Hydrocarbons: Chemistry and Carcinogenicity*; Cambridge University Press: New York, 1991.
- [3] M. J. S. Dewar, *J. Am. Chem. Soc.*, **1952**, 74, 3357-3363.
- [4] R. Wendland, J. LaLonde, *Org. Synth.*, **1954**, 34, 76-79.

- [5] H. Vollmann, H. Becker, M. Streeck, G. Langbein, *Liebigs Ann.*, **1937**, 531, 1-159.
- [6] R. G. Harvey, S. H. Goh, C. Cortez, *J. Am. Chem. Soc.*, **1975**, 97, 3468-3479.
- [7] H. Cho, R. G. Harvey, *Tetrahedron Lett.*, **1974**, 15 (16), 1491-1494.
- [8] J. Hu, D. Zhang, F. W. Harris, *J. Org. Chem.*, **2005**, 70, 707-708.
- [9] G. Venkataramana, P. Dongare, L. Dawe, D. Thompson, Y. Zhao, G. J. Bodwell, *Org. Lett.* **2011**, 13, 2240-2243.
- [10] J. Rudolph, K. L. Reddy, J. P. Chiang, K. B. Sharpless, *J. Am. Chem. Soc.*, **1997**, 119, 6189-6190.
- [11] K. Tabatabaeian, E. Keshavarz, M. Mamaghani, N. O. Mahmoodi, *Arkivoc*, **2010**, 9, 155-162
- [12] D. W. Nelson, A. Gypser, P. T. Ho, H. C. Kolb, T. Kondo, H. L. Kwong, D. V. McGrath, A. E. Rubin, P. O. Norrby, K. P. Gable, K. B. Sharpless, *J. Am. Chem. Soc.*, **1997**, 119, 1840-1858.

Chapter Three

Progress toward a 2,7-Pyrenylene-ethynylene Macrocycle

3.1 Introduction

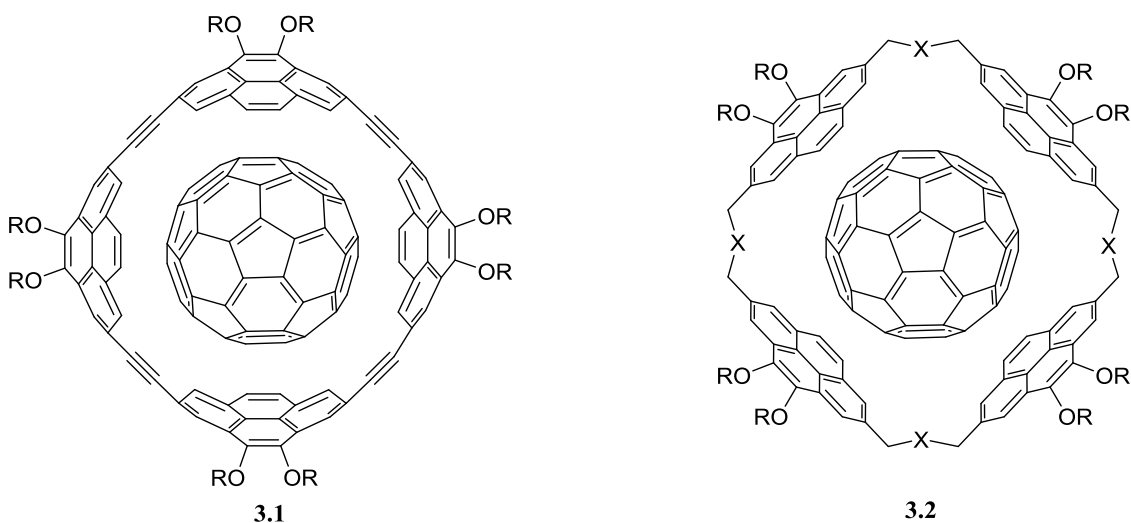


Figure 3.1 Synthetic targets of this work.

As described in Chapter 1, the Bodwell group reported the synthesis of two pyrenylene-ethynylene macrocycles (Scheme 1.4) in 2011.^[1] These pyrenylene-ethynylene macrocycles both featured a (1,8) substitution pattern. The 60° angle formed by the bonds emanating from the 1 and 8 positions means that the (1,8) substitution pattern can be viewed as a *pseudo-ortho* motif. As in the case of benzene, this corresponds to a 120° turn in a macrocyclic system, and thus also, cyclic trimer **1.20** was found to be planar, whereas cyclic tetramer **1.25** was tub-shaped, like cyclooctatetraene. The pyrenylene-ethynylene macrocycles of interest in this Chapter have pyrene systems

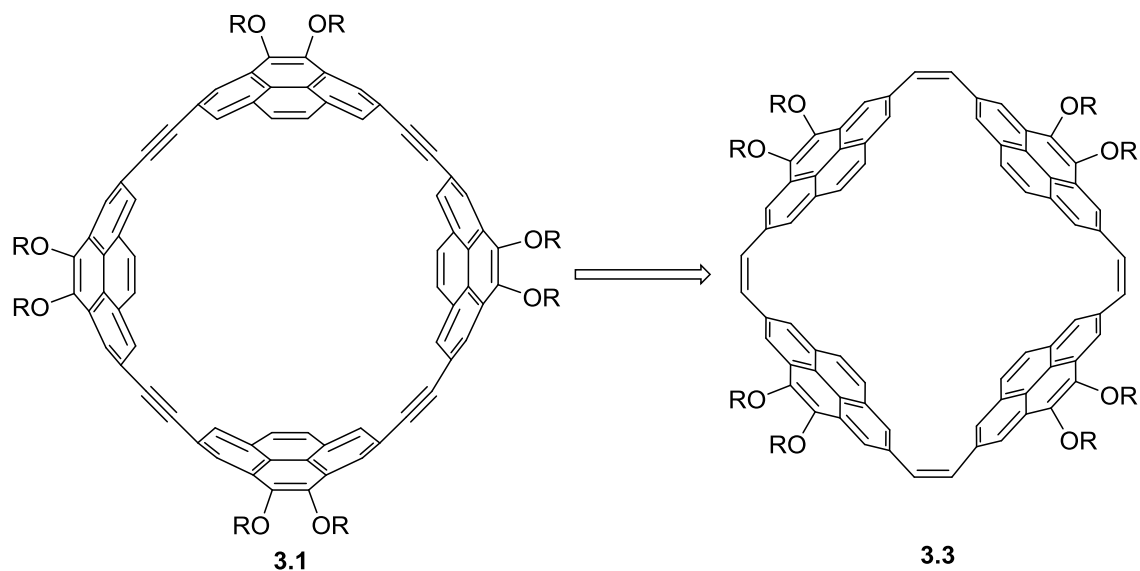
that are connected through the 2 and 7 positions, which is a *pseudo*-para motif (0° turn). Consequently, they would be expected to possess a significant amount of ring strain. Target **3.1** is of interest from both a theoretical and practical point of view. What immediately stands out is the possibility that it would form host-guest type supramolecular inclusion complexes with fullerenes such as C_{60} . Not only would the shape of the macrocycle complement the shape of C_{60} , but the electron-rich concave surface of the macrocycle (especially the bent pyrene systems) would be an electronic match for the electron deficient convex exterior of the fullerenes. This would only be made stronger by the eight π -donating alkoxy groups flanking the macrocycle.^[2] The alkoxy groups would also serve as solubilizing groups throughout the entire synthetic sequence. Furthermore, it is conceivable that they could ultimately play a much more important role as sites for the incorporation of switchable functional groups, which could be used to control the uptake and release of guests.

Kawase *et al.* observed a non-linear relationship between the π -surface area and association constants in their ring-in-ring CPPE complexes. In going from the [9]CPPE \supset [6]CPPE complex to the tribenzo[9]CPPE \supset dibenzo[6]CPPE complex, there is a 33% increase in the surface area of the π -systems, but a 10-fold increase in the apparent association constant. Clearly, the surface area of the π -system plays a large part in the stability of these complexes. Consequently, it seems reasonable to expect that the presence of four pyrene systems in **3.1** would provide an environment for the formation of strong complexes with appropriately-sized fullerenes. Indeed, pyrene has long been known to exhibit strong π -stacking behavior with a wide variety of π -systems in solution,

Such behaviour has been utilized widely across the chemical and biological fields.^[3] Its interaction with fullerenes and nanotubes is stronger still. Nanotubes suspended in pyrene solutions show the FTIR bands of pyrene shifted to lower wavenumbers and the G-bands present in the nanotubes' Raman spectra also similarly shifted proving the pyrene-nanotube interaction is stronger than the interaction seen in pyrene dimers.^[4]

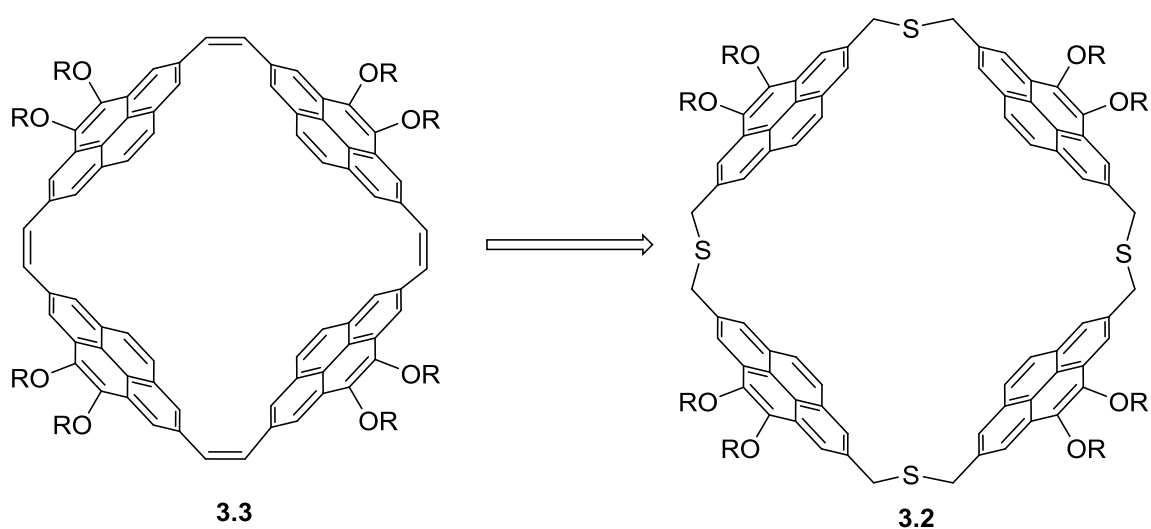
Based on discussions with Dr. Haruka Omachi, an Associate Professor in the Shinohara group at Nagoya University, Japan, some of the late-stage intermediates in the proposed synthesis (*vide infra*) of the pyrenylene-ethynylene macrocycle **3.1** are also very attractive targets. In particular, cyclophanetetraene **3.3** and tetrathiacyclophane **3.2** would also be promising candidates for the encapsulation of fullerenes, but the differences in their cavity sizes might cause them to show selectivity for different fullerenes than pyrenylene-ethynylene macrocycle **3.1**. Thus, the initial objective of the work described in this Chapter was to synthesize the tetrathiacyclophane **3.2** and to then make progress toward the larger goal of the 2,7-pyrenylene-ethynylene macrocycle, **3.1**.

3.2 Retrosynthetic analysis



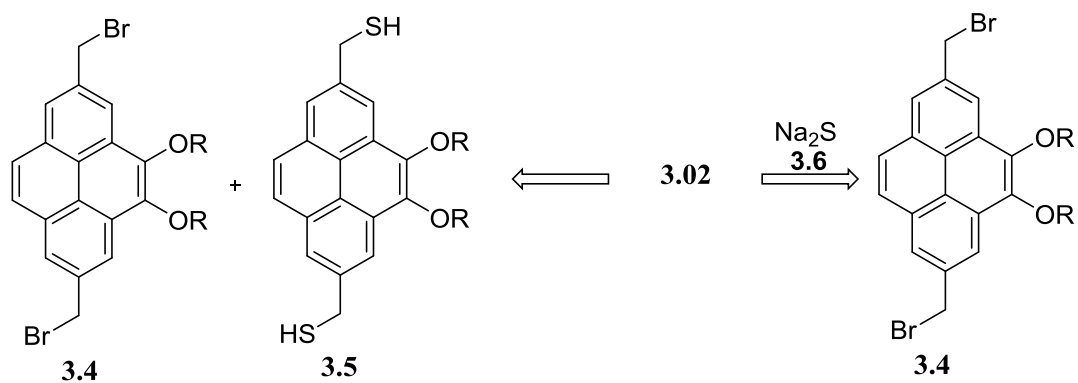
Scheme 3.1 Retrosynthetic analysis of 2,7-pyrenylene-ethynylene macrocycle (**3.1**).

The retrosynthetic analysis of 2,7-pyrenylene-ethynylene macrocycle **3.1** begins with a step back to the corresponding cyclophanetetraene **3.3**. Although alkyne metathesis has been utilized with great success in the synthesis of many shape-persistent macrocycles,^[5] it has never been used in the synthesis of a highly strained target like **3.1**. Accordingly, a bromination/double dehydrohalogenation protocol that has been employed in the vast majority of known arylene-ethynylene macrocycles with significant strain energy (*e.g.* the CPPAs) was envisioned.^[6] Cyclophanetetraene would be the expected product of a thia-Hofmann elimination/Stevens rearrangement sequence starting from tetrathiacyclophane **3.2**.

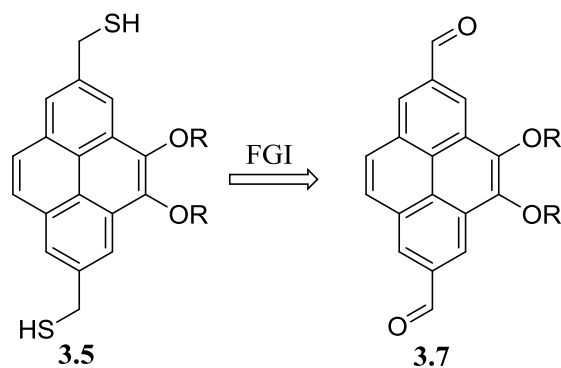


Scheme 3.2 Retrosynthetic analysis of cyclophanetetraene (**3.3**)

Thiacyclophanes have been traditionally made in two ways, which differ in the sets of products they can deliver. Thiol-bromide coupling, *e.g.* **3.4** and **3.5**, will necessarily give macrocycles with an even number of subunits, while sodium sulphide **3.6** mediated macrocyclization, *e.g.* with dibromide **3.4**, has no such restriction. Of course, neither approach was ruled out at this point because both could potentially afford the desired cyclic tetramer. Although the cyclic tetramer was the main compound of interest, other cyclic oligomers would also be worth having.

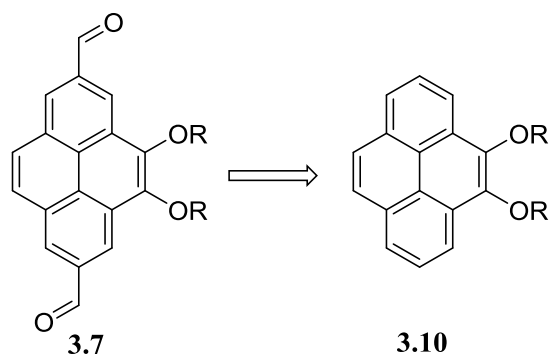


Scheme 3.3 Continued retrosynthetic analysis of tetrathiacyclophane (3.2)



Scheme 3.4 Retrosynthetic analysis of dithiol (3.5)

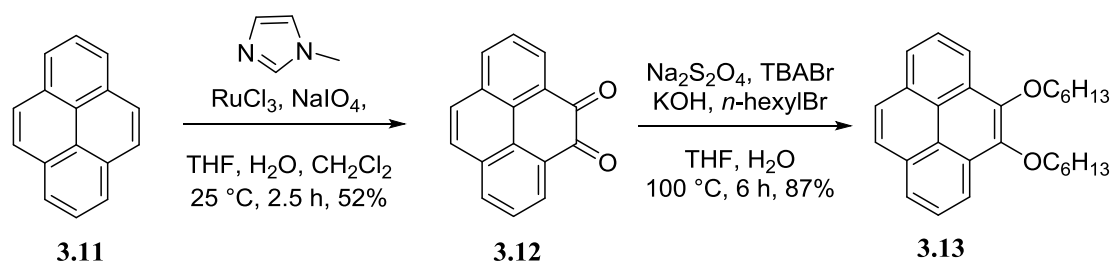
Subsequent functional group interconversions of (3.5) leads to 2,7-pyrenedialdehyde (3.7). Reductive alkylation transform can be taken back to pyrene-4,5-dione according to known reactions within the Bodwell group. Retro-*K*-region oxidation affords pyrene.



Scheme 3.5 Retrosynthetic analysis of dialdehyde (**3.7**)

3.3 Results and Discussion

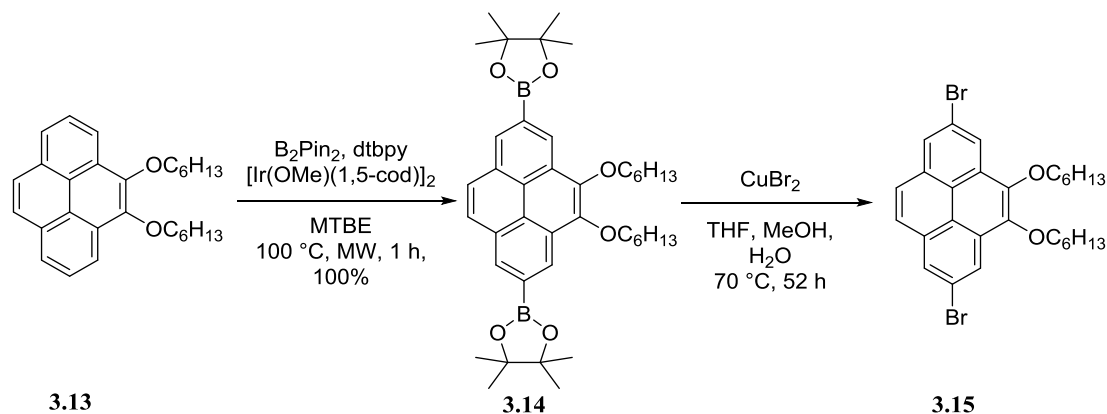
The first step in the synthesis undertaken was the oxidation of pyrene (**3.11**) a relatively cheap starting material owing to its natural abundance (2%) in coal tar. As discussed in Chapter 2, this reaction, which has been used heavily within the Bodwell group, was recently improved through the addition of 5% NMI. With ready access to synthetically-useful amounts of diketone (**3.12**), it was reduced with $\text{Na}_2\text{S}_2\text{O}_4$ and alkylated with 1-bromohexane to provide 4,5-dihexoxy pyrene **3.10** in 85% yield. An important reason for introducing the alkoxy groups was to promote solubility throughout the synthesis. Since functionality at the 2 and 7 positions was required, **3.10** was subjected to the C-H activation borylation reaction developed by Marder.^[7] Surprisingly, there appeared to be no conversion under the published reaction conditions (tlc analysis).



Scheme 3.6 Synthesis of building block **3.13**

The use of solvents other than cyclohexane was then screened (toluene, hexanes, THF and benzene), but still no conversion was observed. Four years after his original publication on the Ir-catalysed borylation, Marder published a one-pot borylation/Suzuki-Miyaura coupling utilizing methyl *tert*-butyl ether as the solvent.^[8] It was speculated that the solvent was sufficiently coordinating to allow the Suzuki-Miyaura coupling to take place, but not coordinating enough to prevent inactivation of the iridium catalyst for the borylation. Fortunately, the use of methyl *tert*-butyl ether as the reaction solvent for the borylation of **3.10** produced the desired product **3.14**. The crude mixture was very “clean” by ¹H NMR analysis and the crude yield was essentially quantitative. Attempts to purify the product by silica gel chromatography led to significant product loss and a decrease in the purity of the product (¹H NMR analysis). Attempted crystallizations were unsuccessful, which supports the notion that the alkoxy groups are excellent solubilizing groups. Consequently, the crude product was used directly in subsequent steps. Following Hartwig’s *ipso*-bromination procedure (CuBr₂ in 1:1 methanol:water),^[9] an attempt was made to convert crude **3.14** into dibromide **3.15**. However two problems were encountered. First, since diborylpyrene **3.14** has two boronate groups, doubling the

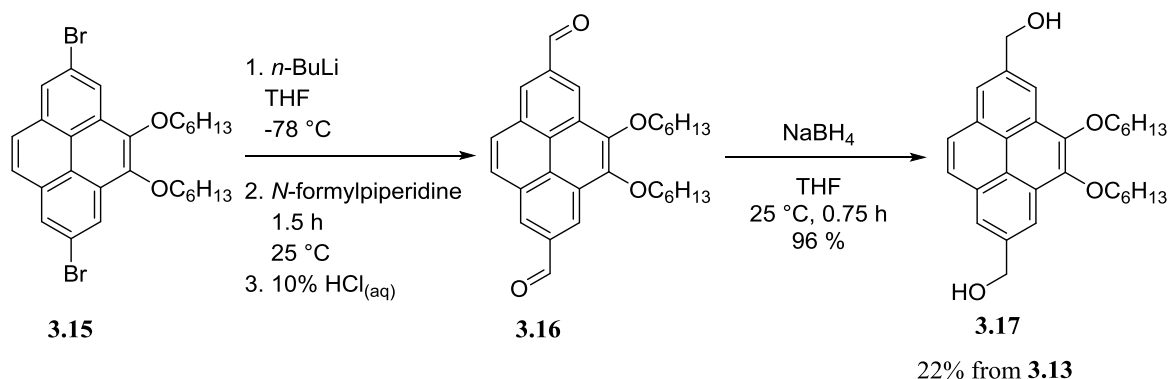
number of molar equivalents of CuBr_2 were required, and this meant that the volume of solvent also had to be doubled. The reason for this is to prevent the formation of the tetrabromocuprate (II) ion that dominates in solution under high bromide concentration and is not a reactive towards boronate esters. Secondly, even under the relatively high-dilution conditions, the starting material **3.14** appeared to be completely insoluble. In any event, the initial result was negligible conversion and significant proto-deborylation. To improve the solubility of **3.14**, a three-solvent system (THF/MeOH/ H_2O , 1:1:1) was employed. Under these conditions, the required dibromide **3.15** was obtained as the major product in an inseparable 5:1 mixture with the corresponding monobromide.



Scheme 3.7 Synthesis of building block **3.15**.

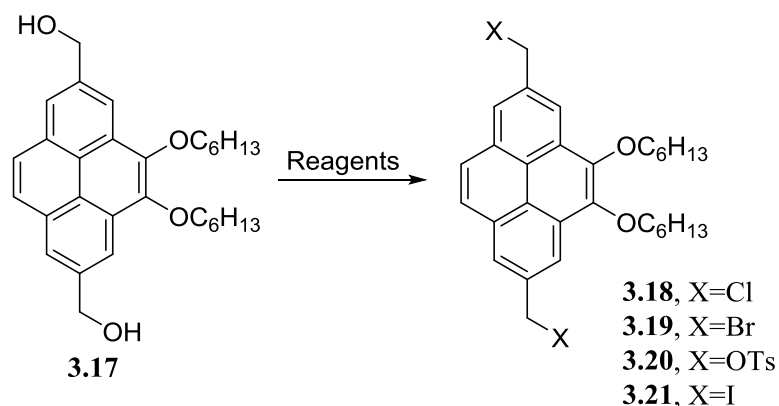
Treatment of this mixture with eight equivalents of *n*-butyllithium followed by *N*-formylpiperidine gave rise to a mixture of dialdehyde **3.16** and the monoaldehyde, which could be separated by silica gel chromatography. The increase in the proportion of the monofunctionalized by-product is likely due to it being a product of both formylation of monobromide impurity and of partial quenching of the dilithiated species produced in the

reaction of dibromide **3.15** with butyl lithium. DMF could also be used as a source of ^+CHO , but the work-up required extensive washing to remove all of the DMF before purification by column chromatography.



Scheme 3.8 Synthesis of building block (**3.17**).

Reduction of dialdehyde **3.16** using sodium borohydride in THF afforded bis(hydroxymethyl)pyrene **3.17** (22% from **3.13**). With this diol in hand, several attempts were made to make an activated species for cyclization. However, this proved to be problematic. First, bromination was attempted using PBr₃, but a complex mixture of products was obtained, which only became more intractable when subjected to attempted purification. The use of concentrated HBr gave similar results. While pyrene is an electron-rich aromatic system and it bears two electron-donating alkoxy groups, it seemed very likely that the benzylic bromides were especially labile. Not surprisingly, attempted tosylation (reagents) and iodination (reagents) were also unsuccessful, presumably for the same reasons.



Scheme 3.9 Attempted synthesis of various electrophiles (**3.18-3.21**).

With the intention of stabilizing the system through the introducing a poorer leaving group, chlorination of diol **3.17** was attempted. Under Appel conditions (CCl_4 , PPh_3), diol **3.17** was completely unreactive. The use of concentrated aqueous HCl appeared to yield traces of the desired dichloride **3.18** (tlc analysis), but it also proved to be unstable under normal purification conditions, yielding several new compounds along with the starting material (tlc analysis). Chlorination using thionyl chloride yielded better results. The reaction yielded the desired dichloride (**3.18**) as a major product among a mixture of compounds (tlc, ^1H NMR analysis). As before, attempted purification of dichloride **3.18** resulted in the formation of intractable mixtures.

Due to the problems associated with purifying dichloride **3.18**, the use of the crude product to generate thiacyclophanes upon treatment with Na_2S was investigated on a small scale (25 mg of **3.18**). Some new mobile spots were observed by tlc and the reaction mixture was subjected to preparative thin layer chromatography. Unfortunately,

LC-MS analysis showed that none of them had the mass of the desired tetrathiacyclophane **3.2** or any higher or lower cyclic homologues.

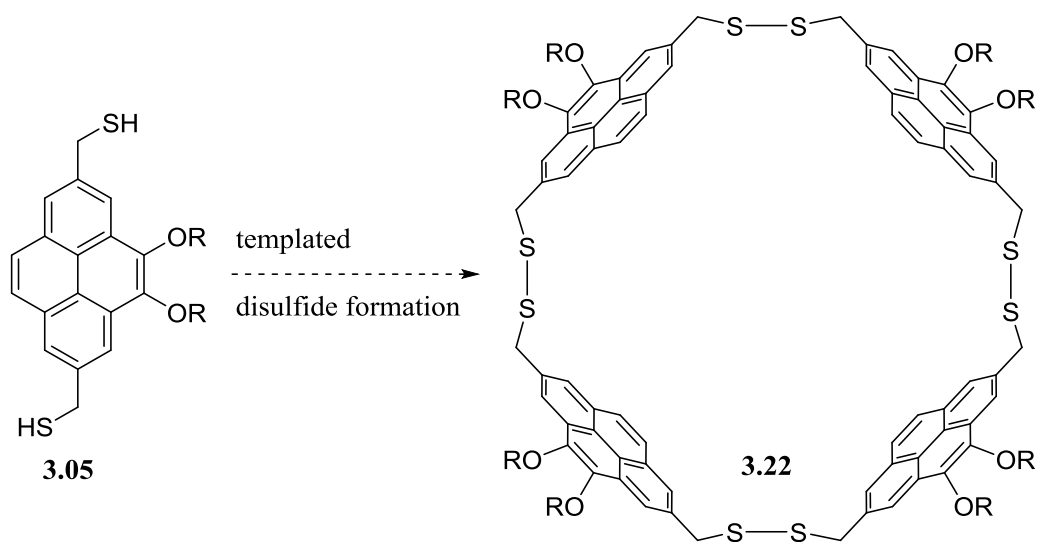
3.4 Conclusion and Future Work

In this chapter the synthesis of an advanced precursor to tetrathiacyclophane was conducted in 10% overall yield from pyrene in six steps. Unfortunately the required macrocyclization to achieve the desired tetrathiacyclophane has not yet been successful.

In the attempted synthesis of tetrathiacyclophane (**3.2**), the apparent high reactivity of electrophilic **3.17** derivatives is a major problem. The inherently electron-rich pyrene core further enhanced by two alkoxy donating groups could simply provide too stable a carbocation. It is worth noting that the ethanol-dichloromethane cosolvent employed in the sulfide coupling reactions could be an unsurmountable problem. If in fact the failed reactions are a result of the high stability of the resulting dialkoxypyrenylic cation the large excess of ethanol compared to sulfide could be quenching the electrophile. This problem spans a wide variety of leaving group ability (Cl to *p*-tosyl) however, weaker leaving groups are well known (*e.g.* acetate).

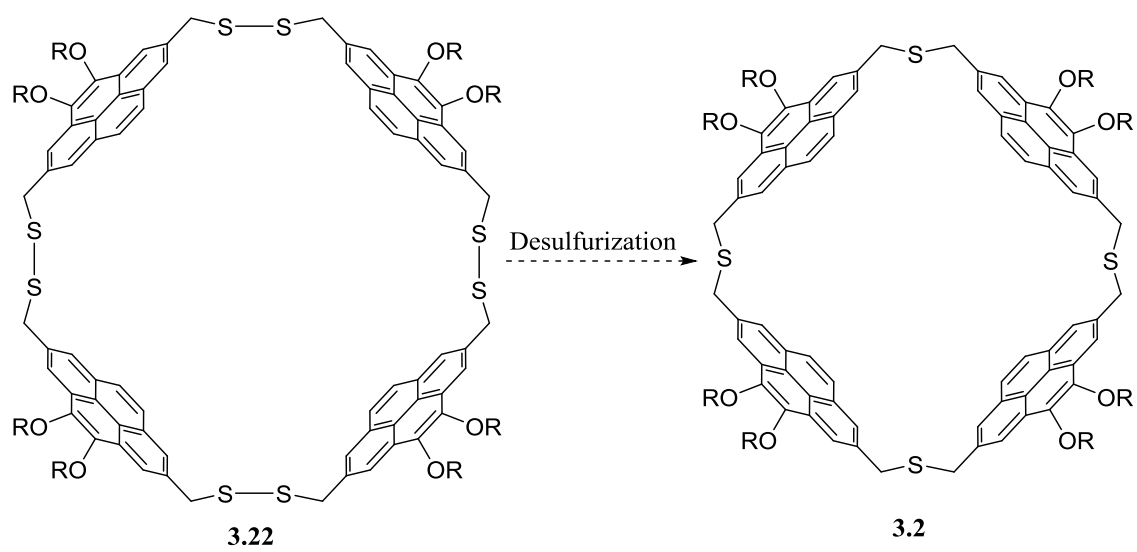
There are some possible synthetic routes accessible from the dihydroxymethylpyrene precursor (**3.17**) bypassing the sodium sulfide coupling stage as the required 2,7-dihalomethylpyrenes are not well behaved compounds (*vide supra*). One possibility is to produce a dithiol (**3.5**) directly from (**3.17**) utilizing the Mitsunobu reaction of hydrogen sulfide. The pKa of 7.0 hydrogen sulfide is well below the required

acidity to generate a useful nucleophile in the reaction. Taking advantage of the dynamic covalent nature of disulfide bond formation ^[10] a templated approach could have a good chance of yielding macrocycles like (**3.22**). There are numerous reported methods for the desulfurization of disulfides yielding thioethers, utilizing one of these methods could



Scheme 3.10 Synthesis of disulfide containing macrocycle (**3.22**).

yield thiacyclophane (**3.2**).^[11-14] This method has several advantages over the current synthetic route as the template approach coupled with dynamic covalent bond forming could open the route to other macrocycles (dimer, trimer) allowing a divergent synthesis from the precursor presented in this work.



Scheme 3.11 Desulfurization revealing the target tetrathiacyclophane (3.2).

3.5 Experimental section

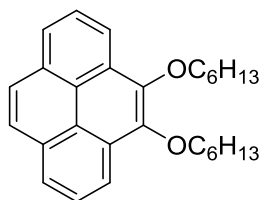
All chemicals utilized in this chapters work were used as received from commercial chemical suppliers (Aldrich, Alfa Aesar, TCI, Matrix Scientific and Precious Metals Online) All reactions were performed without an inert atmosphere unless otherwise indicated. THF was dried over activated 4 Å molecular sieves for 24 h prior to use. Hexanes were distilled before use in column chromatography. Methyl *tert*-butyl ether was subjected to three freeze-pump-thaw cycles before use. Flash chromatography was performed using ZEOChem 60 eco 40-63 μ. Compounds on TLC plates were visualized with UV light (254 and 365 nm) and chemical staining methods (phosphomolybdic acid, 2,4-dinitrophenylhydrazine and iodine).

Instrumentation:

Melting points were measured on an OPTImelt automated melting point system and are uncorrected, recrystallization solvents given in brackets (where applicable). ¹H NMR (300 MHz) and ¹³C NMR (75 MHz) were recorded on a Bruker AVANCE III instrument (CDCl₃, unless otherwise indicated). Chemical shifts are reported relative to internal standards: Me₄Si (δ 0.00 ppm) and CDCl₃ (δ 77.23 ppm). ¹H NMR data are presented as follows: chemical shift, multiplicity (s=singlet, d=doublet, t=triplet, q=quartet, m= multiplet, brs=broad singlet, dd=doublet of doublets), coupling constant (*J* in Hz), integration (number of ¹H). IR spectra were obtained using a Bruker TENSOR 27 FTIR. Low-resolution mass spectra (MS) were taken on LC/MSD (Trap) Agilent 1100 series SL. High resolution mass spectra (HRMS) of some compounds were obtained

using a Waters Micromass GCT premier instrument. MS data are presented as follows: m/z (relative intensity), assignment (when appropriate), calculated mass for corresponding molecular formula. UV-vis and fluorescence spectra were recorded using Agilent HP8453A UV-Visible absorbance spectrophotometer and PTI QuantaMaster 6000 spectrofluorometer.

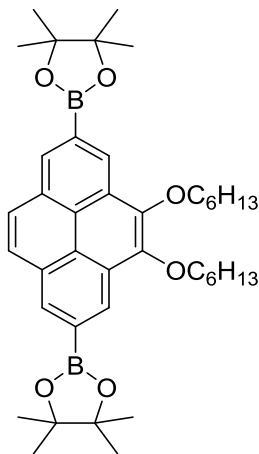
4,5-Dihexoxyppyrene (2.17)



To a suspension of pyrene-4,5-dione (2.00 g, 8.64 mmol) in THF (100 mL) and H₂O (100 mL) was added tetra-*n*-butylammonium bromide (0.835 g, 2.59 mmol) and Na₂S₂O₄ (4.51 g, 25.9 mmol). The reaction was stirred for 5 minutes at room temperature. KOH_(aq) (3.88 g, 69.1 mmol in H₂O (25 mL)) was added to the reaction mixture followed by 1-bromohexane (5.71 g, 34.6 mmol). The deep orange solution was refluxed for 6 h. The reaction was extracted with EtOAc (100 mL). The layers were separated and the aqueous phase was extracted with EtOAc (2 × 50 mL). The combined EtOAc extracts were washed with water (300 mL). The organic phase was dried over Na₂SO₄ and the solvent removed under reduced pressure to yield a brown oil. The crude product was subjected to column chromatography using 10% CH₂Cl₂/hexanes as eluent to yield 4,5-dihexoxyppyrene (3.02 g, 87%) as a pale yellow solid. R_f (10% CH₂Cl₂/hexanes) = 0.30: mp: 40- 45 °C.; ¹H NMR (CDCl₃, 300 MHz) δ 8.46 (dd, *J* = 6.2, 1.3 Hz, 2H), 8.15 (dd, *J* = 6.7, 1.3 Hz, 2H), 7.83 (s, 2H), 7.74 (t, *J* = 7.5 Hz, 2H) ppm; ¹³C NMR (CDCl₃, 75 MHz) δ 180.4, 135.7,

132.0, 130.2, 130.1, 128.4, 128.0, 127.3 ppm. MS [ESI(+)] m/z (%): 402 ($[M]^+$, 100); HRMS [APCI(+)] calcd for $C_{28}H_{34}O_2$ 402.2559, found: 402.2541.

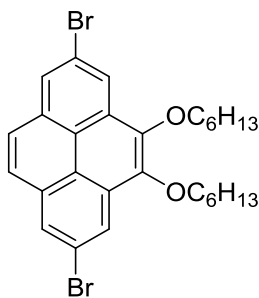
2,7-(4,5-Dihexoxyppyrenylene)bis[4,4,5,5-tetramethyl-1,3,2-dioxaborolane] (3.14)



To a solution of 4,5-dihexoxyppyrene (802 mg, 19.9 mmol) in anhydrous methyl *tert*-butyl ether (4.80 ml) in a 10 mL microwave vial was added B_2Pin_2 (1.02 g, 39.8 mmol), 4,4'-di-*tert*-butyl-2,2'-dipyridyl (48.0 mg, 0.177 mmol) and $[Ir(OMe)(COD)]_2$ (39.6 mg, 0.059 mmol). The headspace was flushed with dry N_2 and the flask was capped. The reaction was subjected to microwave irradiation for 1 h at 80 ° C. Solvent was removed under reduced pressure to

yield crude 2,7-(4,5-dihexoxyppyrenylene)bis[4,4,5,5-tetramethyl-1,3,2-dioxaborolane] as a brown solid. R_f (10% EtOAc/hexanes) = 0.35; 1H NMR ($CDCl_3$, 300 MHz) δ 8.92 (d, J = 0.89 Hz, 2H), 8.56 (d, J = 0.93 Hz, 2H), 8.05 (s, 2H), 4.35 (t, J = 6.55 Hz, 4H), 1.98 (m, 4H), 1.68 (m, 4H), 1.44 (s, 24H), 0.95 (m, 6H) ppm; MS [APCI(+)] m/z (%): 655 ($[M+H]^+$, 100).

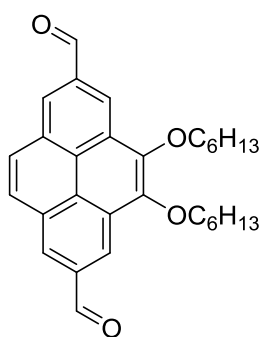
2,7-Dibromo-4,5-dihexoxyppyrene (3.15)



To a solution of 2,7-(4,5-dihexoxyppyrenylene)bis[4,4,5,5-tetramethyl-1,3,2-dioxaborolane] (1.60 g, 2.45 mmol) in THF (240 mL) was added methanol (240 mL), H_2O (240 mL) and $CuBr_2$ (3.28 g, 14.7 mmol). The turquoise solution was brought to

vigorous reflux for 52 h. Organic solvents were removed under reduced pressure. The reaction mixture was extracted with chloroform (2×100 mL) and the combined organic layers were washed with H_2O (200 mL). The organic phase was dried over Na_2SO_4 and the solvent removed under reduced pressure yielding a brown solid. The crude product was subjected to column chromatography using 15% CH_2Cl_2 /hexanes as eluent to yield 2,7-dibromo-4,5-dihexoxyppyrene along with 2-bromo-4,5-dihexoxyppyrene as a cream colored solid. R_f (20% CHCl_3 /hexanes) = 0.55; MS [APCI(+)] m/z (%): 561 ($[\text{M}+\text{H}]^+$, 100).

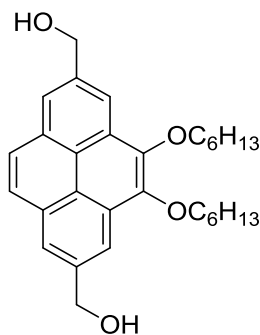
4,5-Dihexoxy-2,7-pyrenedicarboxaldehyde (3.7)



To a -78 °C nitrogen purged solution of crude 2,7-dibromo-4,5-dihexoxyppyrene (444 mg) in anhydrous THF (75 mL) $n\text{-BuLi}$ (6 mL (1.30 M), 6.34 mmol) was added dropwise. The reaction was allowed to stir at -78° C for 5 minutes. N -formyl piperidine (1.62g, 14.3 mmol) was added and the dry ice acetone bath removed. The reaction mixture was allowed to warm to room temperature and stirred for a further 1.5 h. The reaction was quenched with 10% $\text{HCl}_{(\text{aq})}$ (25 mL) and the organic solvents were removed under reduced pressure. The reaction mixture was extracted with CH_2Cl_2 (2×50 mL). The combined organic layers were washed with 10% $\text{HCl}_{(\text{aq})}$ (5×200 mL) and subsequently dried over Na_2SO_4 . Solvent was removed under reduced pressure to yield crude 4,5-dihexoxy-2,7-pyrenedicarboxaldehyde as a dark orange oil. The crude product was subjected to column chromatography using 50% CH_2Cl_2 /hexanes as eluent to yield 4,5-dihexoxy-2,7-pyrenedicarboxaldehyde as a canary yellow solid. R_f (50% CHCl_3 /hexanes) =

0.30; ^1H NMR (CDCl_3 , 300 MHz) δ 10.5 (s, 2H), 8.99 (d, $J = 1.4$ Hz, 2H), 8.65 (d, $J = 1.5$ Hz, 2H), 8.22 (s, 2H), 4.39 (t, $J = 6.7$ Hz, 4H), 1.99 (m, 4H), 1.64 (m, 4H), 1.43 (m, 8H), 0.94 (m, 6H) ppm; MS [APCI(+)] m/z (%): 459 ($[\text{M}+\text{H}]^+$, 100). HRMS [APCI(+)] calcd for $\text{C}_{30}\text{H}_{34}\text{O}_4$ 458.2471, found: 458.2467.

2,7-Bis(hydroxymethyl)-4,5-dihexoxyppyrene



To a solution of 4,5-dihexoxyppyrene-2,7-dialdehyde (0.25 g, 0.545 mmol) in THF (50 mL) NaBH_4 (0.082 g, 2.18 mmol) was added. The solution was allowed to stir for 3 h at room temperature. The solvent was removed under reduced pressure. H_2O (50 mL) and EtOAc (50 mL) was added and the layers separated. The aqueous phase was extracted with EtOAc ($3 \times 25\text{mL}$). The combined organic layers were dried over Na_2SO_4 and the solvent removed under reduced pressure yielding crude 2,7-bis(hydroxymethyl)-4,5-dihexoxyppyrene as a brown solid. The crude product was subjected to preparative thin layer chromatography using 20% THF/hexanes as eluent to yield 2,7-bis(hydroxymethyl)-4,5-dihexoxyppyrene as a white waxy solid (242 mg, 96%). R_f (30% EtOAc / hexanes) = 0.20; ^1H NMR (CDCl_3 , 300 MHz) δ 8.45 (d, $J = 1.3$ Hz, 2H), 8.13 (d, $J = 1.3$ Hz, 2H), 8.02 (s, 2H), 5.15 (s, 4H), 4.3 (t, $J = 6.7$ Hz, 4H), 1.98 (m, 4H), 1.64 (m, 4H), 1.43 (m, 8H), 0.91 (m, 6H) ppm; ^{13}C NMR (CDCl_3 , 75 MHz) δ 144.31, 138.76, 131.32, 129.12, 127.57, 122.83, 122.24, 118.04, 66.13, 31.76, 30.54, 26.02,

25.40, 22.71, 14.30 ppm. MS [APCI(+)] m/z (%): 445 ($[M+H - H_2O]^+$, 100); HRMS [APCI(+)] calcd for $C_{30}H_{38}O_4$ 462.2770, found: 462.2762.

3.6 References

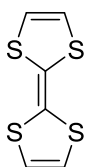
- [1] G. Venkataramana, P. Dongare, L. Dawe, D. Thompson, Y. Zhao, G. J. Bodwell, *Org. Lett.* **2011**, 13 (9), 2240-2243.
- [2] T. Kawase, H. Kurata, *Chem. Rev.*, **2006**, 106 (12), 5250-5273.
- [3] J. Duhamel, *Langmuir*, **2012**, 28, 6527-6538.
- [4] Y. Zhang, S. Yuan, W. Zhou, J. Xu, Y. Li, *J. Nanosci. Nanotechnol.*, **2007**, 7 (7), 2366-2375.
- [5] W. Zhang, J. S. Moore, *Angew. Chem. Int. Ed.*, **2006**, 45, 4416-4439.
- [6] T. Kawase, H. R. Darabi, M. Oda, *Angew. Chem.*, 1996, 108, 458-462.
- [7] D. N. Coventry, A. S. Batsanov, A. E. Goeta, J. A. K. Howard, T. B. Marder, R. N. Perutz, *Chem. Commun.*, **2005**, 2172-2174.
- [8] P. Harrison, J. Morris, P. G. Steel, T. B. Marder, *Synlett*, **2009**, 1, 147-150.
- [9] J. M. Murphy, X. Liao, J. H. Hartwig, *J. Am. Chem. Soc.*, **2007**, 129, 15434-1443
- [10] S. J. Rowan, S. J. Cantrill, G. R. L. Cousins, J. K. M. Sanders, J. F. Stoddart, *Angew. Chem. Int. Ed.* **2002**, 41, 898-952
- [11] S. Antebi, H. Alper, *Tetrahedron Lett.*, 1985, 26, 2609-2612.
- [12] Y. Miyake, H. Takadam, K. Ohe, S. Uemura, *J. Chem. Soc., Perkin Trans.*, **2000**, 1, 1595-1599
- [13] D. N. Harpp, J. G. Gleason, *J. Am. Chem. Soc.*, **1971**, 93, 2437-2445.
- [14] D. N. Harpp, R. A. Smith, *Org. Synth.*, **1988**, 58, 138-141.

Chapter Four

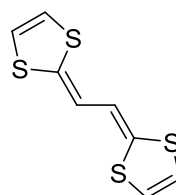
Synthesis of Functional Materials Based on TTFV-PAH Hybrids

4.1 Introduction

Redox chemistry has been used widely in the literature to control a plethora of molecular properties such as molecular recognition,^[1] (dis)association of complexes^[2] and conformations.^[3] Tetrathiafulvalene vinylogues (TTFVs, **4.2**) are an important class of redox-active switchable materials.



4.1

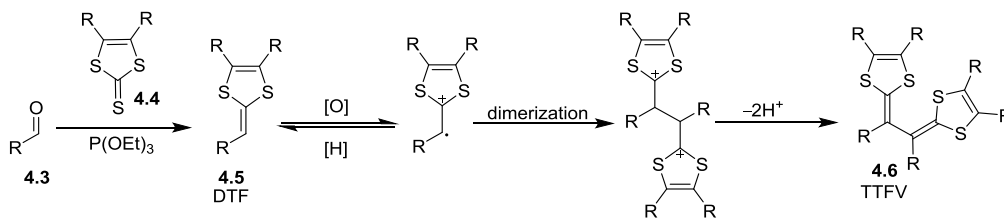


4.2

Figure 4.1 Parent compounds, TTF (**4.1**) and TTFV (**4.2**).

Much like the parent compound, tetrathiafulvalene (TTF **4.1**), TTFVs are strong electron donors and can undergo reversible redox chemistry using mild chemical or electrochemical stimulation. There are numerous ways to synthesize TTFVs. Perhaps the most convenient way in which they can be synthesized from aldehydes in two steps:

Bryce olefination of an aldehyde^[4] (**4.3**) with the thione (**4.4**) to produce a dithiafulvene (**4.5**) followed by chemical or electrochemical oxidative dimerization to yield a TTFV (**4.6**) (Scheme 4.1). The TTFV system undergoes a dramatic conformational change when oxidized or in response to a change in pH. This switching behavior is driven by a complement of steric and electronic effects.



Scheme 4.1 General strategies for the synthesis of TTFVs from aldehydes.

With bulky R groups (often aryl groups), the neutral form of the TTFV (**4.6**) exists mainly in the *pseudo-cis* conformation due to attractive sulfur-sulfur interactions unless R is very large and forces other conformations. Upon oxidation, the molecule changes shape dramatically, adopting a *trans* conformation. This is driven by the Coulombic repulsion of the two positively charged dithiolinium rings (Figure 4.2). A similar change in structure can also be accomplished by changing the pH (Figure 4.3).^[5] According to detailed UV-vis studies,^[8] the protonations are completely reversible and the addition of a base will regenerate the TTFV unit. The large change in conformation coupled with multiple switching stimuli (electrochemical, chemical, pH) make the TTFV subunit a very powerful tool.

PAH-TTFV hybrids are attractive synthetic targets since they can take advantage of PAHs' ability to participate in π stacking and their rich photochemistry while maintaining the switchable behaviour.

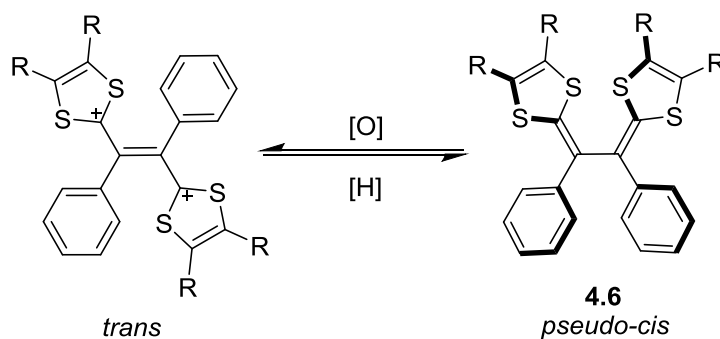


Figure 4.2 Redox switchability of tetrathiafulvalenevinyllogues.

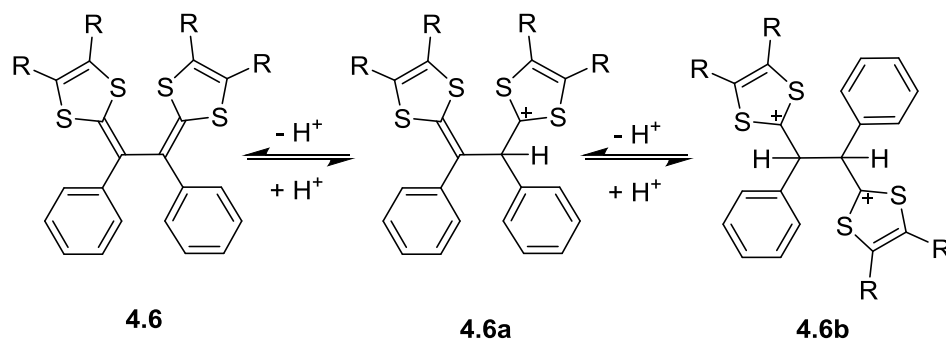


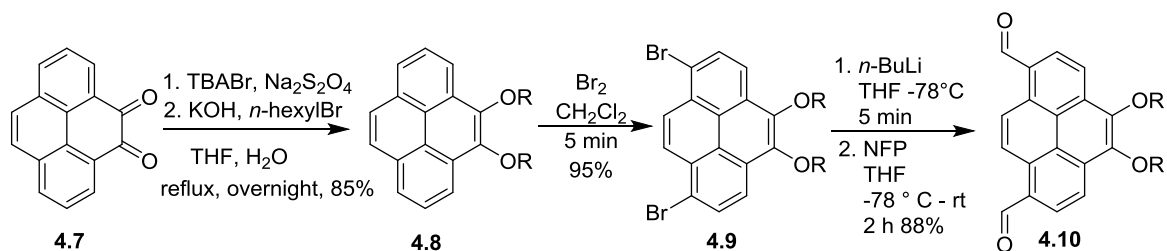
Figure 4.3 pH-induced conformational switching of TTFV.

This allows for the construction of functional organic compounds such as Zhao's TTFV-pyrene hybrid molecular tweezers, which are capable of "catching" a fullerene^[5] through π stacking and then releasing it by inducing a conformational change within the TTFV subunit.

The synthesis, characterization and some applications of other novel PAH-TTFV hybrids are outlined in this Chapter.

4.2 Results and Discussion

The first step in the synthesis undertaken utilized pyrene-4,5-dione (**4.7**), which as described in Chapter 2 had recently become easily available in tens of grams at a time. The quinone **4.7** was subjected to reductive alkylation using a reported procedure for phenanthrenedione^[6] yielding 4,5-dihexoxy pyrene (**4.8**). The 85% yield is comparable to what was obtained using other alkyl groups (+/- 10%). Pyrene derivative (**4.8**) was then brominated selectively in the 1,8-positions to afford 4,5-dihexoxy-1,8-dibromopyrene (**4.9**) in 96% yield. Dibromodihexyloxy pyrene (**4.9**) was then subjected to lithium halogen exchange with *n*-butyllithium and the resulting dilithiated species (not shown) was quenched with DMF to furnish dialdehyde (**4.10**) in 85% yield. The formylation reaction suffered from a somewhat laborious workup.

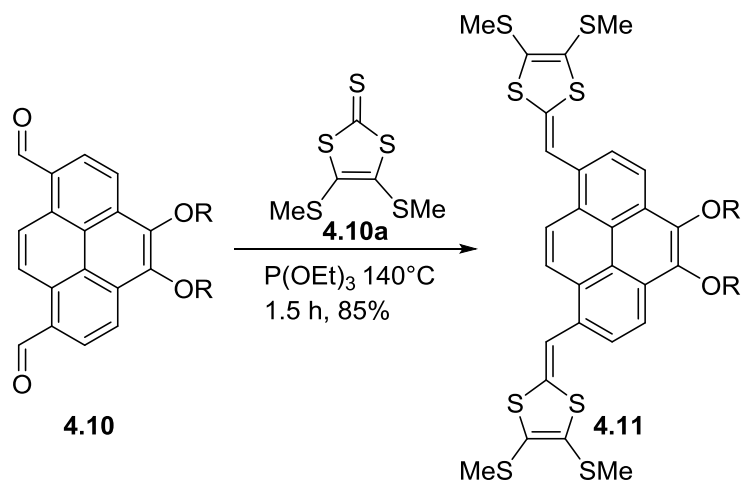


Scheme 4.2 The synthesis of dialdehyde (**4.10**).

In particular, the complete removal of DMF (16 equivalents were used) from the crude reaction mixture prior to column chromatography required considerable effort. Failure to remove all of the DMF resulted in very poor separation of dialdehyde **4.10** from the monoaldehyde byproduct. This problem was conveniently solved by switching the formylating agent from DMF to *N*-formylpiperidine (NFP). NFP has been reported to give higher yields than DMF in the formylation of lithiated species.^[7] In the case of **4.10**, the yield was the same for both formylating agents, but the change to NFP allowed the crude reaction mixture to be columned directly without the need for numerous acid washes. With dialdehyde **4.10** in hand, an opportunity to construct new TTFV-pyrene hybrids arose.

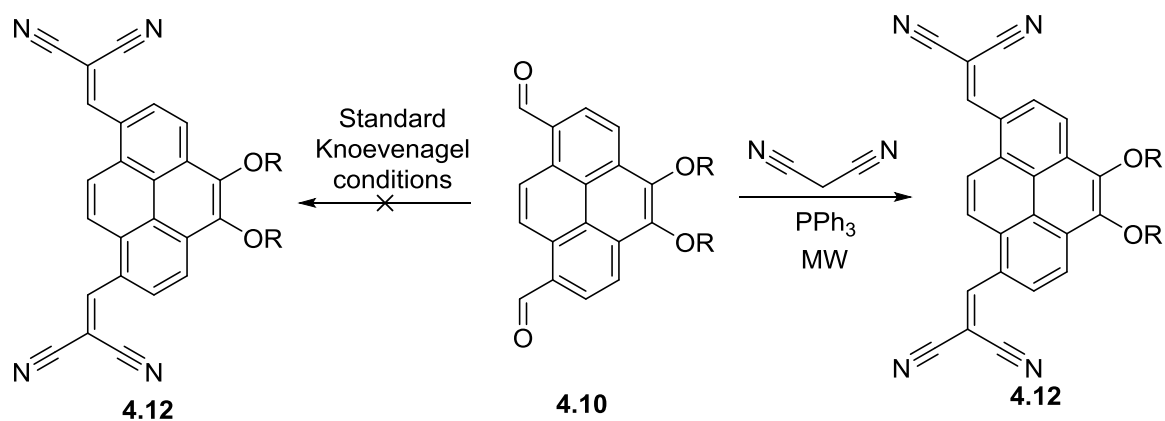
Following Bryce's olefination procedure, dialdehyde (**4.10**) was reacted with cyclic thioxanthate[†] (**4.11**) in triethylphosphite at reflux, which smoothly afforded the di-DTFV-substituted pyrene derivative (**4.12**) in 85% yield (Scheme 4.3). DTF systems are known to be strong electron donors and readily form charge-transfer complexes with appropriate electron-deficient species, so it was of interest to synthesize a pyrene-based

[†] This compound is commonly referred to as a thione, but a thione is the sulphur analog of a ketone. Thus, describing compound **4.10a** as a thione is akin to describing a carbonate as a ketone, *i.e.* it is incorrect. The all-sulfur equivalent of a carbonate is a thioxanthate.



Scheme 4.3 The synthesis of bis(DTF)pyrene (**4.11**).

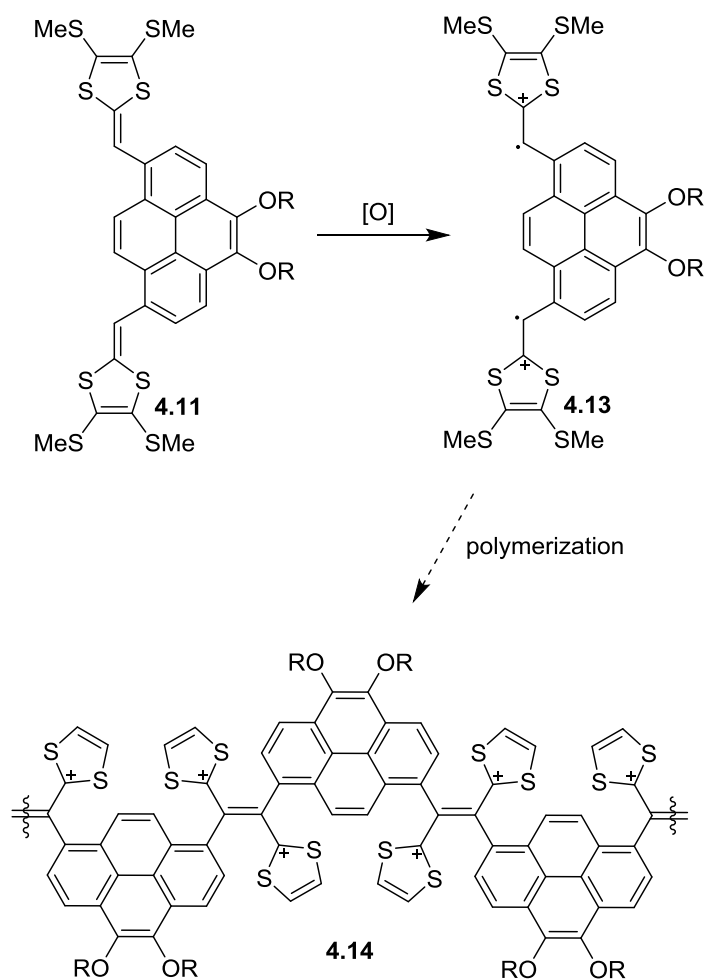
acceptor to match complement (**4.11**). With access to gram quantities of dialdehyde (**4.10**), the synthesis of bis(dicyanoethenyl)pyrene **4.12** was attempted. Unfortunately, under classical Knoevenagel conditions (pyridine at reflux) or ammonium acetate at room temperature), complex product mixtures were obtained. On the other hand, the use of a solventless, phosphine-catalyzed Knoevenagel condensation procedure reported by Yadav *et al.*,^[10] the desired transformation proceeded in a remarkable 96% yield after only 3 minutes of microwave irradiation (Scheme 4.4). Dialdehyde (**4.10**) must be an excellent substrate for these conditions as it underwent a double conversion in higher yield than any single conversion reported by Yadav. Attempts were then made to produce charge-transfer complexes of (**4.12**) and (**4.11**), but after careful titration of dilute solutions of each one into the other in varying ratios, no evidence for complex formation (colour change) was obtained. It may be that **4.12** is not sufficiently electron deficient. It still contains an innately electron rich pyrene system with two electron-donating alkoxy



Scheme 4.4 Knoevenagel condensations of pyrene dialdehyde (**4.10**)

groups. A better candidate for the electron deficient partner would be diketone **2.1**, which would presumably be accessible through removal of the alkyl groups (or perhaps some more easily removable protecting group) at some point in the synthetic pathway.

TTFVs are known to oxidatively dimerize (Figure 4.1), so it was reasoned that compound (**4.11**), by virtue of its spatially distant, disubstituted motif would undergo polymerization (or possibly cyclic oligomerization) when oxidized (Scheme 4.5).



Scheme 4.5 Oxidation of (**4.11**) and the expected product of polymerization (SMe groups omitted for clarity).

Unexpectedly, when compound (**4.11**) was reacted with iodine in dichloromethane, only the starting material was recovered after reductive workup. Cyclic voltammetry was performed on **4.11** to obtain a better understanding of how the material acts under redox conditions. The voltammogram (Figure 4.4) clearly show that the two DTF units undergo sequential pseudoreversible oxidation. When the number of cycles was increased to 12, very little change was seen in the voltammograms over time. This indicated that the di-

(radical cation) is very stable and under the electrochemical redox conditions and consequently does not polymerize.

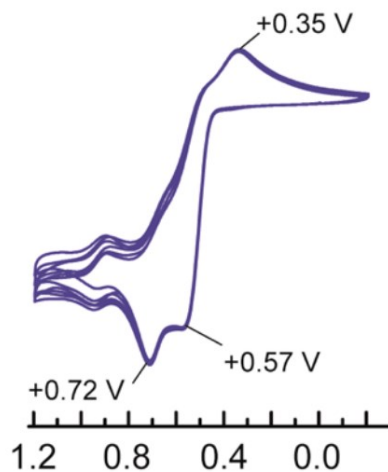


Figure 4.4 Cyclic voltammogram of (4.11) (V vs. Ag/AgCl).

The stability of the di-(radical cation) can be rationalized by the recombination of the diradical through the pyrene system to afford dication **4.13b**, which can be viewed as a naphthalene system flanked by two pentadienyl cations (Figure 4.5). Although the pyrene core is destroyed, so are two radicals. Spectroscopic evidence for the formation of dication **4.13b** comes from the change in the UV-vis spectrum of (4.13) as it is titrated with an oxidant (iodate) (Figure 4.6). The dramatic decrease in the absorption at 475 nm and the emergence of a new broad peak at 650 nm suggests that a new chromophore is produced.

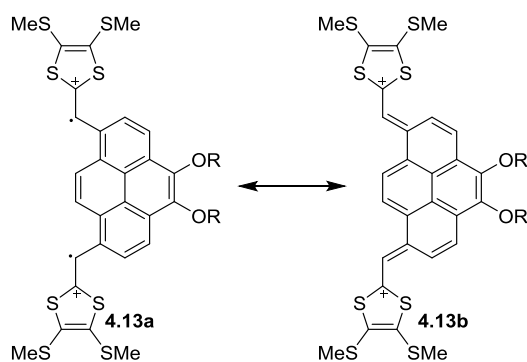


Figure 4.5 Proposed resonance hybrid accounting for low reactivity of (4.11).

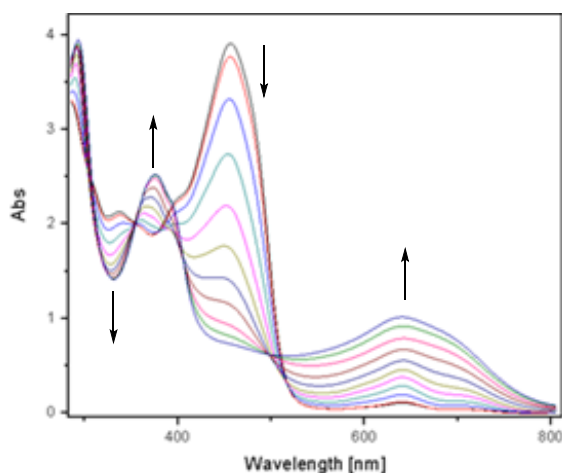


Figure 4.6 UV-vis absorption spectrum of (4.13) titrated with sodium periodate.

After molecule (4.13) failed to polymerize in solution, solid-state reactions were investigated. The hope was that any existing preorganization in the solid state might provide a better scenario for intermolecular reaction. Thus the compound was ground with 6 equivalents of iodine using a mortar and pestle. Interestingly, after only seconds of grinding, the dark brown powder had become a plastic-like material, which adhered to both the mortar and the pestle (Scheme 4.6). The solid had an appearance and malleability similar to lead metal. Excess iodine could be removed by repeated washing

with dichloromethane. Once the wash solvent remained colorless, a black material was left. Attempts to grind this material into a powder between glass slides resulted in the slides being strongly stuck together. Unfortunately, the black material produced was completely insoluble in all solvents tried (CH_2Cl_2 , CHCl_3 , THF, benzene, ethanol, 1,2-dichloroethane, 1,2-dichlorobenzene, ethyl acetate), which precluded further characterization. A Raman spectrum (Figure 4.7) of the bulk material on an aluminium substrate was recorded, but

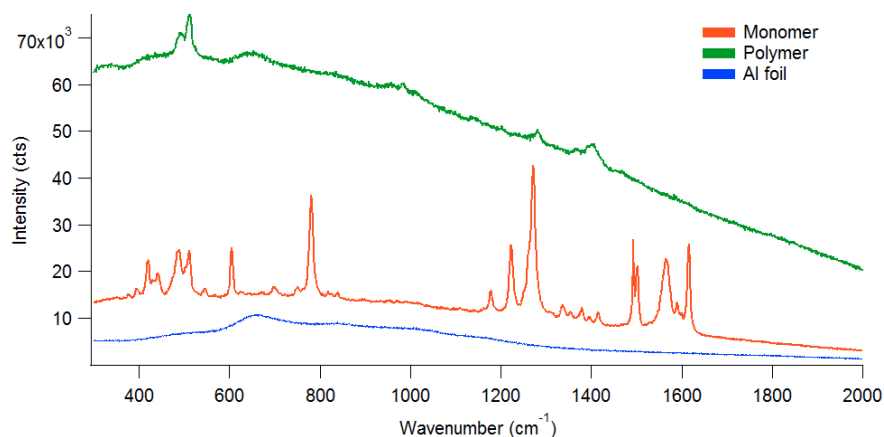


Figure 4.7 Bulk Raman spectra of (4.13)(orange), aluminium(blue) and product of mechanochemical reaction(green).

strong fluorescence and severe baseline drifting limited the information that could be gathered. Since Raman scattering competes with fluorescence, highly fluorescent samples typically have very low signal-to-noise ratios. However, some information could still be gleaned from the result. Peaks present in both monomer and polymer at 500 and 1250 cm^{-1} were tentatively assigned as C–H out-of-plane bending, C–C out-of-plane bending and C–H in-plane bending, C–C in-plane bending respectively. An attempt was made to

enhance the solubility of the presumed polymeric material by subjecting it to reducing conditions. Normally, this is accomplished by stirring a biphasic solution of the oxidized compound in dichloromethane with a concentrated solution of aqueous sodium thiosulfate.^[8] However, since the compound has negligible solubility, the solid was sonicated overnight in a saturated solution of sodium thiosulfate. Interestingly and unexpectedly, starting material (**4.13**) was recovered.

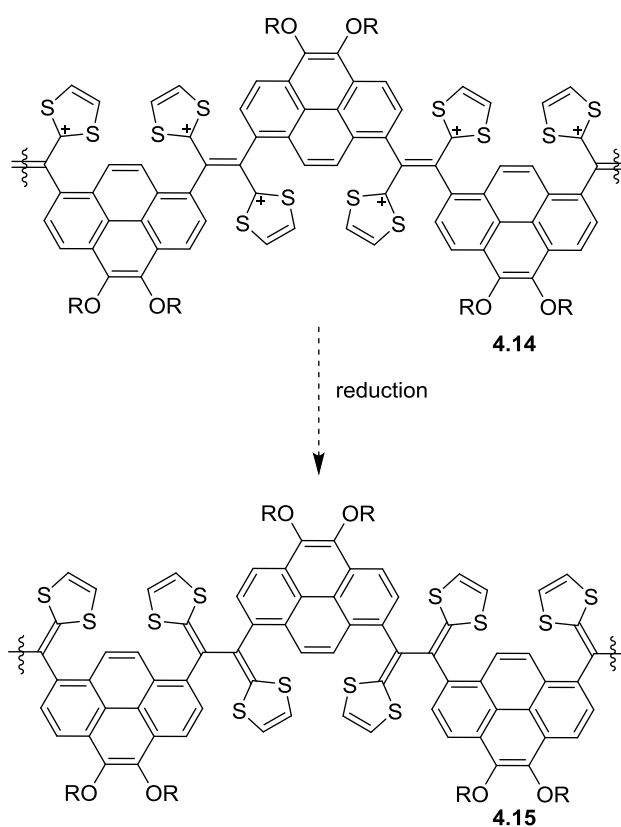
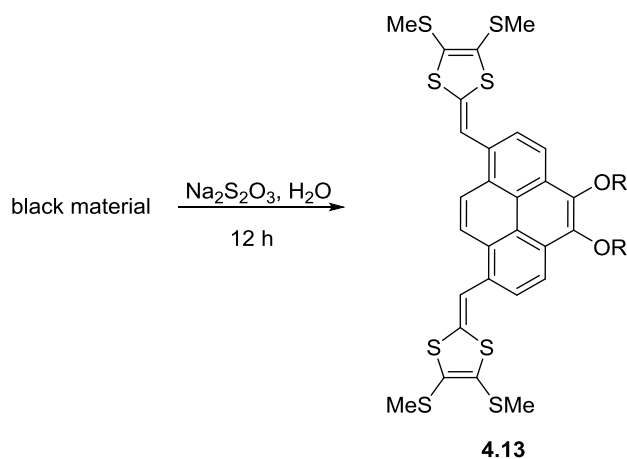
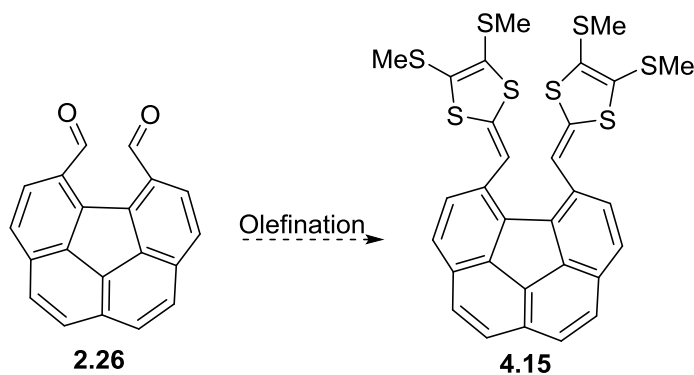


Figure 4.8 Expected product from the oxidation of (**4.13**) with iodine and reductive workup (SMe groups omitted for clarity).



Scheme 4.6 Reduction of black material yielding starting material (**4.13**).

The interesting and unusual dialdehyde **2.26** (the unexpected product of corannulene oxidation) was reported in Chapter 2. After the success in the olefination reaction with pyrene-derived dialdehyde (**4.10**), it was decided to try to synthesize di-DTF compound **4.15** (Scheme 4.7). The main reason for interest in this compound was to determine whether oxidation to corresponding the di-(radical cation) would result in intramolecular radical recombination regenerating the corannulene skeleton.



Scheme 4.7 Proposed olefination of benzofluoranthenedialdehyde (**2.26**).

Subsequent reduction would yield corannulene derivative **4.17**, which has two chemical handles for further functionalization or redox activity. Due to the strain energy present in corannulene (24.2 kcal/mol), this was expected to be a more challenging process than normal, but it seemed likely that radical recombination to form a new C–C bond (*ca.* 84 kcal/mol) would be enough to outweigh the increase in strain.

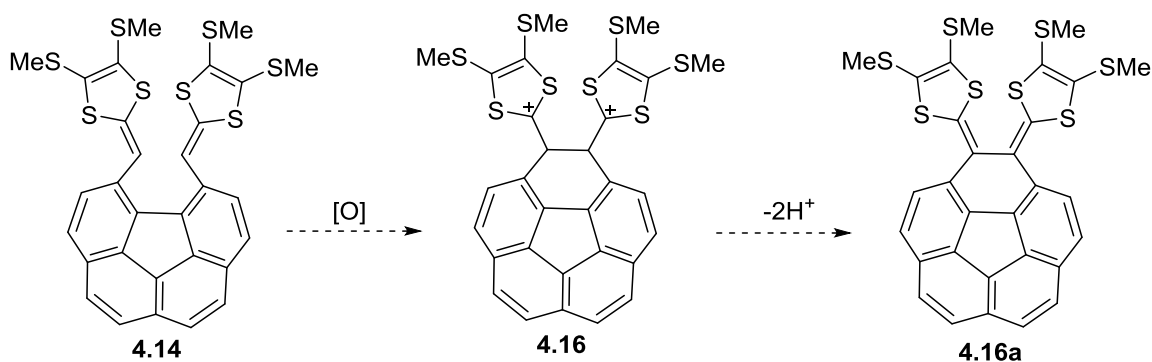
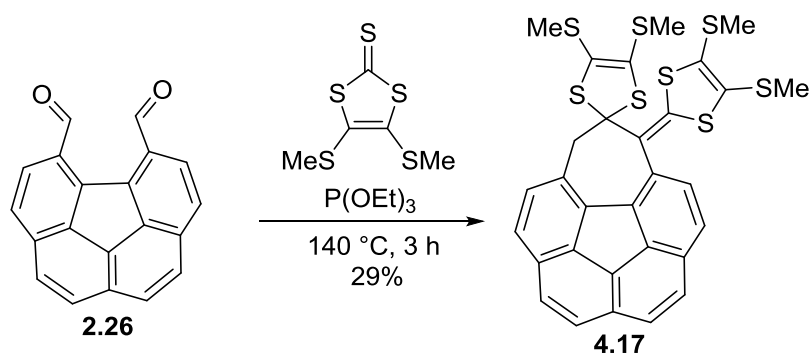


Figure 4.9 Proposed radical ring closure regenerating corannulene system (**4.16**).

When the Bryce olefination reaction was performed on dialdehyde **2.26**, the desired product **4.16a** was not obtained. Instead, another product with the same molar mass ($m/z = 639$) was obtained. No other mobile compounds were formed (tlc analysis). The ^1H NMR spectrum of the new compound contained four 3-proton singlets in the range of δ 2.47-1.84, which indicated that all four SMe groups were in different environments. One of them was at significantly higher field than the others (δ 1.84 ppm). Two coupled doublets with an unusually large coupling constant ($J = 16.8$ Hz) were also observed at δ 4.47 and 4.25 ppm. An HSQC experiment confirmed that the protons responsible for the two doublets were attached to the same carbon atom. A DEPT experiment also showed that the carbon atom in question (δ 44.6 ppm) had two attached protons. All of the NMR

data were consistent with structure **4.17**, which contains a seven-membered rather than the expected six-membered ring. Evidently, the increase in strain associated with forming a six-membered ring disfavoured this reaction pathway and enabled **4.17** to form. However, the isolated yield of (**4.17**) was low (29%). The formation of **4.17** was a very interesting result because it is a derivative of homocorannulene (**4.18**). No homocorannulene appears to have been reported in the open literature.



Scheme 4.8 Unexpected seven-membered ring formation during olefination reaction.

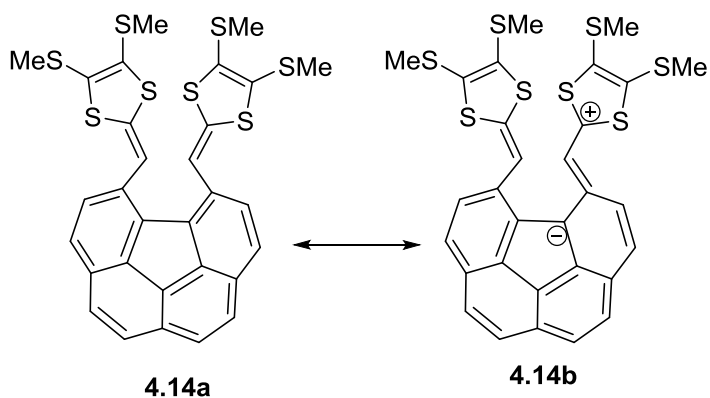
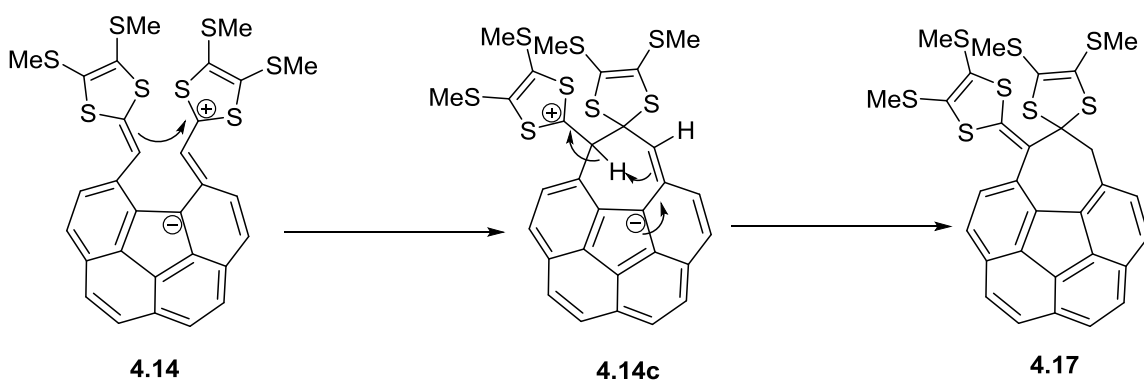


Figure 4.10 Charge separated resonance form resulting in two sextets.

To account the formation of (**4.17**), it can be assumed that the Bryce olefination first afforded the desired di-DTF 4.14a (Scheme 4.9/ Figure 4.10). Inspection of molecular models indicated the two DTF units in (**4.14**) sterically crowd one another and that there are eclipsed conformations where the two carbon atoms that undergo bond formation to give the observed product appear to be oriented appropriately for bond formation to occur. Additionally, there is a charge-separated resonance structure available to all conformers of **4.14**, which places both charges in five-membered aromatic rings (a cyclopentadienyl anion and a dithiolinium cation). Nucleophilic attack of the neighbouring ketene *S,S*-acetal, a reasonable nucleophile, on the dithiolinium-like ring gives rise to a zwitterion **4.18**, which also has both charges in five-membered aromatic rings. Transannular proton transfer then leads to the observed product **4.17**. Examination of molecular models suggested that this process is not highly energetic in nature.

It can be clearly seen in a molecular model of **4.17** that one of the SMe groups is situated over the PAH moiety and would thus be expected to resonate at higher field than the other SMe groups. The two protons on the CH₂ group are diastereotopic and would therefore be expected to appear as coupled doublets in the ¹H NMR spectrum. With regard to the large coupling constants, it is well-documented that diastereotopic protons adjacent to π systems typically have large coupling constants.



Scheme 4.9 Proposed mechanism of the reaction yielding homocorannulene derivative (**4.17**).

4.3 Conclusions and Future Work

In this Chapter, two PAH-DTF hybrids were reported. Pyrene-based di-DTF (**4.13**) was synthesized from the now readily available pyrene-4,5-dione **4.7** in 4 steps in 71% overall yield. Homocorannulene derivative (**4.17**) was synthesized from corannulene in two steps with an overall yield of just 6%, but it is an especially interesting compound.

Di-DTF-pyrene derivative (**4.13**) underwent oxidation with iodine upon grinding in a mortar and pestle. The nature of the oxidation product has not yet been determined, mainly due to its insolubility. Powder XRD and scanning tunneling microscopy experiments may provide some information in this regard.

The formation of **4.17** was unexpected, but it provided access to the first known homocorannulene derivative. In the future, it would be worthwhile to find ways of improving the yield of **4.17** and, more interestingly, to cleave the sulfur-containing

functionality to afford the parent homocorannulene (**4.18**). An especially interesting experiment to perform on **4.18** would be its deprotonation to form anion **4.19**: a formally antiaromatic [16]annulene surrounding a formally aromatic cyclopentadienyl anion.

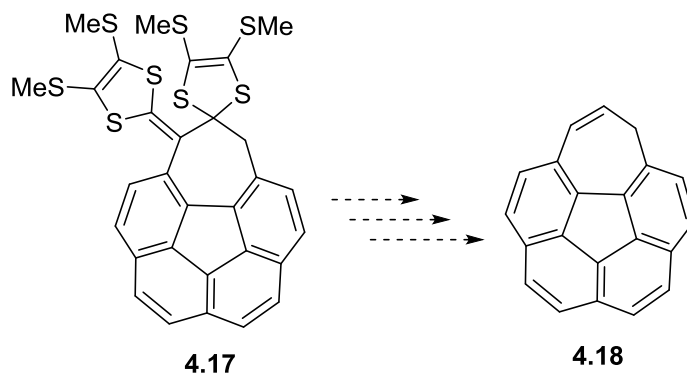


Figure 4.11 Proposed synthetic route to homocorannulene (**4.18**).

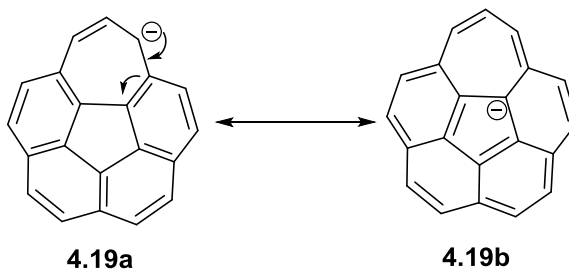


Figure 4.12 Proposed delocalization resulting in a molecule with both anti- and aromatic character.

2.3 Experimental section

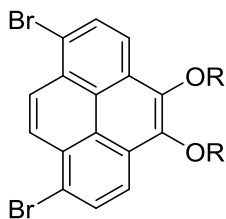
All chemicals utilized in this chapters work were used as received from commercial chemical suppliers (Aldrich, Alfa Aesar, TCI, Matrix Scientific and Precious Metals Online). All reactions were performed without an inert atmosphere unless otherwise indicated. THF was dried over activated 4 Å molecular sieves for 24 h prior to

use. Hexanes were distilled before use in column chromatography. THF was dried over activated molecular sieves for at least 24 h. Flash chromatography was performed using ZEOChem 60 eco 40-63 μ . Compounds on TLC plates were visualized with UV light (254 and 365 nm) and chemical staining methods (phosphomolybdic acid, 2,4-dinitrophenylhydrazine and iodine).

Instrumentation:

Melting points were measured on an OPTImelt automated melting point system and are uncorrected, recrystallization solvents given in brackets (where applicable). ^1H NMR (300 MHz) and ^{13}C NMR (75 MHz) were recorded on a Bruker AVANCE III instrument (CDCl_3 , unless otherwise indicated). Chemical shifts are reported relative to internal standards: Me_4Si (δ 0.00 ppm) and CDCl_3 (δ 77.23 ppm). ^1H NMR data are presented as follows: chemical shift, multiplicity (s=singlet, d=doublet, t=triplet, q=quartet, m= multiplet, brs=broad singlet, dd=doublet of doublets), coupling constant (J in Hz), integration (number of ^1H). IR spectra were obtained using a Bruker TENSOR 27 FTIR. Low-resolution mass spectra (MS) were taken on LC/MSD (Trap) Agilent 1100 series SL. High resolution mass spectra (HRMS) of some compounds were obtained using a Waters Micromass GCT premier instrument. MS data are presented as follows: m/z (relative intensity), assignment (when appropriate), calculated mass for corresponding molecular formula. UV-vis and fluorescence spectra were recorded using Agilent HP8453A UV-Visible absorbance spectrophotometer and PTI QuantaMaster 6000 spectrofluorometer.

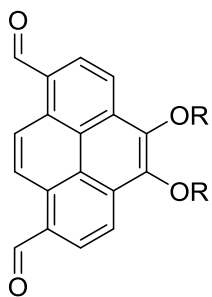
1,8-Dibromo-4,5-dihexoxyppyrene (4.9)



To a solution of 4,5-dihexoxyppyrene (2.00g, 5.00 mmol) in CH₂Cl₂ (50 mL) was added bromine (1.75 g dissolved in 10 mL CH₂Cl₂). The reaction was stirred for 5 minutes at room temperature. Excess bromine was quenched with saturated sodium thiosulfate solution.

The layers were separated and the aqueous phase was extracted with EtOAc (2 × 50 mL). The organic phase was dried over Na₂SO₄ and the solvent removed under reduced pressure to yield a brown solid. The crude product was subjected to column chromatography using 10% CH₂Cl₂/hexanes as eluent to yield 1,8-dibromo-4,5-dihexoxyppyrene (2.65 g, 95%) as a pale yellow solid. R_f (10% CH₂Cl₂/hexanes) = 0.50: ¹H NMR (CDCl₃, 300 MHz) δ 8.51 (s, 2H), 8.37 (d, *J* = 8.5, 2H), 8.27 (d, *J* = 8.5, 2H), 4.31 (t, *J* = 6.7 Hz, 2H) 1.95 (m, 4H), 1.60 (m, 4H), 1.40 (m, 8H), 0.93 (m, 6H) ppm; MS [APCI(+)] *m/z* (%): 561 [M+H]⁺, 100.

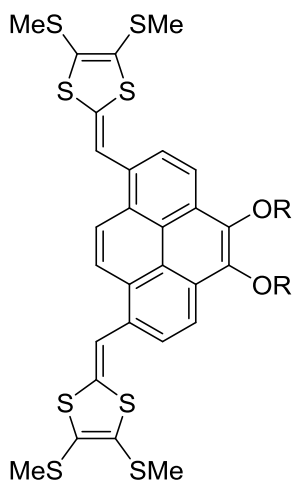
4,5-dihexoxyppyrene-1,8-dicarboxaldehyde (4.10)



To a -78 °C nitrogen purged solution of crude 1,8-dibromo-4,5-dihexoxyppyrene (444 mg) in anhydrous THF (75 mL) *n*-BuLi (6 mL (1.3 M), 6.34 mmol) was added dropwise. The reaction was allowed to stir at -78° C for 5 minutes. *N*-formyl piperidine (1.62 g, 14.3 mmol) was added and the dry ice acetone bath removed. The reaction mixture

was allowed to warm to room temperature and stirred for a further 1.5 h. The reaction was quenched with 10% HCl_(aq) (25 mL) and the organic solvents were removed under reduced pressure. The reaction mixture was extracted with CH₂Cl₂ (2 × 50 mL). The combined organic layers were washed with 10% HCl_(aq) (2 × 200 mL) and subsequently dried over Na₂SO₄. Solvent was removed under reduced pressure to yield crude 4,5-dihexoxy-1,8-pyrenedicarboxaldehyde as a dark orange oil. The crude product was subjected to column chromatography using 50% CH₂Cl₂/hexanes as eluent to yield 4,5-dihexoxy-1,8-pyrenedicarboxaldehyde as a canary yellow solid. R_f (50% CHCl₃/hexanes) = 0.30; ¹H NMR (CDCl₃, 300 MHz) δ 10.82 (s, 2H), 9.56 (s, 2H), 8.72 (d, *J* = 8.2, 2H), 8.54 (d, *J* = 8.2, 2H), 4.38 (t, *J* = 6.7 Hz, 4H) 2.00 (m, 4H), 1.61 (m, 4H), 1.42 (m, 8H), 0.95 (m, 6H) ppm; MS [APCI(+)] *m/z* (%): 561 ([M+H]⁺, 100. HRMS [APCI(+)] calcd for C₃₀H₃₄O₄ 458.2471, found: 458.2411.

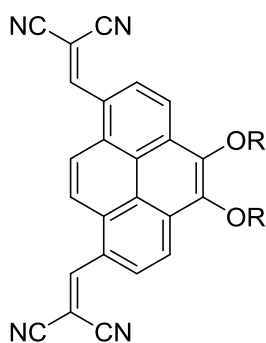
1,8-bisDTF-4,5-dihexoxypyrene



To a solution of 4,5-dihexoxy-1,8-dialdehyde (2.00g, 4.36 mmol) in P(OEt)₃ (100 mL) was added dimethyl thione (**4.10a**) (0.835 g, 25.9 mmol). The reaction was stirred at reflux under nitrogen for 3 h. The bulk of P(OEt)₃ was removed by vacuum distillation then the crude product was subjected to a plug column removing the last traces of P(OEt)₃. Finally the

crude material was again subjected to column chromatography using 10% CH₂Cl₂/hexanes as eluent to yield 1,8-bis(DTF)-4,5-dihexoxyppyrene (3.02 g, 85%) as a shining orange solid. *R_f* (10% CH₂Cl₂/hexanes) = 0.25: ¹H NMR (CDCl₃, 300 MHz) δ 8.47 (d, *J* = 8.2, 2H), 8.21 (s, 2H), 8.04 (d, *J* = 8.26, 2H), 7.32 (s, 2H), 4.31 (t, *J* = 6.7, 2H), 2.49 (s, 3H), 2.37 (s, 3H), 1.97 (m, 4H), 1.62 (m, 4H), 1.42 (m, 8H), 0.94 (m, 6H), ppm; ¹³C NMR (CDCl₃, 75 MHz) δ 144.00, 134.69, 130.49, 128.13, 127.53, 124.54, 124.45, 123.46, 123.29, 119.49, 112.67, 73.87, 31.82, 30.60, 26.01, 22.72, 19.02, 18.97, 14.13 ppm; MS [APCI(+)] *m/z* (%): 815 ([M+H]⁺, 100. HRMS [APCI(+)] calcd for C₄₀H₄₆O₂S₈ 814.1263, found: 814.1244.

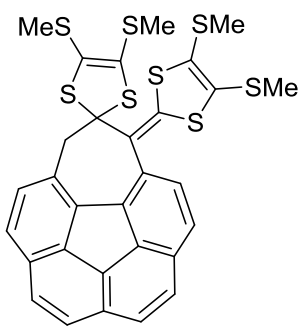
1,8-bis(malonylethenyl)-4,5-dihexoxyppyrene (4.12)



In a 10 mL microwave vial, 4,5-dihexoxyppyrene-1,8-dialdehyde (250 mg, 1.08 mmol), triphenylphosphine (40.2 mg, 0.153 mmol) and malononitrile (122 mg, 1.84 mmol) were added. The tube was capped and irradiated for 6 minutes at 170 °C. The resulting red solid was adsorbed to silica gel and subjected to column chromatography using 75% CH₂Cl₂/hexanes as eluent to afford (3.02 g, 87%) as a matte red solid. *R_f* (75% CH₂Cl₂ / hexanes) = 0.55: ¹H NMR (CDCl₃, 300 MHz) δ 8.91 (s, 2H), 8.90 (d, *J* = 8.62, 2H), 8.75 (d, *J* = 8.5 2H), 8.48 (s, 2H) 4.39 (t, *J* = 6.7 Hz, 4H) 1.99 (m, 4H), 1.62 (m, 4H), 1.42 (m, 8H) , 0.95 (m, 6H) ppm; ¹³C NMR (CDCl₃, 75 MHz) δ 155.87, 146.49, 133.69, 130.02, 126.94, 125.0, 124.08, 122.37, 122.05, 114.06, 112.95,

84.79, 74.56, 31.70, 30.44, 25.88, 22.65, 14.08 ppm; MS [APCI(-)] m/z (%): 554 ($[M]^-$, 100.

Homocorannulene derivative (4.17)

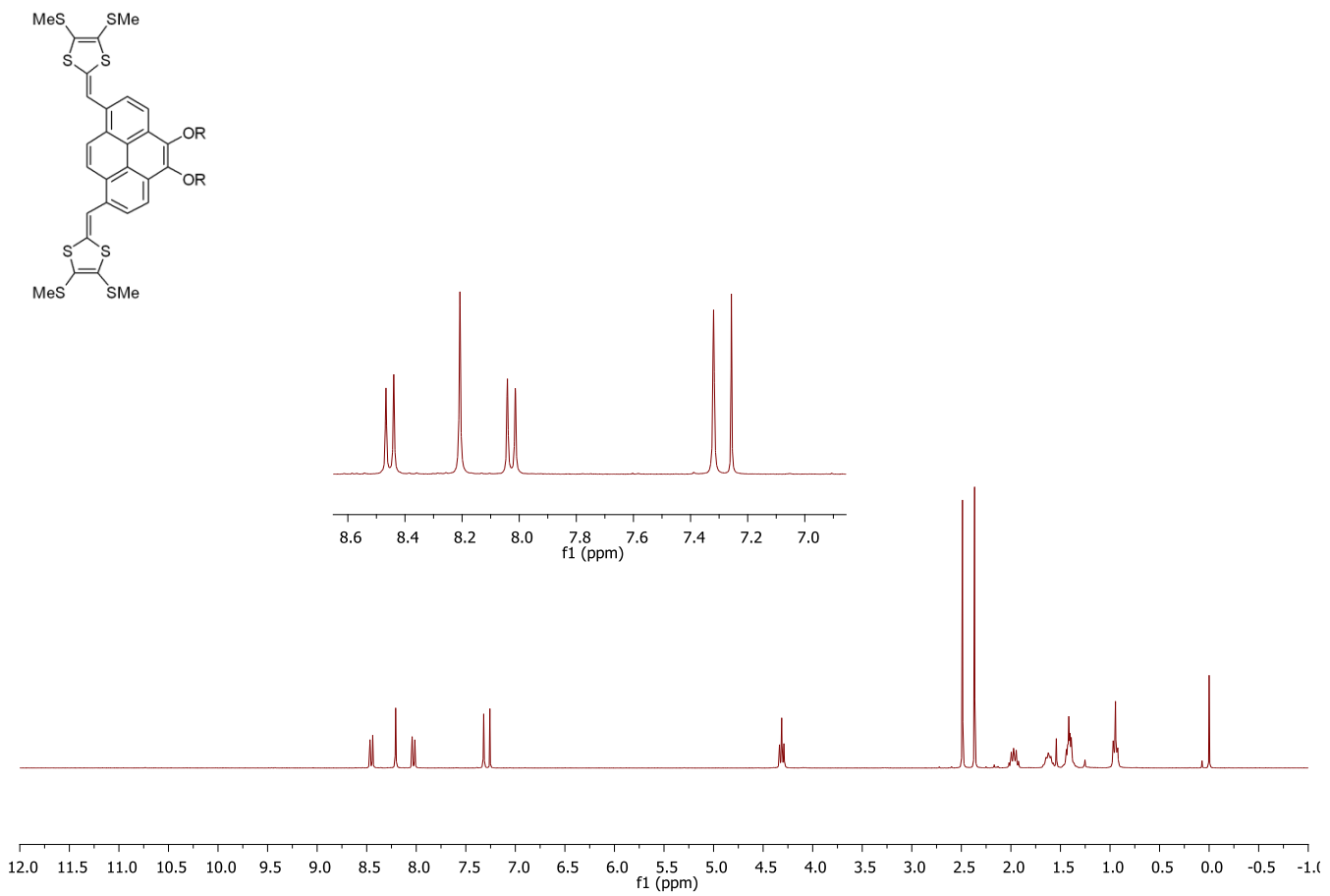


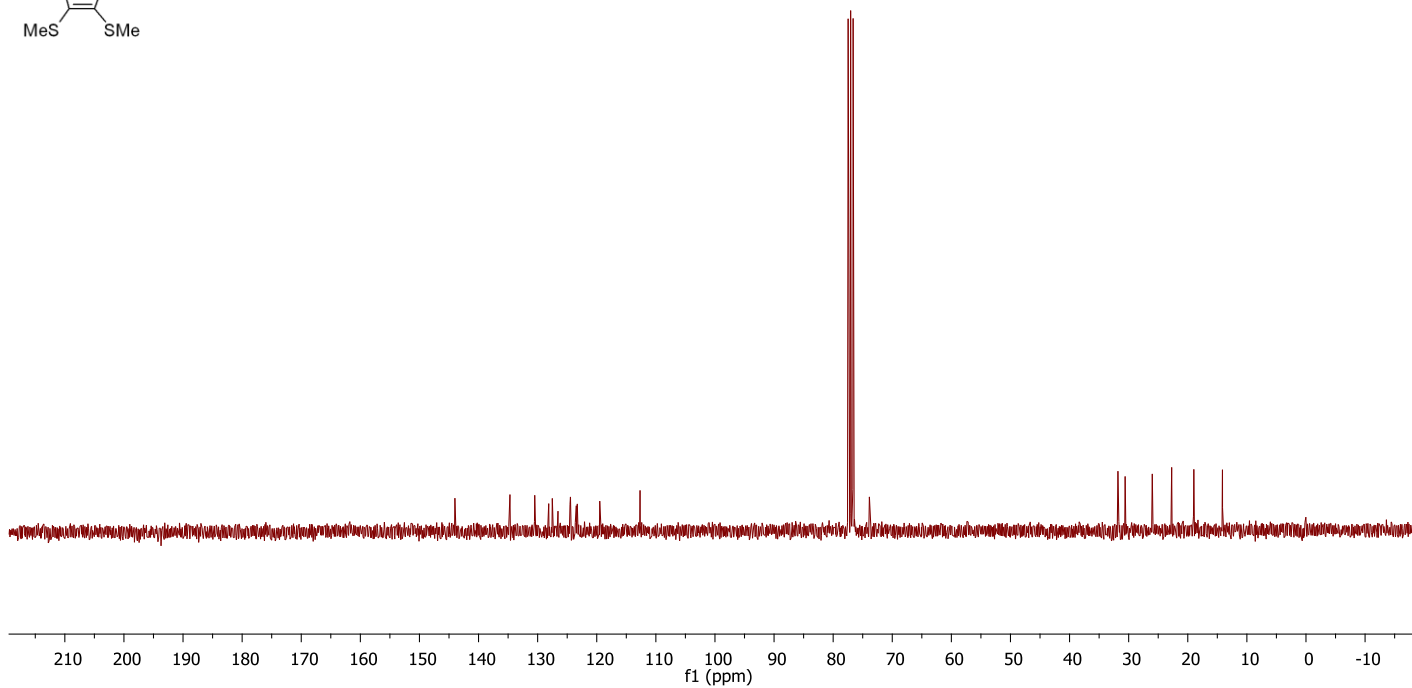
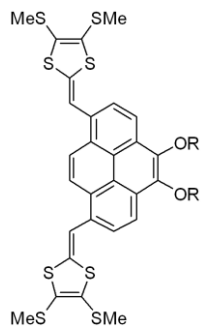
To a solution of benzo[*ghi*]fluoranthene-5,6-dicarboxaldehyde (250 mg, 0.886 mmol) in P(OEt)₃ (30 mL) was added dimethyl thione (**4.10a**) (0.601 g, 2.66 mmol). The reaction was stirred at reflux under nitrogen for 3 h. The bulk of P(OEt)₃ was removed by vacuum distillation then the crude product was subjected to a plug column removing the last traces of P(OEt)₃. Finally the crude material was again subjected to column chromatography using 25% CH₂Cl₂/hexanes to yield homocorannulene derivative (**4.17**) (164 mg, 29%) as an orange solid. R_f (30% CH₂Cl₂/hexanes) = 0.35: ¹H NMR (CDCl₃, 300 MHz) δ 7.93 (d, J = 8.2, 2H), 8.21 (d, 2H), 8.04 (d, J = 8.26, 2H), 7.32 (d, 2H), 4.31 (d, J = 16.6, 1H), (d, J = 16.6, 1H), 2.59 (s, 3H), 2.47 (s, 3H), 2.25 (s, 3H), 1.85 (s, 3H), ppm; ¹³C NMR (CDCl₃, 75 MHz) δ 144.00, 134.69, 130.49, 128.13, 127.53, 124.54, 124.45, 123.46, 123.29, 119.49, 112.67, 73.87, 31.82, 30.60, 26.01, 22.72, 19.02, 18.97, 14.13 ppm; MS [APCI(+)] m/z (%): 815 ($[M+H]^+$, 100. HRMS [APCI(+)] calcd for C₄₀H₄₆O₂S₈ 814.1263, found: 814.1244.

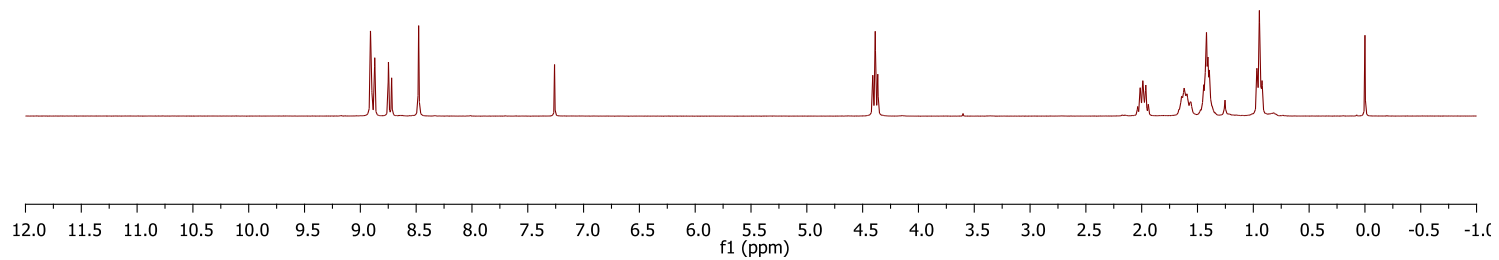
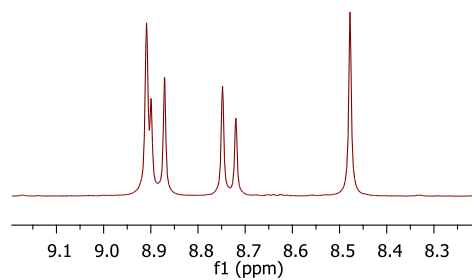
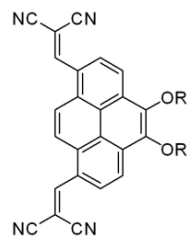
4.4 References

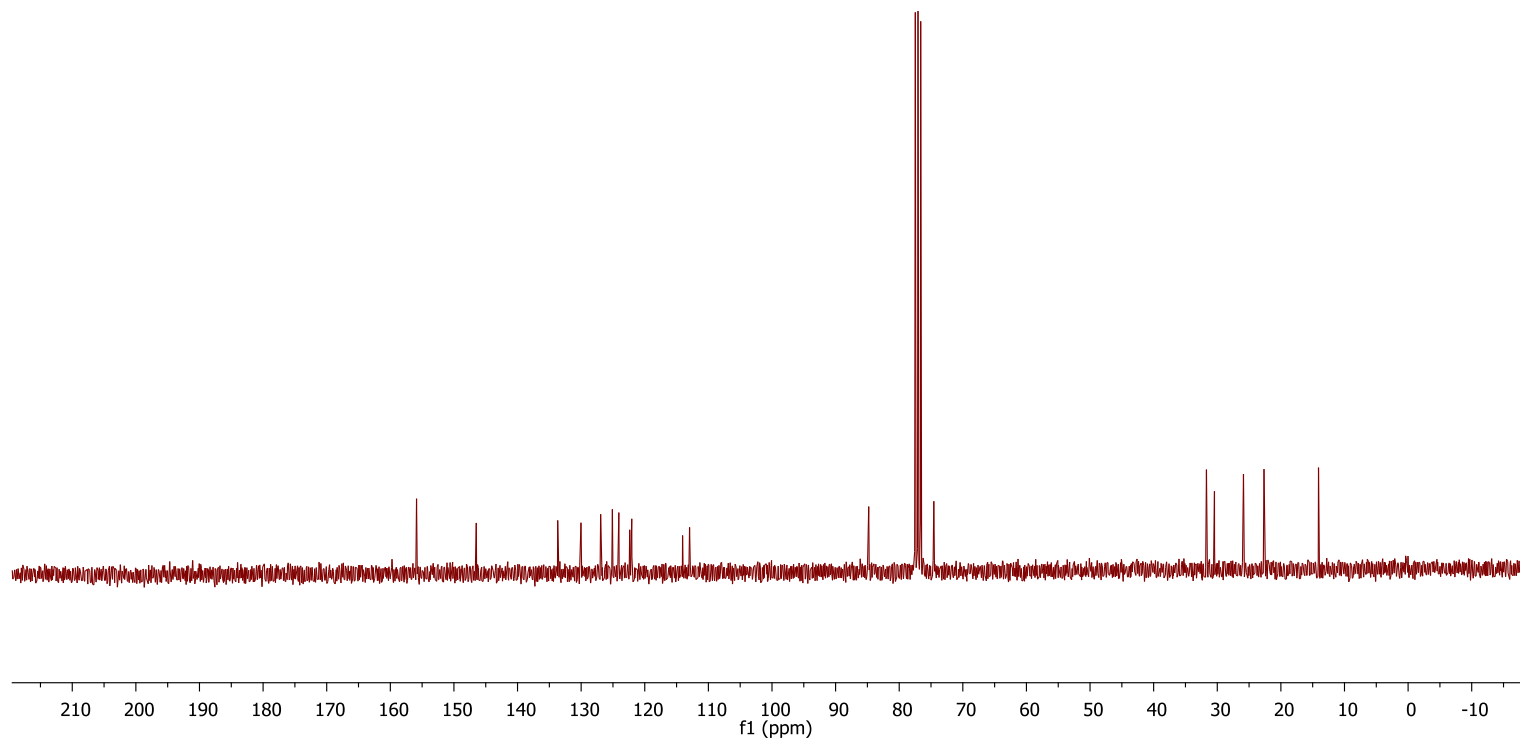
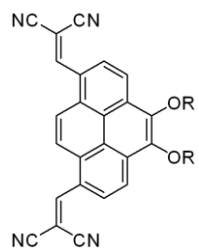
- [1] K. A. Nielsen, S. Bähring, J. O. Jeppesen, *Chem. Eur. J.*, **2011**, 17, 11001-11007.
- [2] A. Niemz, V. M. Rotello, *Acc. Chem. Res.*, **1999**, 32, 42-52.
- [3] Y. Yamashita, M. Tomura, M. B. Zaman, K. Imaeda, *Chem. Commun.*, **1998**, 1657-1658.
- [4] C. A. Christensen, A. S. Batsanov, M. R. Bryce. *J. Org. Chem.*, **2007**, 72, 1301
- [5] K. Mulla, H. Shaik, D. W. Thompson, Y. Zhao, *Org. Lett.*, **2013**, 15, 4532-4535.
- [6] K. Paruch, T. Katz, C. Incarvito, K. Lam, B. Rhatigan, A. J. Rheingold, *J. Org. Chem.*, **2000**, 65, 7602-7608.
- [7] L. Bondarenko, I. Dix, H. Hinrichs, H. Hopf, *Synthesis*, **2004**, 16, 2751-2759.
- [8] Y. Zhao, G. Chen, K. Mulla, I. Mahmud, S. Liang, P. Dongare, D. W. Thompson, L. N. Dawe, S. Bouzan, *Pure Appl. Chem.*, **2012**, 84, 1005-1025.
- [9] N. Mase, T. Horibe, *Org. Lett.*, **2013**, 15, 1854-1857.
- [10] J. S. Yadav, B. S. S. Reddy, A. K. Basak, B. Visali, A. V. Narsaiah, K. Nagaiah, *Eur. J. Org. Chem.*, **2004**, 546-551.

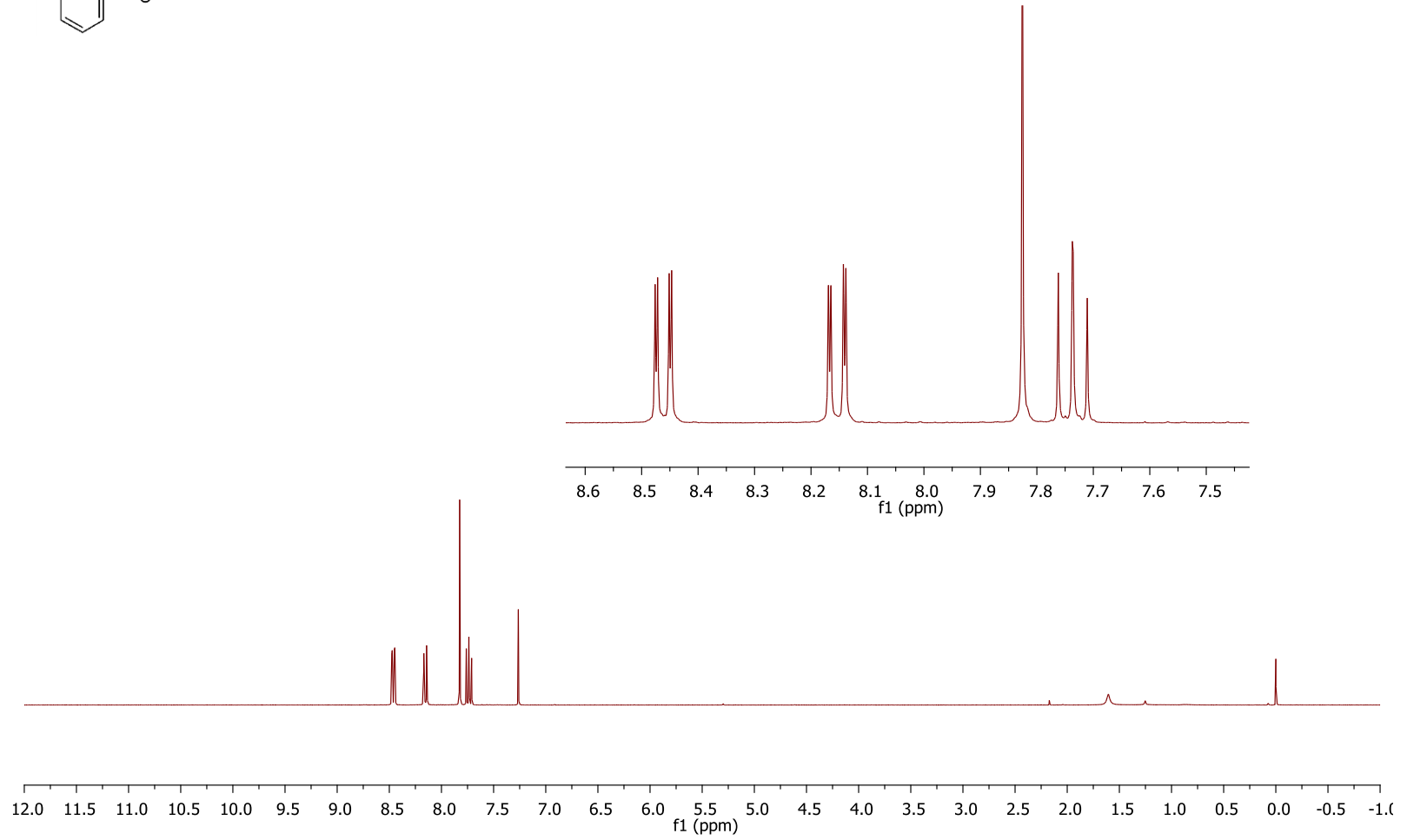
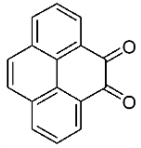
Appendix

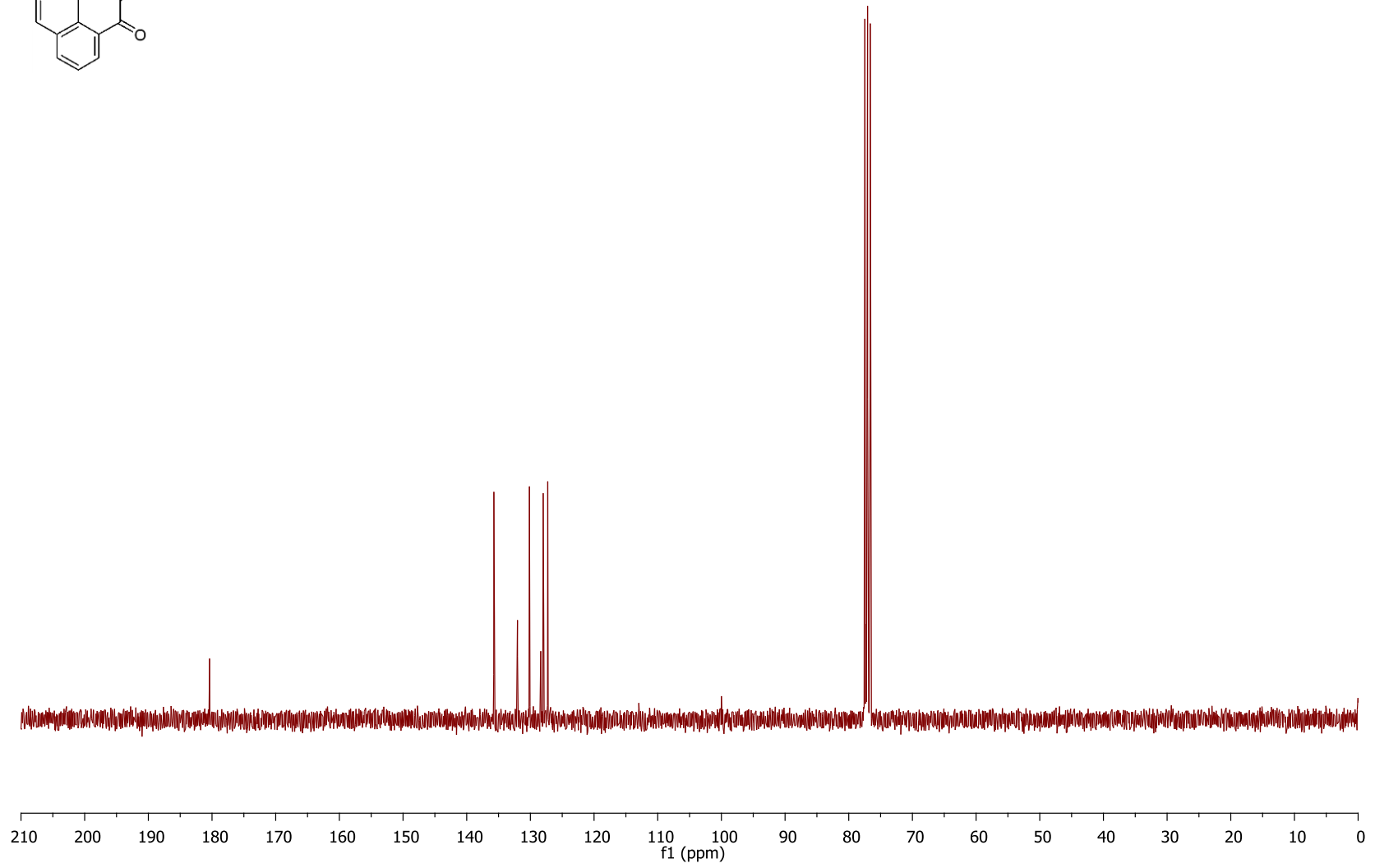
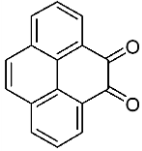




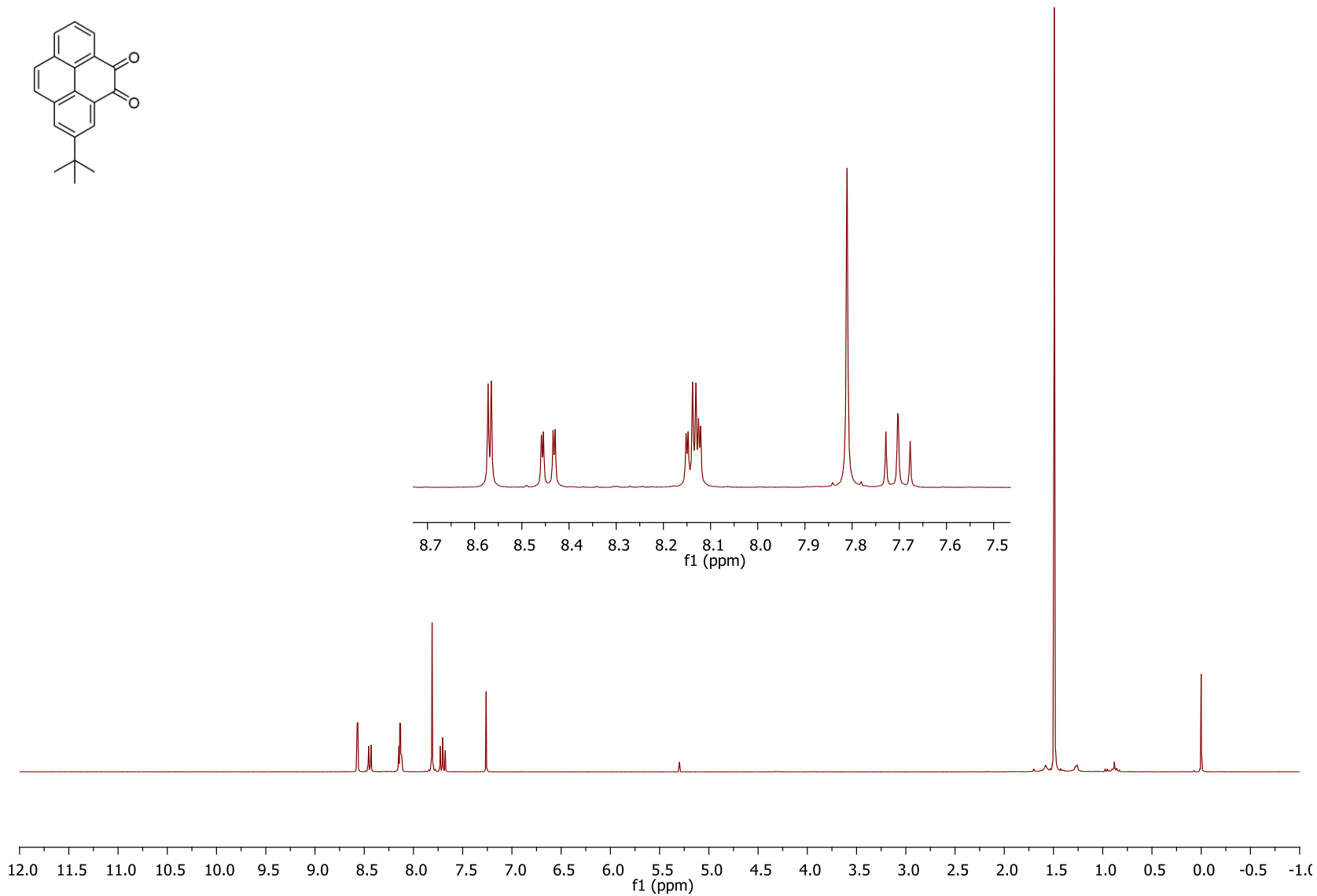
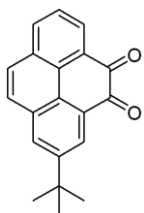


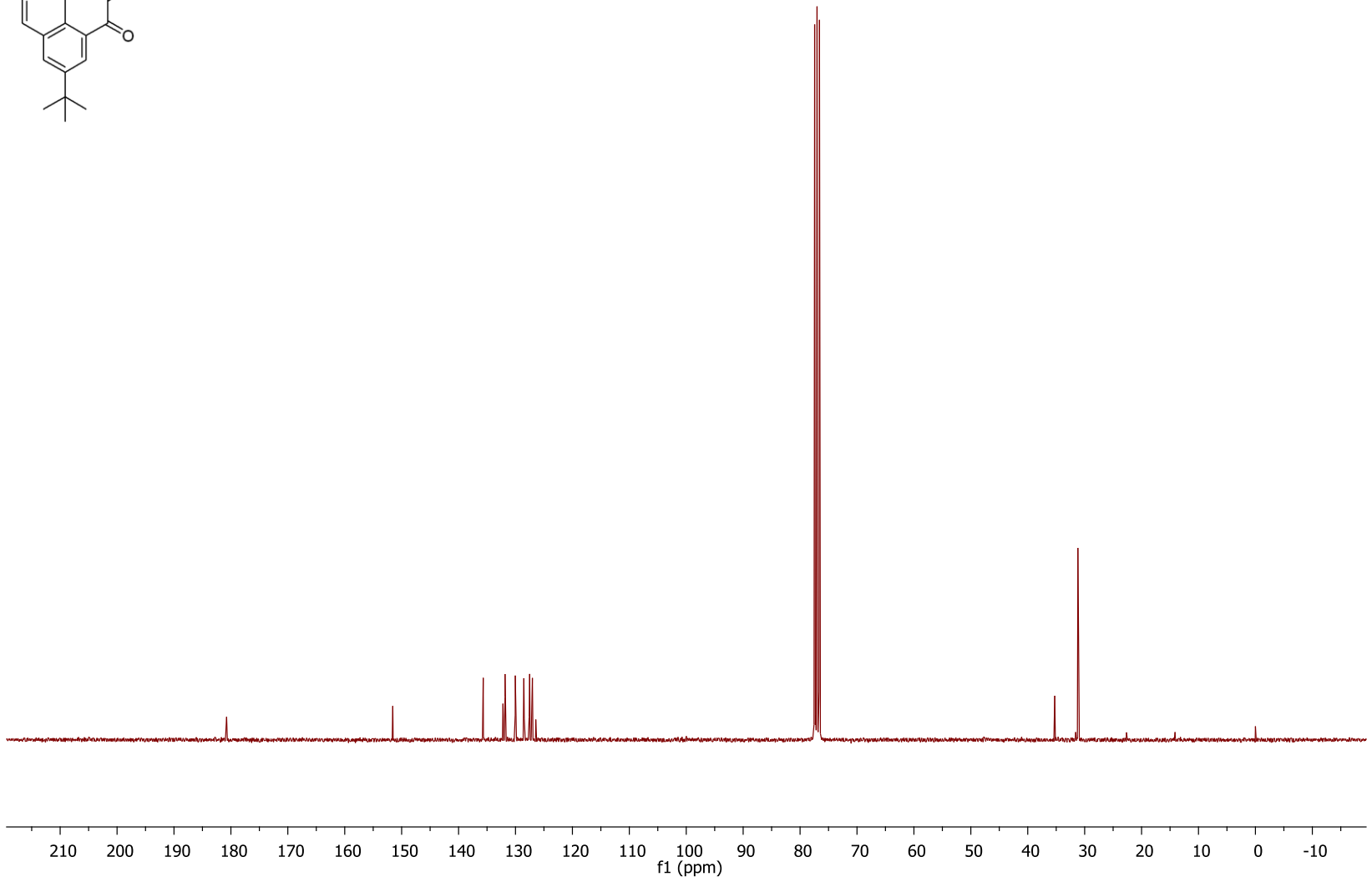
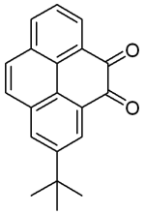


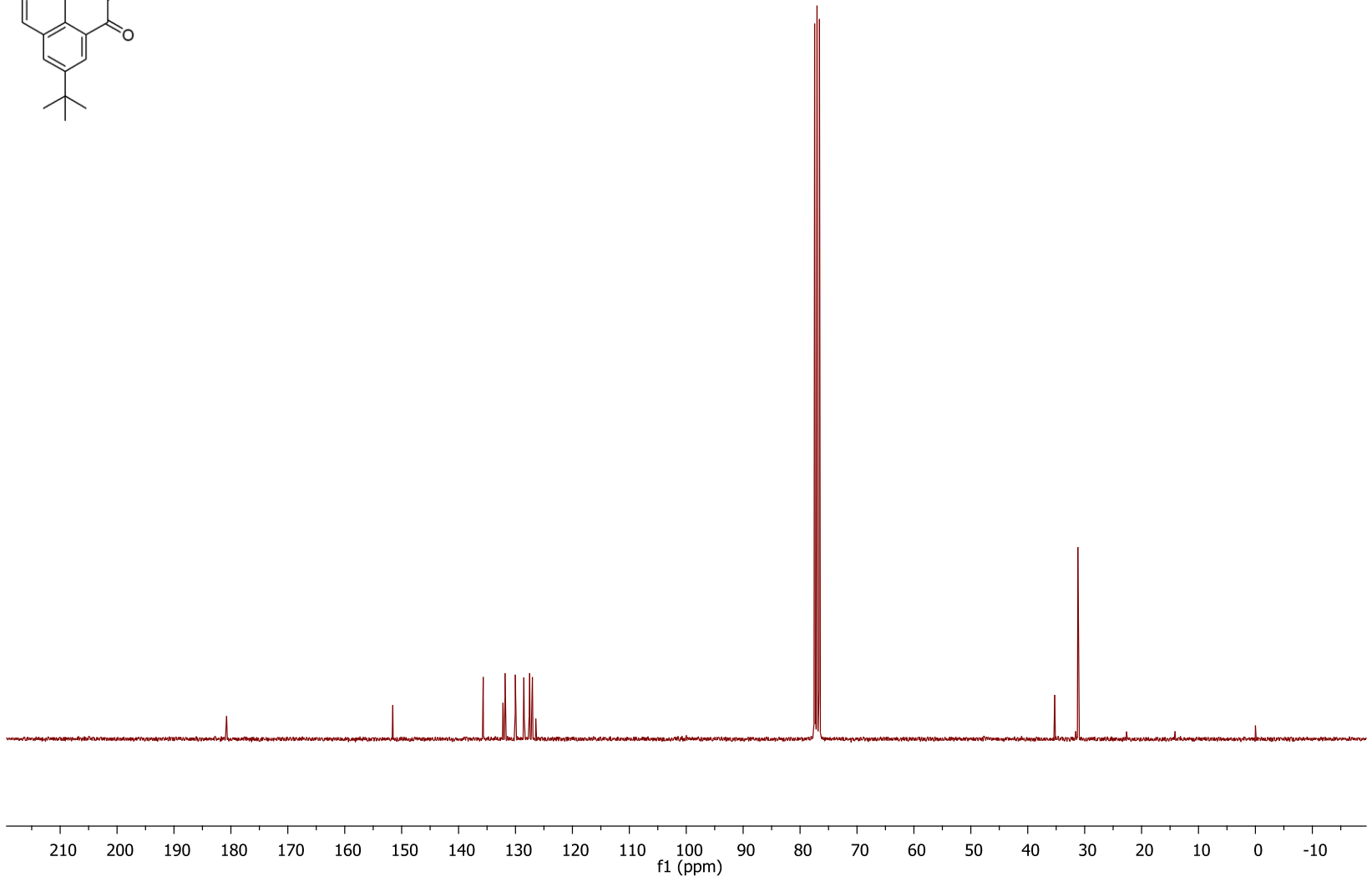
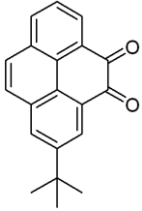




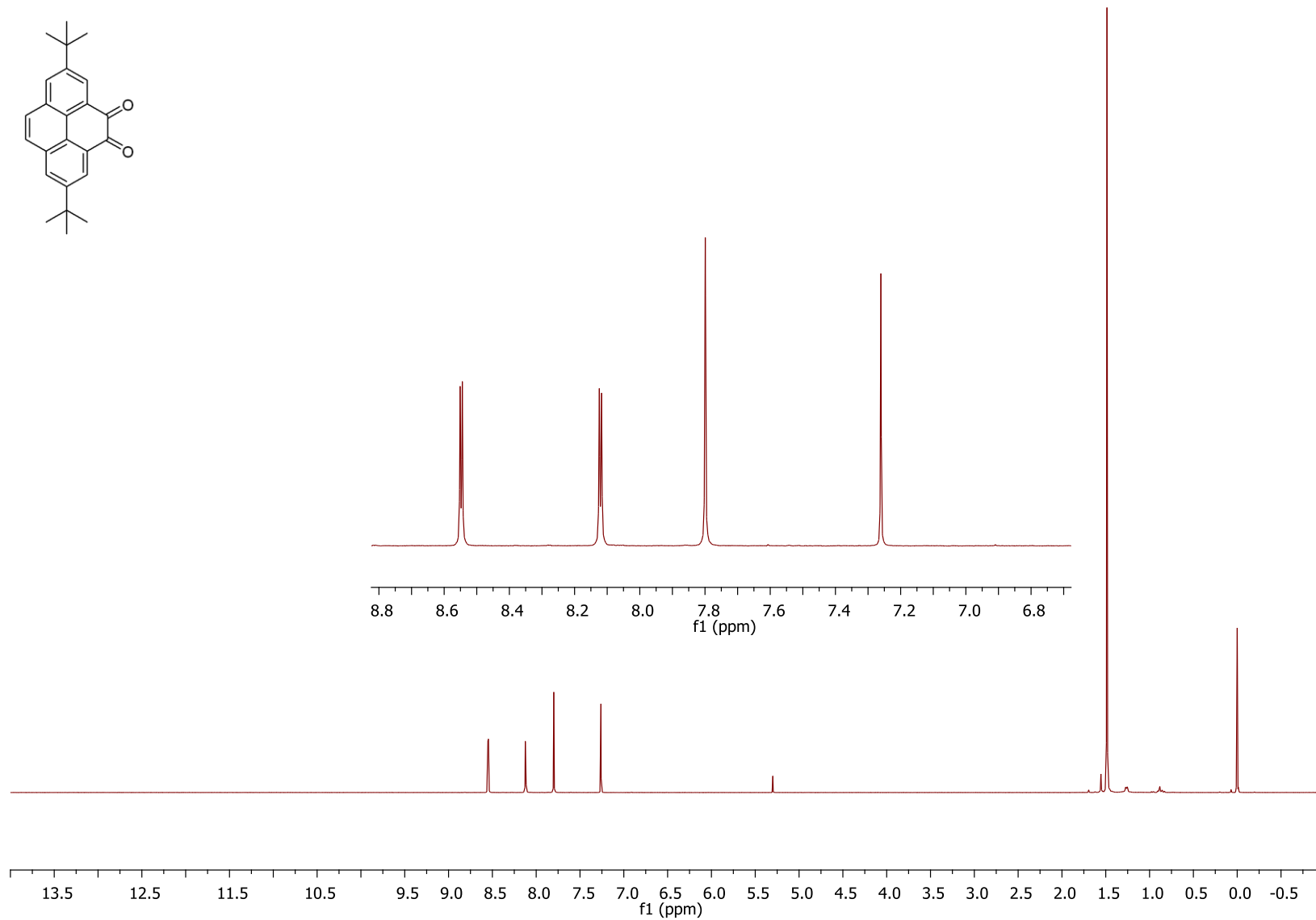
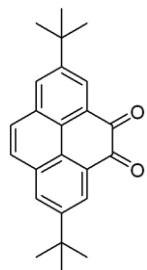
vi



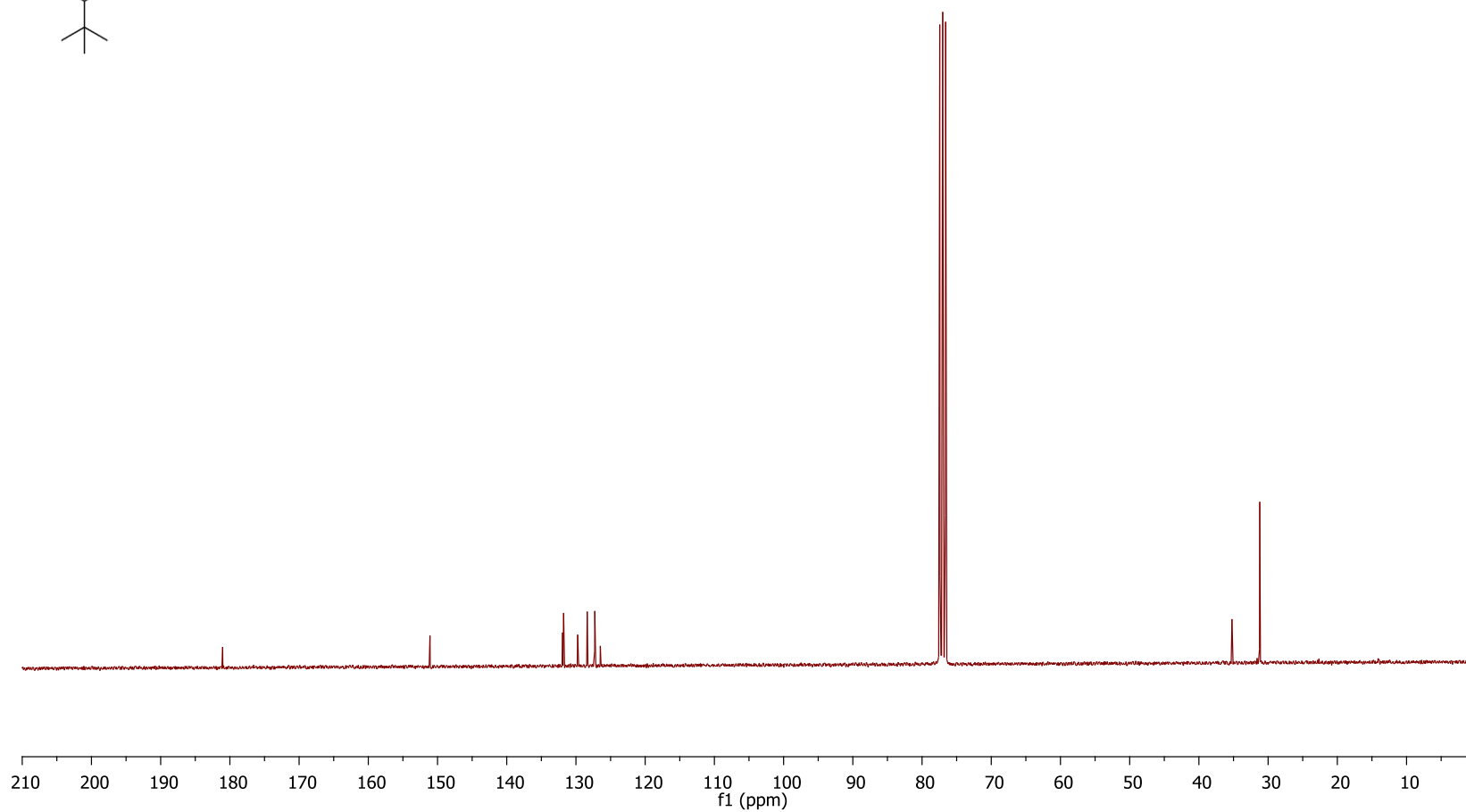
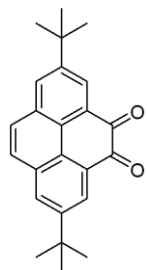




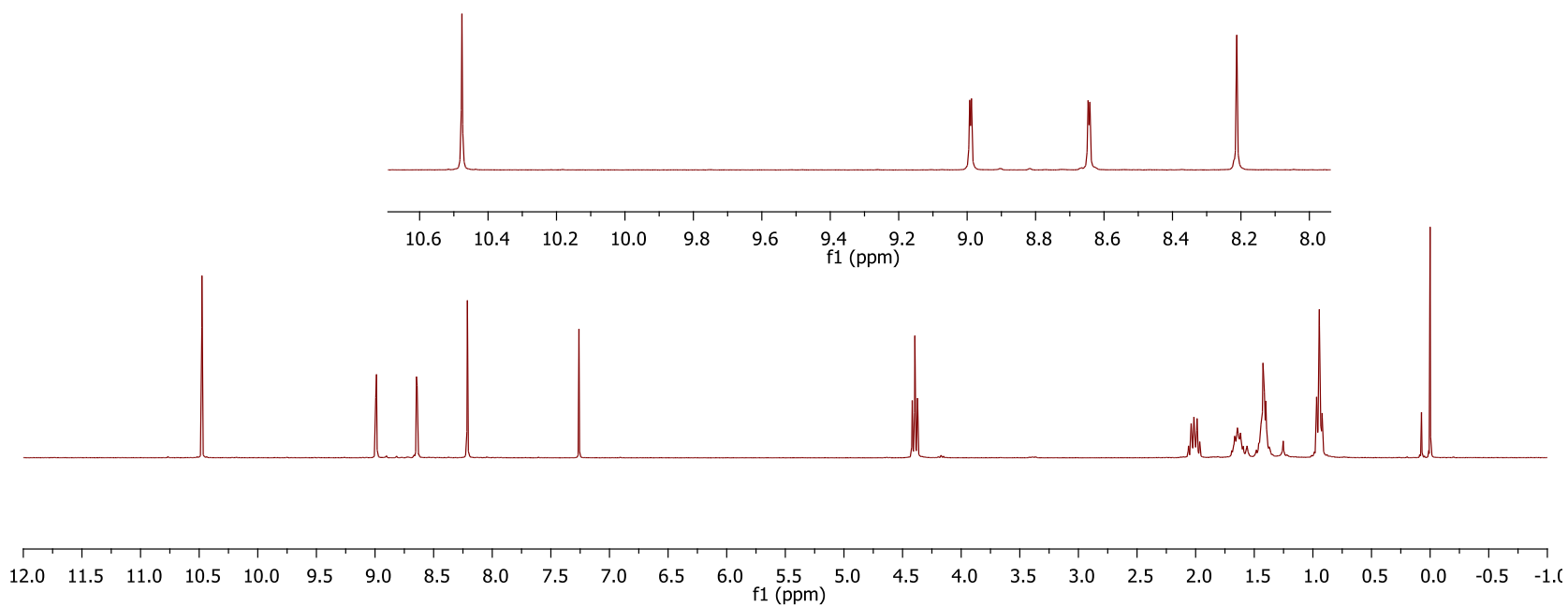
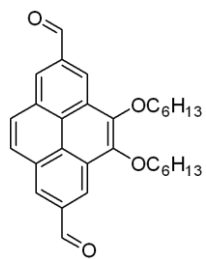
ix

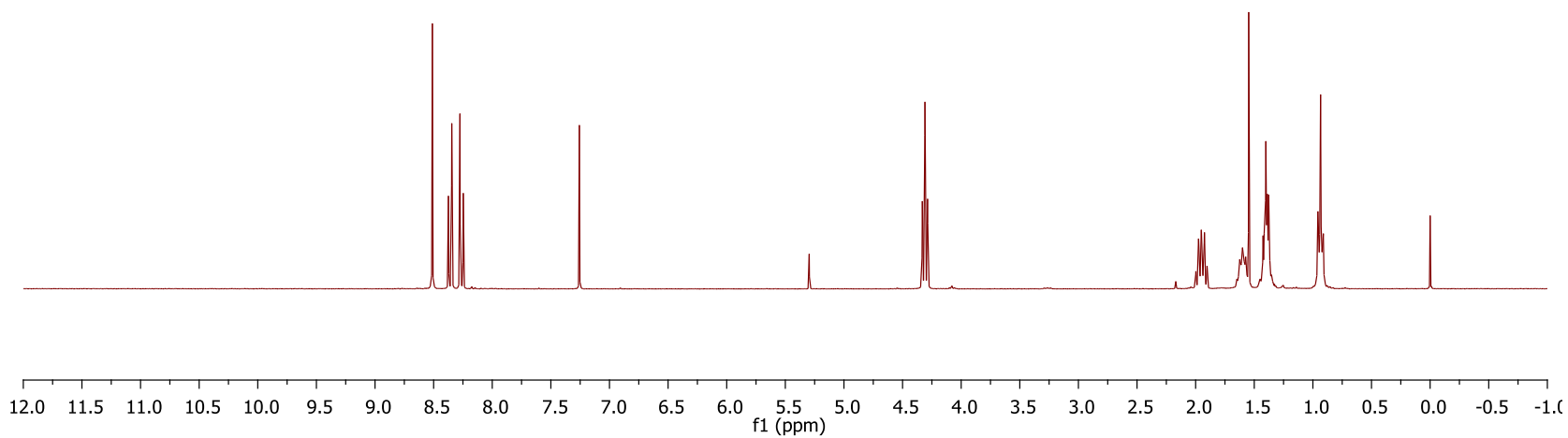
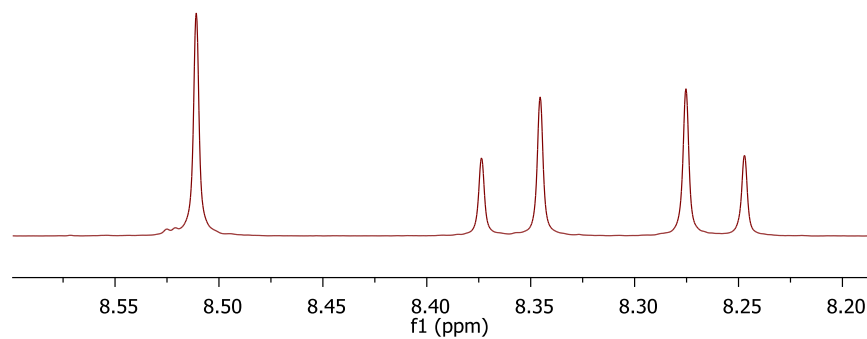
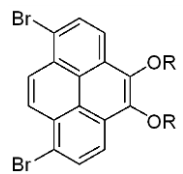


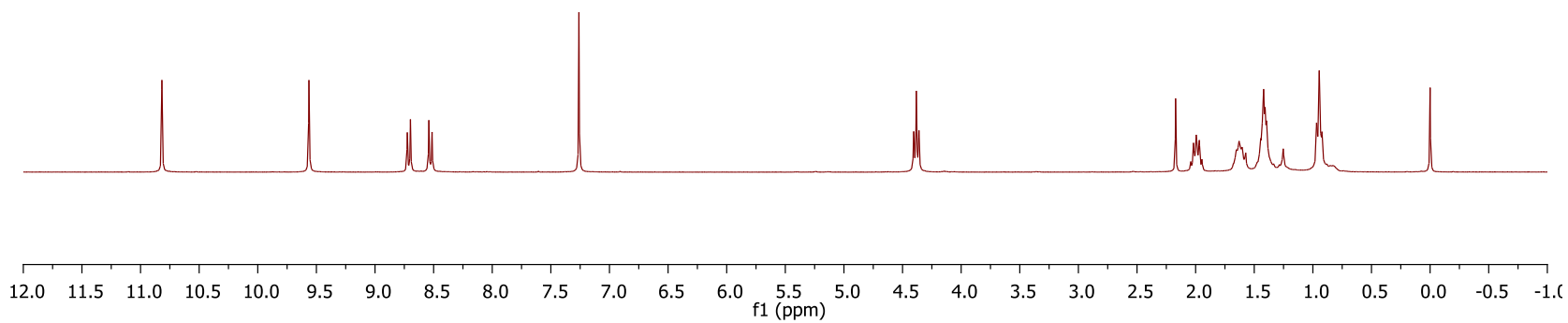
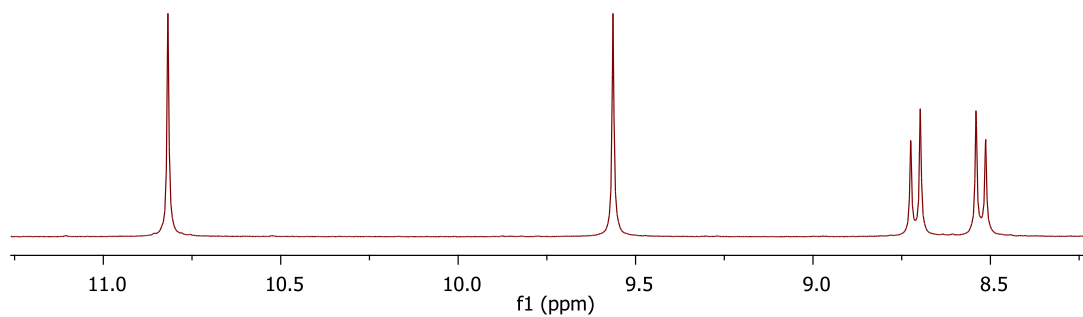
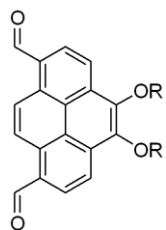
X



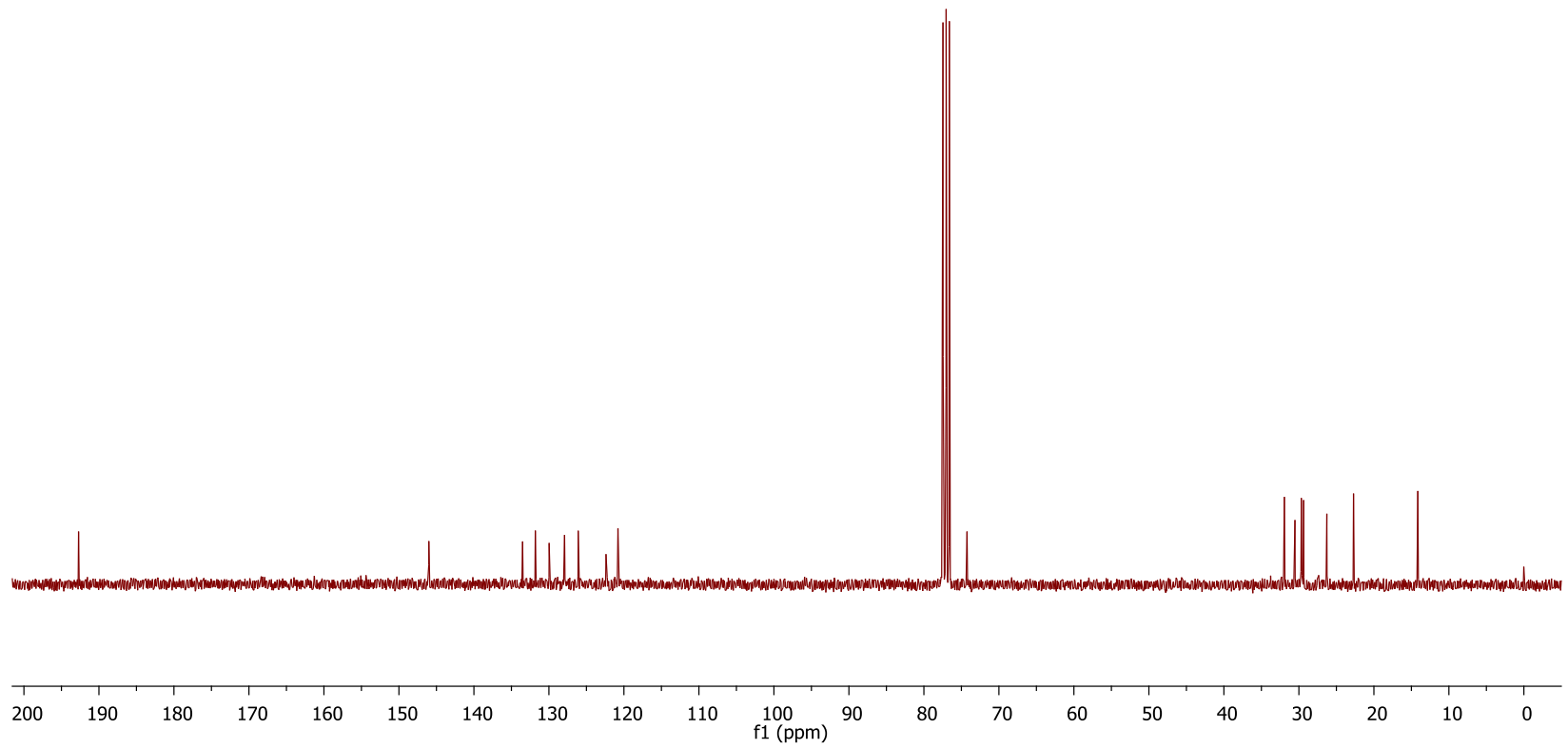
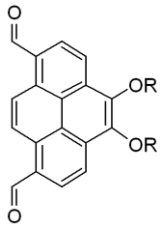
xi



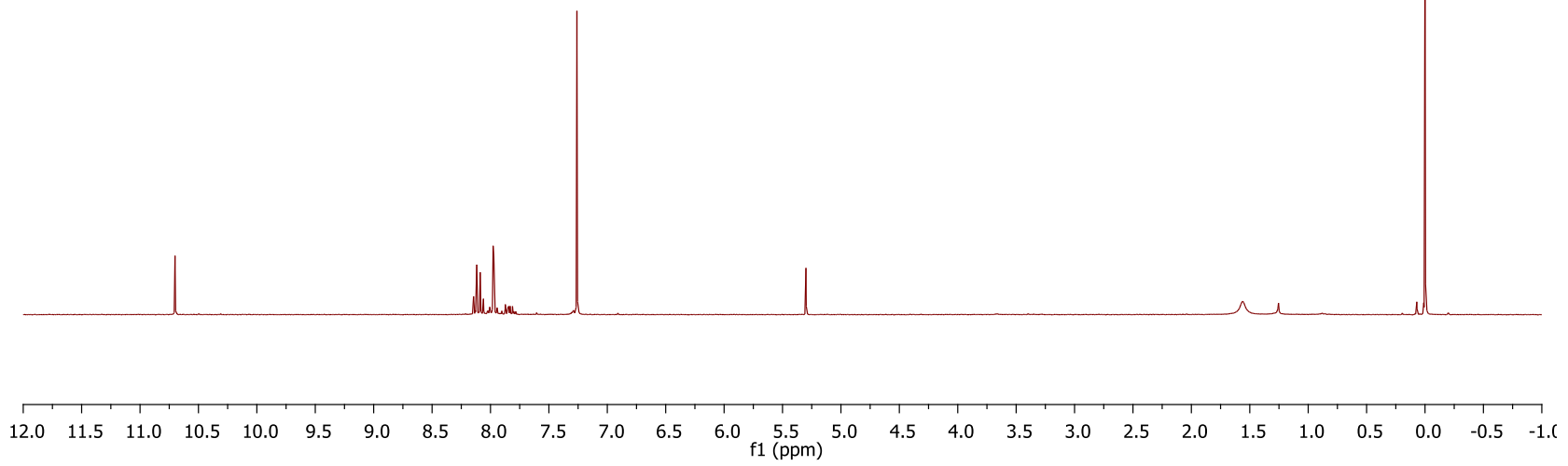
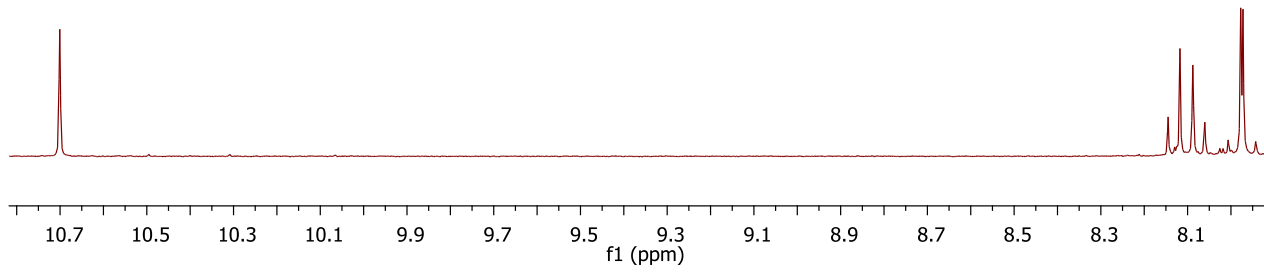
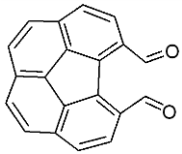




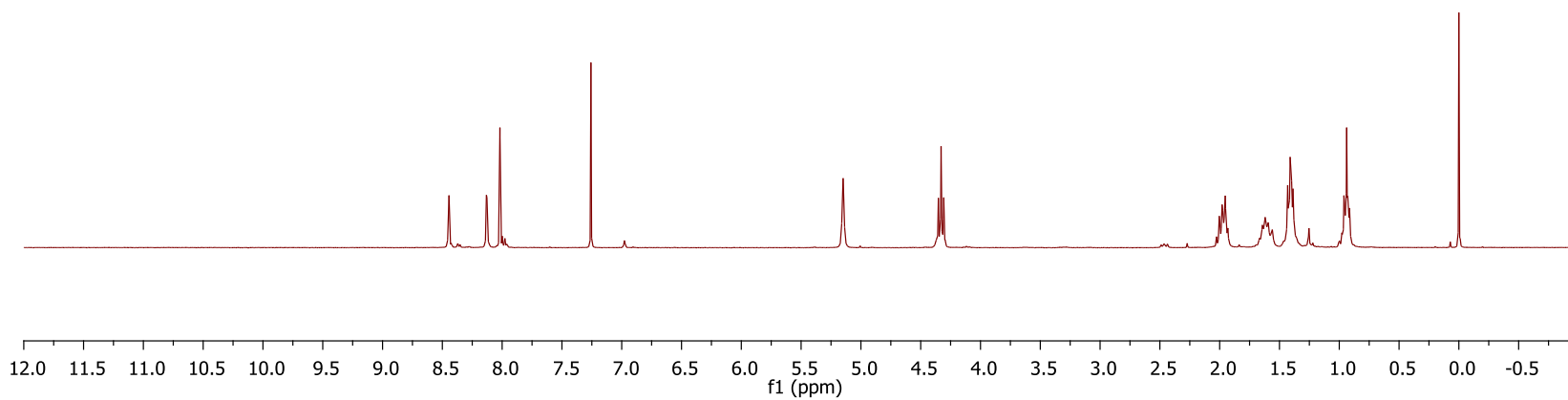
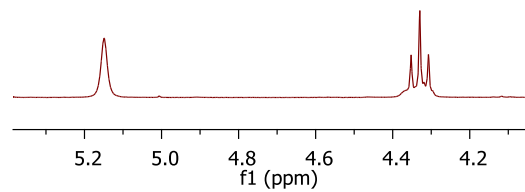
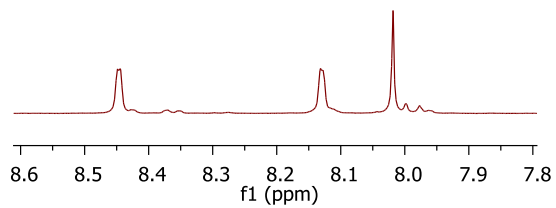
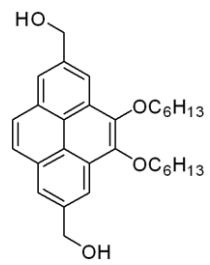
Xiv

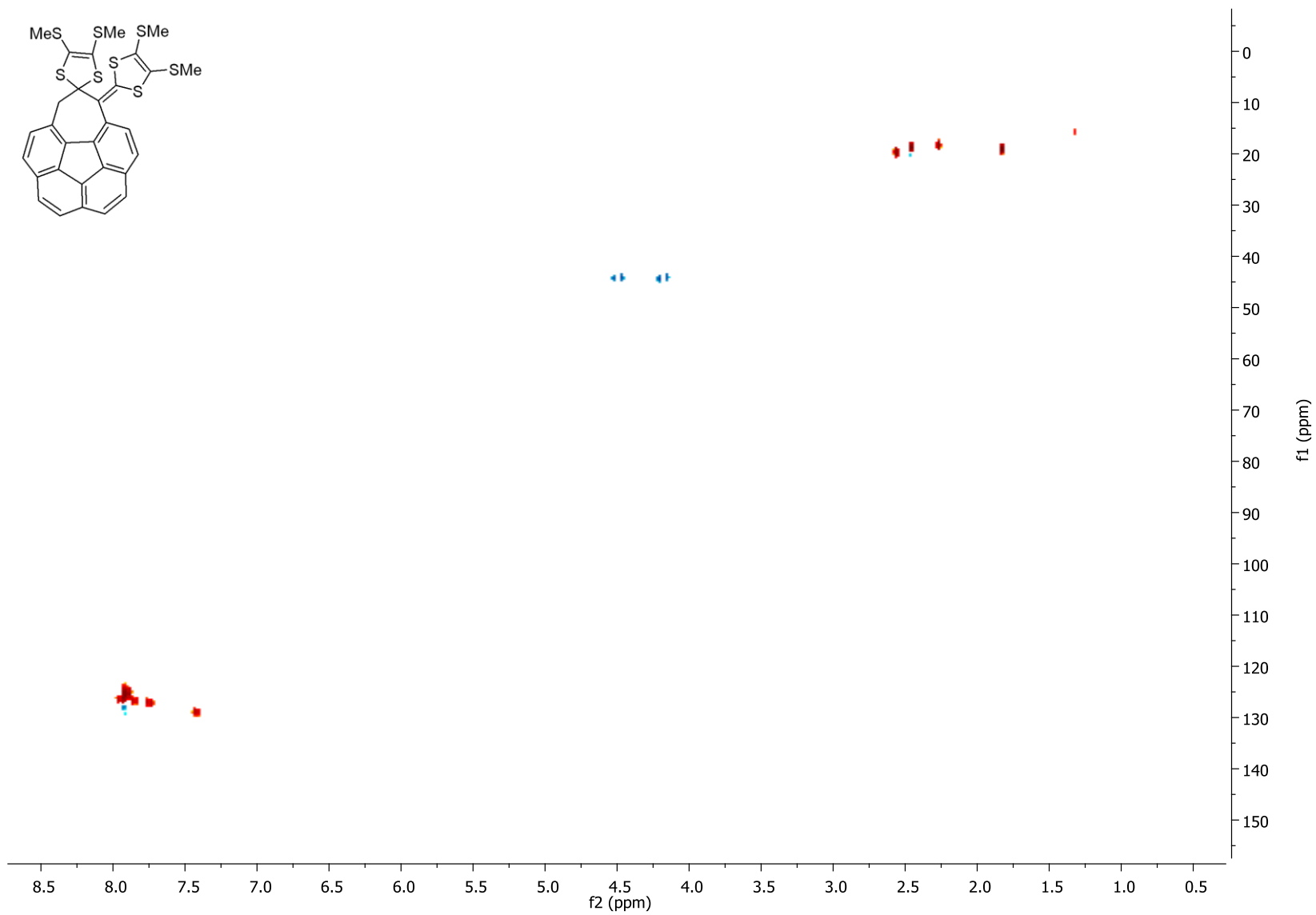
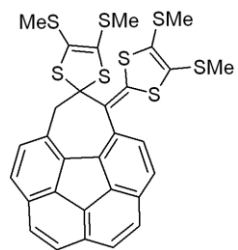


XV



xvii





XX